MASTERARBEIT | MASTER'S THESIS

Titel | Title

In vitro characterization of anti-inflammatory effects of non-pungent capsaicin analogs on the skin

verfasst von | submitted by

Elena Zoe Bogensperger BSc

angestrebter akademischer Grad | in partial fulfilment of the requirements for the degree of

Master of Science (MSc)

Wien | Vienna, 2025

Studienkennzahl lt. Studienblatt | Degree programme code as it appears on the student record sheet:	UA 066 659
Studienrichtung lt. Studienblatt | Degree programme as it appears on the student record sheet:	Masterstudium Lebensmittelchemie
Betreut von | Supervisor:	Dipl.Ern.Wiss. Dr. Barbara Lieder Privatdoz.

Acknowledgements

I would like to thank my supervisor Univ.-Prof. Dipl.Ern.Wiss. Dr. Barbara Lieder, Privatdoz. for her valuable insights while guiding me throughout the entire Master project. I would like to thank María Fernanda Cervantes Recalde, B.Sc. MSc. for teaching me cell culture, PCR and ELISA. I would like to thank Symrise AG, who kindly provided the homovanillic acid esters used for testing to make this research possible and also Dr. Joachim Hans for his introduction to the structure activity relationship. Finally, I want to express my deep gratitude to the ones I love - especially my parents, my brother, Alessa, Adelina, Selina and Jana- for their support on this journey.

Index

Index of Abbreviations

ATP Adenosine Triphosphate

CAP Capsaicin

CAPZ Capsazepine

Ca^{2+} Calcium Ions

cDNA Complementary Deoxyribonucleic Acid

CGRP Calcitonin Gene-Related Peptide

CLDN1 Claudin-1

COX-2 cyclooxygenase-2

CTE Capsiate

CXCL8 C-X-C Motif Chemokine Ligand 8

cryo-EM cryo-electron microscopy

ddH_2O double-distilled water

DMEM Dulbecco's Modified Eagle Medium

DMSO Dimethyl Sulfoxide

DNA Deoxyribonucleic Acid

ELISA Enzyme-Linked Immunosorbent Assay

EGFR Epidermal Growth Factor Receptor

FBS Fetal Bovine Serum

GAPDH Glyceraldehyde-3-Phosphate Dehydrogenase

gDNA Genomic Deoxyribonucleic Acid

HaCaT Human Adult Low Calcium High Temperature

hCa^{2+} High Ca^{2+} Content

HRP Avidin-Horseradish Peroxidase

HPRT Hypoxanthine-Guanine-Phosphoribosyltransferase

IL Interleukins

IL-8 Interleukin 8

LTB4 Leukotrien B4

LTMRs low-threshold mechanoreceptors

MMPs Matrix Metalloproteinase

mRNA Messenger Ribonucleic Acid

MTT 3-(4,5-Dimethylthiazol-2-yl)-2,5-Diphenyltetrazolium Bromide

nCa^{2+} Low Ca^{2+} Content

NaCl Sodium Chloride

NF-κB Nuclear Factor Kappa B

NFW Nuclease-Free Water

NGF Nerve Growth Factor

PBS Phosphate-Buffered Saline

PGE2 prostaglandin E2

RNA Ribonucleic Acid

RNase Ribonucleases

rpm Rotations Per Minute

RT-qPCR Quantitative Real-Time Polymerase Chain Reaction

SD Standard Deviation

SMILES Simplified Molecular Input Line Entry System

SP Substance P

S1-6 Transmembrane Helices 1-6

TJ Tight Junction

TNF-α Tumor Necrosis Factor-Alpha

TRP Transient Receptor Potential Cation Channel

TRPA1 Transient Receptor Potential Cation Channel Subfamily Ankyrin Member 1

TRPV1 Transient Receptor Potential Cation Channel Subfamily Vanilloid Member 1

VGiCs voltage-gated ion channels

Index of Figures

Index of Tables

1. Introduction

The skin is the primary interface between the human body and its external environment, serving as an essential barrier against chemical, physical, and microbiological stimuli (C. Cao et al., 2020). Epidermal keratinocytes (cells of the outermost skin layer) play an important role in maintaining skin homeostasis and initiating inflammatory responses. Specialized ion channels expressed in keratinocytes, including "Transient Receptor Potential" (TRP) channels, act as polymodal sensors for environmental stimuli. (Gouin et al., 2017) Capsaicin, the active ingredient in chili peppers, activates TRPV1, inducing a burning sensation both when consumed and when applied to the skin, resulting in redness and pain. Despite this, capsaicin is widely recognized for its analgesic properties and is valued as a spice in various cuisines.(Ilie et al., 2019) Although the role of TRPV1 in pain-related signaling pathways is well-documented, there is still some debate in the literature regarding its involvement in inflammatory processes, particularly in non-neuronal cells, which have received less attention in research (Chéret et al., 2013). In this context, homovanillic acid esters which are structurally related to capsaicin but less pungent (R. Gupta et al., 2021), represent a suitable model to explore whether structural analogues of capsaicin may influence inflammation and barrier function in human keratinocytes. Their reduced pungency makes them attractive for further investigation, with the hypothesis that they might elicit similar biological effects while allowing for an evaluation of potential TRPV1-dependent mechanisms. As polymodal receptors are widely present throughout the human body, TRPV1 channels are of significant research interest, due to their potential therapeutic implications for conditions associated with wound healing and inflammation (Bagood & Isseroff, 2021). This study aims to investigate various homovanillic acid esters, which are structurally related to capsaicin, with respect to their anti-inflammatory and barrier-enhancing effects in human keratinocytes, alongside an exploratory assessment of a potential involvement of TRPV1 ion channels. Furthermore, a central objective of this work was to identify specific structural features within these compounds that are associated with reduced inflammatory responses and increased *CLDN1* gene expression in human keratinocytes.

Therefore, 16 homovanillic acid esters have been tested on human epidermal keratinocytes to evaluate their anti-inflammatory and barrier-enhancing properties. This research is particularly critical as capsaicin's application on the skin often leads to an unpleasant burning sensation (Ilie et al., 2019). Thus, identifying compounds that retain the beneficial anti-inflammatory and barrier-stabilizing effects without causing discomfort could provide valuable treatment options for individuals with various skin conditions. Due to the fact that, skin alterations frequently correlate with systemic or other inflammatory diseases, such as psoriasis, atypical dermatitis (C. Cao et al., 2020) or rosacea (George et al., 2023).

2. Scientific Background

2.1. The human Skin- physiological function and structure

The skin is the largest protective organ in the human body. In addition, it also consists of a network of immune cells which play an important role in defense against infection and injury, the maintenance of homeostasis, and facilitating the repair of the skin. These characteristics make the skin a barrier and important in the body's immune functions. (Nguyen & Soulika, 2019)

The skin performs different activities to maintain the overall health of the human body, which will be further elucidated in more detail in the next paragraphs. Furthermore, the skin has an important thermoregulatory function which lies in maintaining a constant internal temperature. The skin can also act as an organ to perceive different senses which enables humans to feel touch, pressure, temperature, and pain. (Khavkin & Ellis, 2011) It also retains water within the hypodermis layer and absorbs lipophilic compounds. The skin is also involved in the expression of emotions. Another important skin function is the vitamin D synthesis. Vitamin D is synthesized into the skin when exposed to sunlight. (McKnight et al., 2022)

Anatomically, the skin is made up of three layers: the epidermis, dermis, and hypodermis. Starting off with the very outer layer of the skin: the epidermis. It provides a barrier against the entry of injurious substances, microorganisms, and UV radiation. It controls the water loss to preserve hydration. This layer also contains cells, such as melanocytes, involved in melanin biosynthesis responsible for skin pigmentation and further protection from UV damage. (Nguyen & Soulika, 2019) The epidermis can be further divided into several sublayers. the stratum basale, stratum spinosum, stratum granulosum, stratum lucidum (not present in thin skin), and stratum corneum (Arda et al., 2014). The stratum basale is the deepest epidermal layer and is composed of basal keratinocytes, as well as a few immune cells like Langerhans cells and T cells. Continuing with the stratum spinosum which is the thickest layer of the epidermis, consisting of several layers of cells, mostly keratinocytes. (Arda et al., 2014) In the stratum granulosum, keratinocytes contain granules with high contents of cysteine and histidine, which help to link keratin filaments together. The stratum lucidum consist of a thin layer of dead keratinocytes. On the top, ending with the stratum corneum, where terminally and enucleated differentiated keratinocytes can be found, which are continuously replaced by migrating cells from the stratum basale. (Nguyen & Soulika, 2019). It is also within the epidermis that the sensory receptors, by which one can interact with the environment, are found. Sensory receptors give the ability to perceive external stimuli such as touch, pressure, temperature, and pain. (Baroni et al., 2012) (Khavkin & Ellis, 2011)

Lying beneath the epidermis is the dermis - a layer, composed of blood vessels, nerves, hair follicles, and sweat glands and collagen supporting the epidermis (Nguyen & Soulika, 2019). Due the location of the sweat glands in the dermis, the dermis takes part in the thermoregulation and the cooling of

the body. (Arda et al., 2014) The dermis can be further differentiated into papillary and reticular sub-layers. (Nguyen & Soulika, 2019) The dermis supports the epidermis due to its blood supply and assists in transmitting stimuli by carrying a great number of nerves. The hypodermis, or subcutaneous tissue, is the deepest layer of skin consisting of fat cells that insulate the body and protect it against physical impact. (Yousef et al., 2025) Besides this structural role, the hypodermis is an active tissue producing a variety of mediators, including growth factors, adipokines, and cytokines. It also contains multiple immune cells which contribute to the immune function of the skin. (Nguyen & Soulika, 2019) The epidermis, dermis, and hypodermis interact together to maintain health and integrity of the skin by regulating homeostasis, sensory perception and also emotional expression. (McKnight et al., 2022)

2.1.1. Keratinocytes- skin cells of the epidermis

Keratinocytes are the most abundant cell types of the epidermis, which have an influence on the skin due to their importance in keratin production. Keratin is a protein involved in water impermeability and the strengthening of the skin. (Ranzato et al., 2008) Keratinocytes also take part in regeneration and repair processes of the skin, especially during wound healing. (Piipponen et al., 2020) Moving from the basal layer, the keratinocytes progress to the top layer, where they differentiate and finally undergo programmed cell death. (Nguyen & Soulika, 2019) This process is crucial in terms of skin health and functionality. Understanding keratinocytes behavior plays a major part in the development of methods to treat skin trauma and wounds. Therapies that enhance the function of keratinocytes may therefore provide ways of improving and healing deficient mechanisms of skin repair in humans. (Ranzato et al., 2008) During this master thesis the HaCaT cell line was used. The abbreviation HaCaT stands for Human adult low calcium high temperature (Colombo et al., 2017). This is a human keratinocyte cell line expressing many properties of epidermal keratinocytes. It's also one of the most used cell lines in studies dealing with skin biology and the mechanism of wound healing (Ranzato et al., 2008). Furthermore, HaCaT keratinocytes are of wide use in scientific research, due to their high capacity for differentiation and proliferation *in vitro*. A high level of calcium leads to differentiation and stratification, whereas a low concentration leads to a basal state. (Colombo et al., 2017). The HaCaT- cells were cultured under high calcium concentration (1.8 mM Ca^{2+}) and seeded under low calcium concentration (0.06 mM Ca^{2+}) based on the previous experiments of Cervantes Recalde et al., 2024. This, skin model was used in the master thesis to investigate inflammatory processes in non-neuronal skin cells. (Piipponen et al., 2020)

2.1.2. Tight junctions

The skin's barrier function is one of its defense mechanisms against the invasion of microbes, viruses, fungi, toxins, irritants, and allergens. Impaired integrity of the epithelial barrier plays a critical role in developing or promoting such invasions. It was suggested that the disruption of the skin barrier is a crucial factor in various cutaneous diseases, including atopic dermatitis, allergic and irritant contact dermatitis, and bacterial or viral infections. (Deng et al., 2019) Tight junctions are integral intercellular structures that maintain epithelial barrier function. Among key proteins forming tight junctions are the claudins, or *CLDNs*, a family of four-pass transmembrane proteins. (Otani & Furuse, 2020) More than 20 claudin genes have been identified in the human genome. They have a critical role in regulating the paracellular permeability of the epithelium and in the assembly of tight junction strands, affecting pore formation, strand number, and complexity. (Günzel & Yu, 2013) Moreover upholding the physical barrier is the crucial first line of defense against harmful external factors, which is also associated with the innate immune system, therefore upholding the function of tight junctions is very important as their actions seem interdependent with the immune system (Deng et al., 2019).

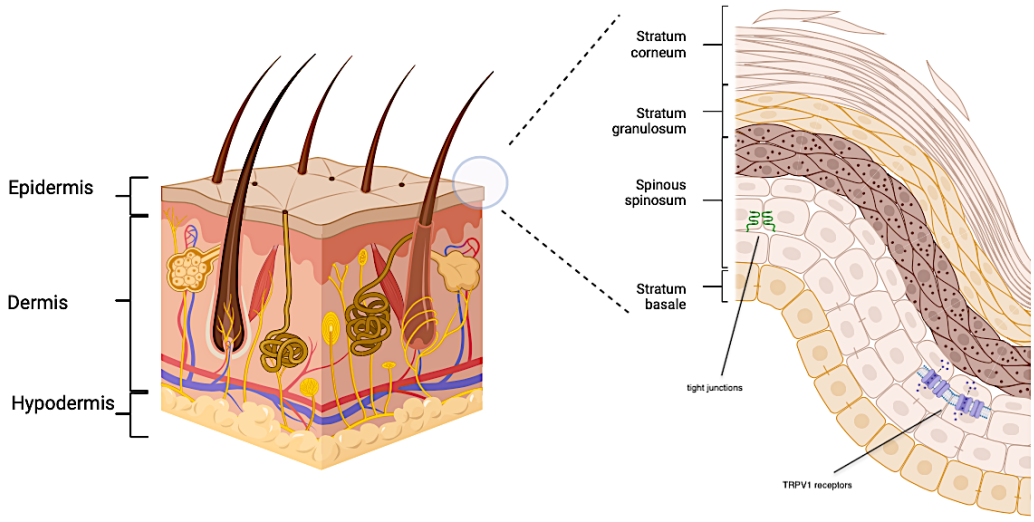

Figure 1 Cross-section of the skin, showing the major layers: epidermis, dermis and hypodermis (Left) Cross-sectional view of human skin layers with a zoomed-in detail of the epidermis highlighting TRPV1 receptors and tight junctions (Right). Zoomed-in view of the epidermis, showing its four distinct layers: stratum basale, stratum spinosum, stratum granulosum, and stratum corneum. (Arda et al., 2014) TRPV1 receptors (violet structures) are shown on keratinocyte membranes within the stratum spinosum. These receptors detect thermal and chemical stimuli, contributing to the skin's protective response to environmental stressors. (Nadezhdin et al., 2021) Tight junctions (green lines) are located between keratinocytes in the stratum spinosum and are composed of proteins such as claudin and occludin, which strengthen the skin barrier by limiting water loss and preventing pathogen entry. (Deng et al., 2019) This figure was created using BioRender.

2.2. Inflammation in keratinocytes

As before mentioned, the barrier function and the immune system are intertwined, the physical barrier depends on the expression and function of junction adhesion molecules and tight junction proteins. Disruption in either of their expressions or functions brings about insufficient barrier formation, thereby leading to skin disorders. (Deng et al., 2019) The skin employs various mechanisms to maintain homeostasis and defend against external influences. (He et al., 2024) (Nguyen & Soulika, 2019). One key part of this, is the biomolecules it produces, like antimicrobial proteins (AMPs) and lipids, which help fight off bacteria. The skin's slightly acidic pH also creates an environment that's less welcoming to certain pathogens. On top of that, both immune cells—like myeloid and lymphoid cells—and non-immune skin cells play a role in defense. Most skin cells, including keratinocytes, fibroblasts, adipocytes, melanocytes, and endothelial cells, have pattern recognition receptors (PRRs). When activated, these receptors trigger the production of cytokines and chemokines, further enhancing the skin's immune response. (Nguyen & Soulika, 2019) Keratinocytes are special in that way that they express almost all intracellular and extracellular PRRs and therefore help the body to defend itself against infection. (Piipponen et al., 2020). Furthermore keratinocytes are in a constant interaction with the local immune system due there production of cytokines chemokines. (Takashima et al., 1995).

IL-8, a chemokine mainly released by keratinocytes and macrophages, plays a key role in attracting neutrophils to inflamed areas. Neutrophils act as the body's first line of defense, working to eliminate pathogens and clear damaged tissue during immune responses.. (Piipponen et al., 2020) Whereas TNF-α (tumor necrosis factor-alpha) is a cytokine predominantly produced by immune cells like macrophages and monocytes, and it plays a crucial role in amplifying the inflammatory response (Idriss & Naismith, 2000). It induces the production of other pro-inflammatory cytokines and chemokines such as IL-6 (De Cesaris et al., 1998). Moreover TNF-α may stimulate IL-8 production in keratinocytes and other skin cells, which leads to a positive feedback loop that sustains the inflammation (Young et al., 2008) TNF-α interacts with TNF receptors on various cells, initiating a signal transduction which can lead to the activation of NF-κB (Nuclear Factor kappa-light-chain-enhancer). (Idriss & Naismith, 2000) This pathway can be activated due to UV radiation, which in turn leads to the increase of proinflammatory cytokines such as TNF-α, interleukin (IL)-1β, IL-6, and IL-8 (S. Han et al., 2018). NF-κB acts as a transcription factor upregulates the expressions of inflammatory genes and amplifying the inflammatory response with coordination of the immune response (Liu et al., 2017). Therefore it can be summarized that TNF-α itself induces inflammation, defending the human body against pathogens, however an unresolved inflammation leads to chronic inflammation (Idriss & Naismith, 2000).

Another pathway worth mentioning when talking about keratinocytes, is the STAT3 signaling pathway. In a murine psoriasis model, it was found that keratinocytes produce inflammatory

cytokines and chemokines, and especially IL-25 can activate this pathway. This suggests that keratinocytes play a significant role in the development of the disease. (Nguyen & Soulika, 2019) Psoriasis is immune mediated disease leading to quick hyperproliferation of keratinocytes which are activated by the immune system (Yamanaka et al., 2021). Furthermore, keratinocytes also offer different mechanisms to stop the inflammatory process form overreacting (Nguyen & Soulika, 2019).

2.3. Introduction to TRP channel receptors

The skin contains specialized receptors allowing the perception of a wide range of stimuli, including pain (nociceptors), itch (pruriceptors), temperature (thermoreceptors), and touch (low-threshold mechanoreceptors, or LTMRs). Some of these receptors, like the nociceptors, pruriceptors, thermoreceptors, and some mechanoreceptors, are present as free nerve endings. (Nguyen & Soulika, 2019)

Sensory nerves, originate from the dorsal root ganglion and innervate the skin. These nerves are divided into myelinated types (Aβ- and Aδ-fibers) and unmyelinated types (C-fibers). C-fibers can be distinguished into peptidergic and non-peptidergic subtypes, with their endings located in the epidermis. (Bagood & Isseroff, 2021) Thermoreceptors of the skin are necessary to detect changes in the temperature of the body and the external environment. When thermoreceptors are activated by changes in temperature, this stimulates physiological responses as the body attempts to return to a thermal balance, through vasodilation, vasoconstriction, sweating, or shivering. The ligand-gated ion channels (resembling voltage-gated potassium channel (Liao et al., 2014)) are directly involved in the detection of pain and temperature stimuli is the transient receptor potential *(*TRP) family. (Nguyen & Soulika, 2019) TRP channels were first discovered in 1977 and six subfamilies are known of today. (P. Yang et al., 2017) All of the TRP channels have six transmembrane domains with the N- and C-terminal regions located inside the cell and are assembled as tetramers to form nonselective cation-permeable pores (Liao et al., 2014).

In the skin, TRP channels are not only found in sensory nerve endings but are also expressed in various non-neuronal cell types, including keratinocytes and skin-resident immune cells. These channels play crucial roles in maintaining skin homeostasis by participating in the formation and maintenance of the skin barrier, hair follicle growth, and regulating immune and inflammatory processes. (P. Yang et al., 2017) As such, they contribute to both normal skin function and the development of skin disorders (Nguyen & Soulika, 2019). Importantly, several TRP channels in the skin act as primary sensors for temperature, mechanical, and chemical stimuli, allowing us to perceive sensations such as temperature, touch, itch, and pain, under both healthy and disease conditions (P. Yang et al., 2017). Members of the TRP family are for example, TRPA1 (Transient Receptor Potential Ankyrin 1) which are receptors are detectors of cold, while TRPV1 (Transient Receptor Potential Vanilloid 1) and TRPV2 are detectors of heat. (Nguyen & Soulika, 2019)

2.3.1. TRPV1 Structure and function

TRPV1 expression has been identified in C-fibers, mast cells, keratinocytes, sebocytes, hair follicles, nociceptors and other components. (Bagood & Isseroff, 2021) TRPV1 expression in human keratinocyte was first discovered by Denda et al ,2001. In non-neuronal cells, TRPV1 also acts as nociceptive sensor and interacts with the inflammatory processes of the skin (Gouin et al., 2017).

The TRPV1 gene is situated on chromosome 17p13.2 and encodes a protein consisting of 838 amino acids, which assembles into a homo-tetrameric structure (Ilie et al., 2019). The ability of TRPV1 lies in the detection of physical and chemical factors leading to the transmission of inflammatory and chronic pain signals. Structurally, TRP channels resemble voltage-gated ion channels, with a tetrameric structure around a central ion. (Liao et al., 2013) Each of the four subunits contains six transmembrane segments (S1-S6), with a hydrophobic region between S5 and S6 forming the ion-conducting pore (Ilie et al., 2019). Moreover TRPV1 has a selectivity filter (Liao et al., 2013). Despite this structural similarity with voltage gated ion channels, TRP channels are more diverse, due to their cytoplasmic N-terminal and C-terminal domains (Hellmich & Gaudet, 2014). According to Bagood and Isseroff, 2021, the N- and C-terminal regions of each channel subunit are positioned intracellularly. The N-terminus contributes to the channel's responsiveness to activators, while the C-terminal TRP box plays a crucial role in maintaining channel stability and regulating its function. (Bagood & Isseroff, 2021) Furthermore, these domains are also important to distinguish the different subtypes of TRPs and play a crucial part channel gating (Diver et al., 2022).

The activation state of the TRPV1 channel can be regulated through sensitization or desensitization, depending on its modulation. This regulation occurs either through the binding of calmodulin (CaM) at specific sites on TRPV1 or via phosphorylation by protein kinase C (PKC), protein kinase A (PKA), or calcium/calmodulin-dependent kinase II (CaMKII). (Szolcsányi & Sándor, 2012) Furthermore, TRPV1 is also widely known for its activation by natural reagents like capsaicin (Diver et al., 2022), but also other reagents like vanilloids and endovanilloids, as well as noxious heat exceeding 43°C, acidic environments, cations, and various animal toxins can lead to its activation. Moreover, pathways can be triggered independently, but activators can also work together, adding to the complexity of channel activation. (Bagood & Isseroff, 2021)

Zhang et al. (2021) explains that outer pore regions of TRPV1 are structurally flexible which allows the permeation of bigger organic cations. Such flexible regions can be displayed due to widening during channel activation and thereby enabling dynamic ion selectivity. However, the complete physiological impact of this structural plasticity is still unknown. Nonetheless it would also further explain the activation of TRPV1. Zhang et al. also demonstrated that, TRPV1 operates through a two-step process, using single-particle cryo-electron microscopy (cyro-EM). Suggesting that extracellular protons, changed the structure of the upper gating to facilitate opening of the lower gate. (Zhang et al., 2021)

A) Apo structure of TRPV1

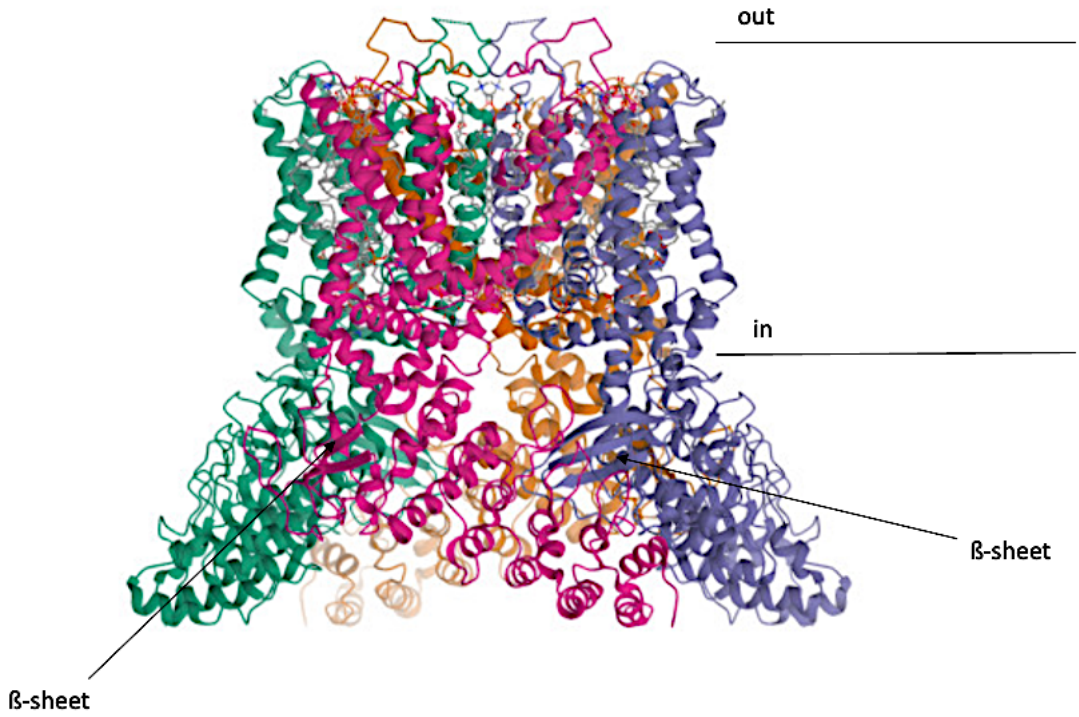

B) Linear diagram of a TRPV1 subunit

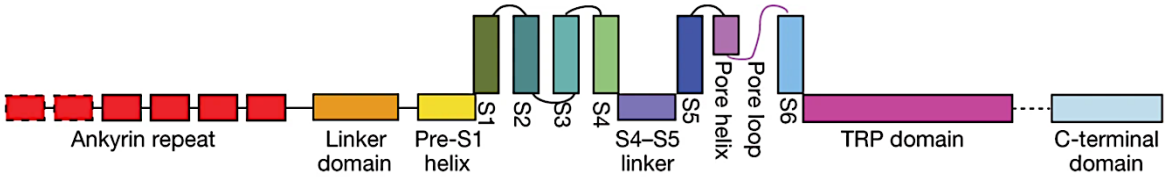

Figure 2 molecular structure of TRPV1 and the linear diagram of the major structural domains (A) TRP channels are polymodal molecular sensors which play an indispensable role in a wide range of physiological functions and various human diseases. The cryo-EM structure of full-length TRPV1 from thirteen-lined ground squirrel is presented by (Nadezhdin et al., 2021) adapted from (Liao et al., 2013) indicating the membrane as well as ß-sheet structures and four different colors to differentiate the subunits of TRPV1. The Protein Data Bank (RCSP PDB) was used to find the structure. (B) Depicts the Linear diagram with major structural domains in a TRPV1 subunit.

After activation, the TRPV1 channel opens and the cell membrane permeabilizes, especially calcium ions are favored. The downstream signaling triggered by calcium influx is shaped by intracellular processes, which also determine its functional effects on the cell. (Bagood & Isseroff, 2021) Additionally, research suggests that alternative splicing of TRPV1 can result in nonfunctional channels or splice variants that inhibit the function of the receptor. (Vos et al., 2006). All of this knowledge about TRPV1, the structure, the activation and the downstream effects make developing therapy which targets this receptor highly complex (Bagood & Isseroff, 2021).

2.3.1.1. TRPV1 in keratinocytes and its role in Inflammation

As before mentioned, heat, photoaging, and intrinsic aging could increase the expression of TRPV1 in human keratinocytes (*ex vivo* and *in vitro* models). In general, changes in intracellular free Ca^{2+} concentration are crucial in keratinocyte homeostasis because an increase in intracellular Ca^{2+} concentration triggers the differentiation and inhibits the proliferation of keratinocytes. More recently, it has been suggested that stimulation of TRPV1 may facilitate the polarization and migration of keratinocytes. (Xiao et al., 2023) Additionally, factors such as UV irradiation and capsaicin can activate TRPV1 in keratinocytes (leading to a calcium influx) triggering various downstream effects which impact the keratinocyte-dependent inflammation. UV radiation has been shown to enhance TRPV1 trafficking to the cell membrane via Src kinase-mediated mechanisms.(S. Han et al., 2018) Additionally, intracellular calcium levels and TRPV1 expression appear to be interdependent (Graham et al., 2013). It has also been suggested that TRPV1 activation by capsaicin or heat may impair barrier recovery (Denda et al., 2007). Calmodulin signaling on the other hand plays a key role in desensitizing TRPV1 following activation, via two different pathways, either way through an increase in intracellular Ca^{2+} or through the absence of extracellular Ca^{2+} (Rosenbaum et al., 2004). Under acidic conditions it might be observed that TRPV1 activation stimulates the production of growth factors and cytokines, promoting keratinocyte proliferation *in vivo* (Bagood & Isseroff, 2021). Beyond its role in keratinocyte function, TRPV1 plays a significant part in keratinocyte-mediated inflammation. In vitro studies with HaCaT cells have demonstrated that TRPV1 activation, through capsaicin or acidification, results in increased intracellular calcium levels and the release of cyclooxygenase-2 (COX-2), different interleukins like (IL-8, IL-1β, IL-2, IL-4), TNF-α and prostaglandin E2, LTB4, as well as several MMPs, including MMP-13, 9, 3, and 2. This further highlights the receptor's involvement in promoting inflammatory responses. IL-8 and PGE2 are both important mediators of inflammation and pain. TRPV1 also contributes to neurogenic inflammation through promoting the release of neuropeptides from sensory nerves, which also increases the inflammatory response in keratinocytes. (Southall et al., 2003) Further studies showed, that a calcium influx led to a TRPV1 activation and can stimulate PKCα (Protein Kinase C alpha) signaling, leading to increased MMP1 levels in HaCaT cells after contact with UV radiation, heat, and capsaicin. Another pathway which can be activated in HaCaT skin cells by UV radiation is the cytoplasmic 1 (NFATc1) pathway, which upon activation of TRPV1 followed by a calcium influx, which turns on the calcineurin/nuclear factor of activated T-cells. (Bagood & Isseroff, 2021). Pro-inflammatory effects are associated with the activation of TRPV1, and excessive activation contributes to chronic inflammation, which is harmful to the skin. Thus, controlling the activity of TRPV1 might be an important role in the treatment of skin inflammatory conditions. (Gouin et al., 2017) The figure below will give an overview of the before mentioned activators of TRPV1 and their downstream effects.

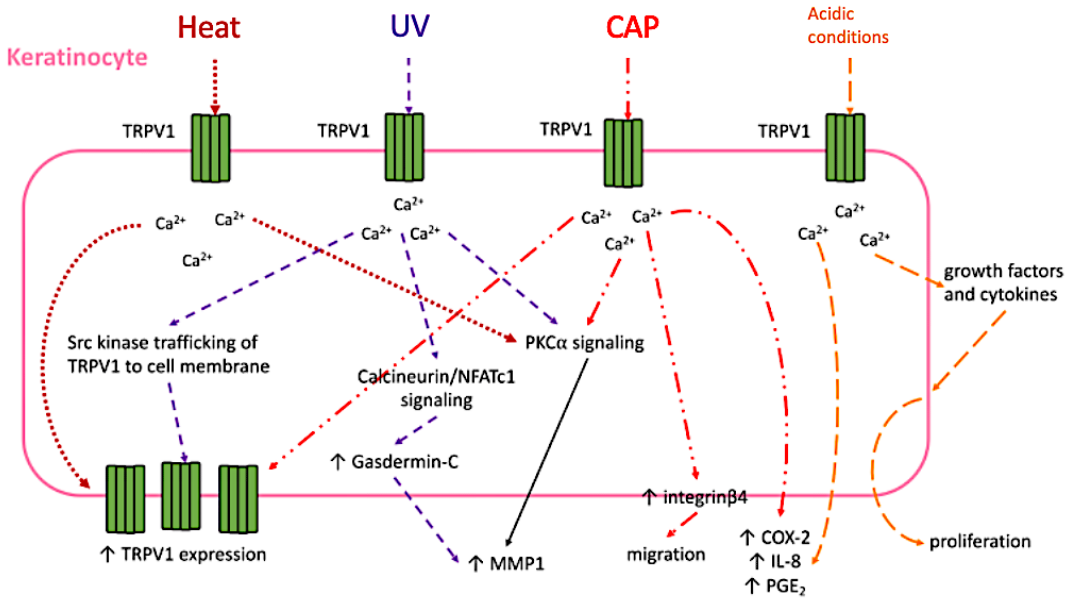

Figure 3 Different factors which activate TRPV1 in keratinocytes and their downstream effects. Adapted from Bagood and Isseroff, 2021.

2.4. Capsaicin-Agonist of TRPV1 and its effect on pungency

Fruits of the genus *Capsicum* are used for their pungency, which is usually added in many cuisines to elevate the flavors. These fruits are consumed worldwide not only for their high pungency but also for the wide range of health benefits they have. Various studies have established the fact that their pungency is mainly due to compounds known as capsaicinoids, which are biosynthesized via two different pathways: by reactions between vanillylamine moieties with branched fatty acid moieties derived from amino acids (Chen et al., 2019) or the phenylpropanoid pathway (Aza-González et al., 2011). Capsaicin is a protoalkaloid and chemically known as trans-8-methyl-N-vanillyl-6-nonenamide. It is a crystalline and an off-white color. It possesses lipophilic properties, is colorless, odorless, and melts between 62-65°C. Capsaicin structurally resembles other vanilloids due to its aromatic ring, long hydrophobic chain, and polar amide group. (Ilie et al., 2019) The structure is presented below with the head of capsaicin marked in green with the aromatic ring structure, the amid group as the neck of capsaicin in the middle and lastly the hydrophobic chain as the tail marked in orange (figure 4).

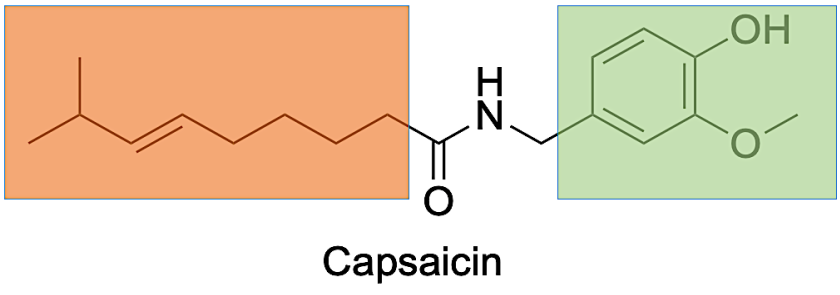

Figure 4 Capsaicin structure: the aromatic ring structure (Head) marked green, Neck in the middle and the Tail as the aliphatic side chain in orange

Upon capsaicin-mediated activation, TRPV1 allows sodium and calcium ions to flow into the cell. This influx of ions depolarizes the nociceptive neurons, causing an action potential to fire in response to the sensation of spiciness. (F. Yang & Zheng, 2017) (E. Cao et al., 2013) However according to Chen et al, 2019, the exact mechanism of pungency has not yet been perfectly explained because the pungent molecules interact very intricately with human sensory receptors such as TRPV1. Some observations are based upon sensory evaluations of pure capsaicinoids. These suggest that the vanillyl group and the length of the alkyl chain-particularly, the presence of appropriate carbon-carbon double bonds or branched methyl groups-are both important to pungency. However according to Chen et al., it is not possible to make a direct use of these findings because they are based on the action of particular chemical groups on pungency, in a quantitative prediction of pungency for related compounds.(Chen et al., 2019) Also, another factor highlights this claim; even chemically different compounds - for example drimane sesquiterpenes - are pungent (Mathie et al., 2017), whereas similarly structured capsinoids - like capsiate - are not (K. Han et al., 2013). So, specific structural features of pungent chemicals are responsible for their pungency, however they still remain unknown and therefore more studies are needed to make a conclusive statement. (Liedtke & Heller, 2007) Furthermore, understanding spiciness and also the effect of capsaicin on the human body would lead to new analgesics which target TRPV1. (E. Cao et al., 2013)

2.5. TRPV1 activation through capsaicin

Even though, TRPV1 is a polymodal receptor, it expresses remarkable sensitivity and specificity for capsaicin. Minor modifications in its chemical structure drastically reduce potency or, in most instances, turn it into an antagonist. (E. Cao et al., 2013)

Precise location of the capsaicin-binding pocket was obtained from the cryo-EM data, formed by S3 and S4 and the S4-S5 linker region within the membrane. A small electron density was observed inside the channel in the capsaicin-bound structure, providing evidence on the location of capsaicin inside the channel. Electron density in the same pocket in the closed-apo state of TRPV1 suggested occupation of this pocket by a lipid molecule. This molecule would be displaced upon activation of the receptor by capsaicin. (F. Yang et al., 2015a) Furthermore, the structural comparisons between the closed and capsaicin-bound open states revealed that capsaicin binding is associated with a slight outward motion of the S4-S5 linker. This could serve to enhance the opening of the central ion-conducting pore through interactions with the activation gate. (Liao et al., 2013)

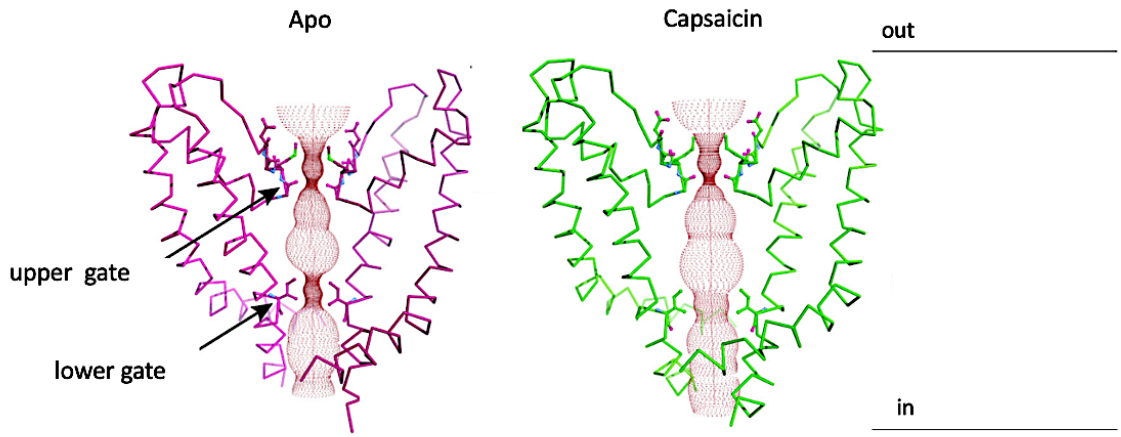

Figure 5 side by side comparison of the apo state structure and the capsaicin structure. This is shown by diagonally opposed subunits of TRPV1. Key residues in the upper gate and lower gate are highlighted to display side chain movements associated with gating adapted from (E. Cao et al., 2013).

These insights provided by the cryo-EM structure did not fully explain the orientation of the capsaicin molecule within its binding pocket or the specific interactions between capsaicin and the channel protein. One paper tried to elucidate the binding of capsaicin to TRPV1. Yang et al, 2015 addressed the linkage of the molecule and the receptor through computational docking along with functional studies. Considering the very peculiar chemical environment of the membrane, the computation- predicted a configuration that showed capsaicin adopting a "tail-up, head-down" orientation. It was suggested that its flexible tail allowed multiple conformations. This was further stabilized by van der Waals and two critical hydrogen bonds: one between the "neck" of capsaicin and residue T551 (threonine) and another between the "head" and residue E571 (glutamate). (F. Yang et al., 2015b)

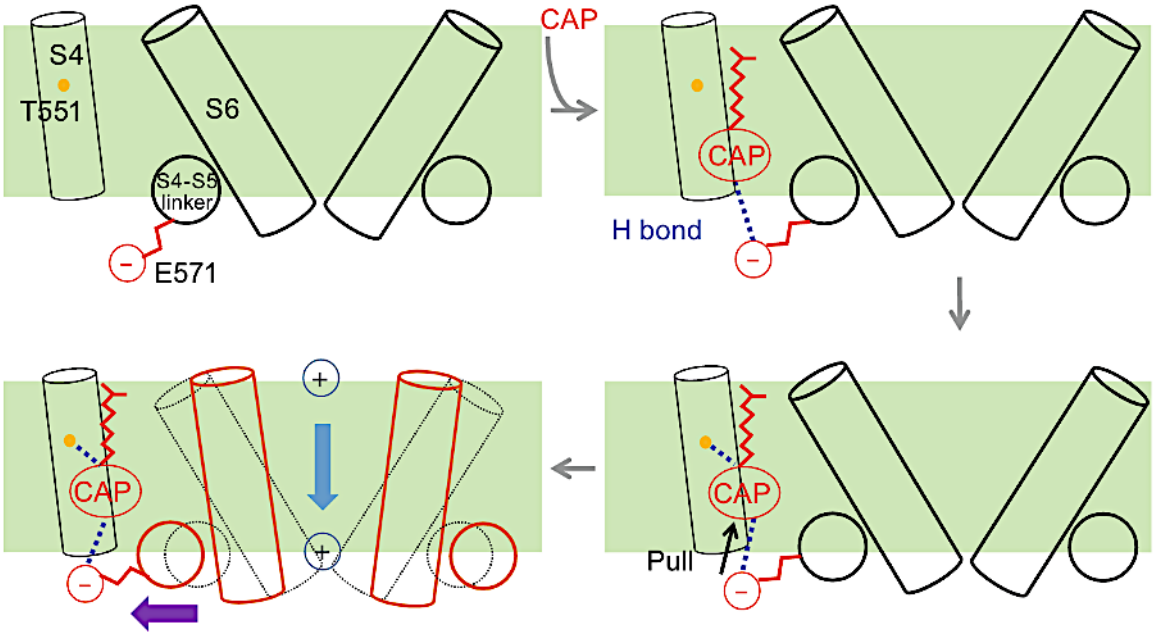

Figure 6 The diagram illustrates the binding of capsaicin and the subsequent activation of the TRPV1 channel. Highlighted are two amino acid residues, T551 which plays a key role in capsaicin binding through hydrogen bonding. (adapted from Yang & Zheng, 2017)

Furthermore Yang & Zheng, 2017 tried to back up these findings via a thermodynamic mutant cycle analysis with capsaicin analogs and TRPV1 mutants. These results confirmed the interaction between capsaicin's neck and T551 and the head with E571. Moreover, it could also be detected that the tail was critical for binding, through capsaicin analogues possessing a shortened tail. It can be said that the initial contact of capsaicin with TRPV1 is through the tail and neck, which is then followed by the formation of a hydrogen bond between the head and E571 on the S4-S5 linker. This bond is stabilizing the outward movement of the linker that underlies opening of the S6 activation gate in channel activation. (F. Yang & Zheng, 2017)

2.5.1. The structural features necessary to activate TRPV1

The general structure of a TRPV1 ligand consists of three distinct parts. The "head" which fits into the vanilloid pocket of the channel, where it establishes hydrogen bonds with four specific polar amino acid residues. The "neck" is a polar segment that further stabilizes the interaction by forming additional hydrogen bonds with nearby hydroxyl groups. Finally, the hydrophobic "tail" strengthens the ligand’s attachment by engaging in Van der Waals interactions, ensuring a firm and effective binding. (Caballero, 2022) Capsaicin represents a molecule with a vanillyl ring and an aliphatic tail that is structurally optimized to engage with the TRPV1 receptor (Ilie et al., 2019). Structural features like this contribute to capsaicin's TRPV1 activation through generation of specific electrostatic, hydrogen-bonding, steric, and hydrophobic interactions, which stabilize the receptor in an active state. These properties of capsaicin appear critical for the binding affinity and activation potency toward TRPV1. (Chen et al., 2019)

When capsaicin binds to TRPV1, it adopts a **“**tail-up, head-down” configuration which in turn enables the aliphatic tail of capsaicin to engage in these binding forms like, Van der Waals and hydrogen bond interactions (Domene et al., 2022) However, capsaicin is not unique in its pungency and activation of TRPV1. This suggests that while structural similarity can be a factor in determining a compound's interaction with TRPV1, the activation of TRPV1 is dictated by more subtle parameters than simple molecular mimicry. (Chen et al., 2019) Furthermore, there is emerging evidence that other receptors might also be involved in the mechanism of action of capsaicin and related compounds, suggesting thereby that the network of targets could be more complex than the involvement of TRPV1 alone (R. Yang et al., 2014)

2.5.2. Anti-inflammatory and barrier promoting properties of capsaicin in keratinocytes

The research on non-neuronal cells and the effect of capsaicin is rather scarce.(Guo et al., 2023) This has a few reasons. Keratinocyte research is more focused on wound healing, inflammation, and skin barrier function, areas where capsaicin's role is less defined (Bagood & Isseroff, 2021). Unlike in neurons, where capsaicin has a clear desensitizing effect, its role in keratinocytes seems more complex—it can have pro-inflammatory (Southall et al., 2003) and anti-inflammatory effects (Cervantes Recalde et al., 2024). However, therapeutic effects of capsaicin on skin diseases like

psoriasis and atopic dermatitis (Basharat et al., 2020) and the role of keratinocytes are getting more and more attention (Yamanaka et al., 2021).

Anti-inflammatory effects were described by Cervantes Recalde et al, 2024. The study concluded that the activation of the TRPV1 channel by capsaicin plays a crucial role in the skin's inflammatory response. This activation is believed to aid in restoring the skin barrier function by influencing keratinocyte behavior during inflammation. Furthermore it was reported that the capsaicin pre-treatment led to a significant reduction in the pro-inflammatory cytokine IL-8. (Cervantes Recalde et al., 2024) Furthermore, a study on rats after postoperative pain concludes that capsaicin, when administrated subcutaneously, has analgesic effects, which was attributed to the desensitization of TRPV1 in nociceptors. However, this study also showed the effect on keratinocytes because capsaicin inhibited the proliferation of these cells. Moreover, the expression of interleukin-1β (IL-1β) and TNF-α, in keratinocytes was reduced. Also suggesting that capsaicin might have an effect on the inflammatory responses and the modulation of keratinocytes. (Guo et al., 2023). Furthermore, another study demonstrated that the activation by capsaicin has been shown to elevate integrin β4 levels in murine migrating cells, thereby promoting keratinocyte migration (S. Han et al., 2018)

An indirect way to show the connection between capsaicin and inflammation is the usage of the TRPV1 antagonist capsazepine. Capsazepine was able to prevent the intracellular calcium increase and the release of pro-inflammatory mediators induced by capsaicin, thus demonstrating that through this receptor, keratinocytes may actively take part in inflammation (Ilie et al., 2019). A general structure could be established which blocks TRPV1. Antagonists of TRPV1 have a central hydrogen bond acceptor/donor motif flanked by a lipophilic side chain on one side and the other a polar aromatic group incorporating a hydrogen bond acceptor. (Szallasi et al., 2007)

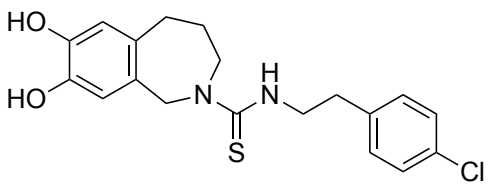

Capsazepine

Additionally, the barrier function can be affected by capsaicin in keratinocytes. One research on HaCaT skin cells demonstrated that pre-treating cells with capsaicin reduced the TNF-α (20 ng/ml) induced increase in *CLDN1* during the first 6 hours. This suggests that capsaicin may modulate the inflammatory response, potentially preventing excessive signaling that could disrupt skin barrier function. Furthermore, long term effects on tight junction proteins were suggested, due to fact that protein levels of CLDN1 in cells treated with both capsaicin and TNF-α, increased significantly, compared to cells treated with TNF-α alone. (Cervantes Recalde et al., 2024). However, Deng et al., 2019 discovered that capsaicin (100μmol/L) reduces the expression of *CLDN1* and *CLDN3 in vitro* in HaCaT keratinocytes in a dose dependent manner. They also suggested that, the reduction in *claudins* may interfere with skin barrier integrity. (Deng et al., 2019) Capsaicin was also found to

influence the cytoskeleton and tight junctions both in epithelial and endothelial cells. It has been demonstrated that it irreversibly opens tight junctions in microvascular endothelial cells and may promote increased permeability of macromolecules across the blood-brain barrier. (Kaiser et al., 2018) Capsaicin was reported to upregulate *CLDN3* in esophageal squamous cell carcinoma, which is accompanied by decreased cell migration and invasion. While this work is related to *CLDN3*, it could suggest a similar role of capsaicin in skin-related applications for other claudins such as *CLDN1*. (Feng et al., 2022) However more studies need to be conducted to further elucidate the effect of capsaicin and *CLDN1* in keratinocytes (Deng et al., 2019).

2.6. Capsiate-non pungent analogue of capsaicin

Capsiate is a non-pungent analogue of capsaicin and belongs to the capsinoid family (E.-J. Lee et al., 2010), which involves esters of vanillyl alcohol with fatty acids. Capsiate was identified in the fruits of a non-pungent *capsicum* variant, *capsicum annuum*. (Iida et al., 2003) Even though capsinoids and capsaicinoids are both featured with similar structural features, the central linkage between the two is different: ester bonds for capsinoids and amide bonds for capsaicinoids. (R. Gupta et al., 2022) (Iida et al., 2003)

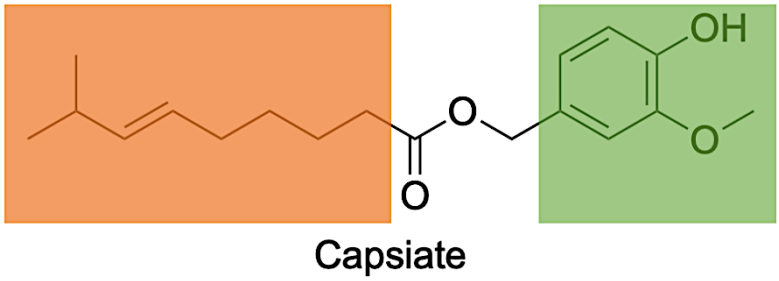

Figure 7 Capsiate structure: The aromatic ring structure (Head) marked green, Neck in the middle with the ester bond and the Tail as the aliphatic side chain in orange

Capsiate is a colorless oily liquid with a molecular formula of $C_{18}H_{26}O_4$ and a molecular weight of 306.4 g/mol (Castillo et al., 2007). Compared with capsaicin, capsiate is more lipophilic (Iida et al., 2003). Capsiate also shows cis-trans isomerism due to internal rotation hindered by a double bond in its structure.(Sancho et al., 2002) Pharmacologically, capsiate has demonstrated a wide range of activity: it increases thermogenesis and energy expenditure, reduces body weight, and exhibits antidiabetic, anticancer, analgesic, cardioprotective, and gastroprotective activity (R. Gupta et al., 2022). Unfortunately, the ester bond of capsiate and other capsinoids makes them easily hydrolyzed while passing through mucosal tissues, thereby reducing their effectiveness in stimulating TRPV1 receptors. That is also one reason why capsaicin is the most studied capsaicinoid regarding analgesic effects and inflammation. (Iida et al., 2003) However, capsiate is also an agonist like capsaicin, also inducing the nociceptive response in mice by activation of TRPV1 in a dose-dependent manner (subcutaneously). It was suggested that a topical application does not provide any significant response. Tominaga, 2005 therefore claimed that capsiate has to be directly available to the nerve endings to initiate its responses. (Tominaga, 2005) Furthermore, it was also

demonstrated in a study on mice (intraplanar injection) that capsiate had a greater efficacy compared with capsaicin in facilitating membrane transport of the analgesic drug N-ethyl lidocaine (QX-314). A combination of QX-314 with capsiate led to a more intense analgesic response than a capsaicin-QX-314 combination, suggesting that capsiate has its own self-analgesic property. (Nakagawa H and Hiura A, 2014) In another study, capsinoid derivatives differing in the C1 position acyl chains and at the C4 position alkoxy groups were studied for antinociceptive activity in mice after subcutaneous injection. The derivatives synthesized were relatively non-pungent like other capsinoids. They exhibited moderate analgesic activity pharmacologically, showing that antinociceptive efficacy decreased with the elongation of the acyl chain in the C1 position. However, the elongation of the alkoxy chain at the C4 position enhanced the activity. (He et al., 2009). Sancho et. al, 2002, also suggested that capsiate has indeed anti-inflammatory properties *in vivo* (mice) due to fact that it can suppress the NF-κB pathway (Sancho et al., 2002). In conclusion, the research is still ambiguous, and more data is needed to establish a full picture of capsiate. Furthermore homovanillic acid esters which were tested in the course of the present master thesis, have similar structures to capsiate. This suggests that they may lack the desired effect on the anti-inflammatory and barrier-promoting properties due the instability of the ester bond, preventing the interaction with TRPV1. (Iida et al., 2003) However, in this study, the compounds were not applied topically, but directly to keratinocytes cultured in low-calcium conditions, which simulate the undifferentiated basal layer of the epidermis (Arda et al., 2014). This approach was chosen to specifically examine early keratinocyte responses, as most existing studies focus on the effects of such compounds on the outer, more differentiated layers of the skin (Tominaga, 2005). As a result, relatively little is known about how capsiate or the structurally similar compounds like the homovanillic acid esters influence basal-layer keratinocytes.

2.7. Aim of the thesis

This master's thesis focuses on various homovanillic acid esters, structurally similar to capsaicin. The objective was to investigate whether these capsaicin-O analogs exhibit anti-inflammatory effects and promote skin barrier integrity. The hypothesis is that specific structural elements of the aliphatic chain in homovanillic acid esters contribute to their anti-inflammatory and barrier-enhancing properties. In skin cells, specialized ion channels known as "transient receptor potential" (TRP) channels detect harmful environmental stimuli. These channels act as sensors for thermal, chemical, mechanical, painful, and inflammatory stimuli, playing a crucial role in inflammatory responses. (Bagood & Isseroff, 2021) The involvement of TRPV1 in inflammatory responses is intricate and requires further investigation, particularly in non-neuronal cells, despite its well-documented role in pain mediation within neuronal cells (F. Yang & Zheng, 2017) because TRPV1 expression is linked to pain- and itch-related inflammatory skin diseases like psoriasis and atopic dermatitis. (C. Cao et al., 2020) Further investigation into the binding mechanisms of capsaicin with its receptor, TRPV1, has shown that factors such as electrostatic interactions, hydrogen bonding, steric hindrance, and hydrophobicity play significant roles in governing pungency. Additionally, it is acknowledged that

TRPV1 is not the sole receptor responsible for capsaicin's pungent effects. (Yang et al., 2015) Understanding these binding parameters is essential for gaining deeper insights into the interactions of capsaicin and its analogs with TRPV1, which is a central focus of this master's thesis.

To investigate the inflammatory roles of TRPV1 in epidermal keratinocytes, HaCaT cells were treated with specific agonists and antagonists. An inflammatory model was used (TNF-α), which induced the expression *of CXCL8*/*IL-8* and *CLDN1* and secretion of IL-8. Both TNF-α and IL-8 are integral to the initiation and progression of inflammatory responses, including skin inflammation, whereas *CLDN1* serves as a marker for the integrity of the skin barrier. HaCaT cells underwent treatment with the respective agonists and antagonists for 24 hours, followed by TNF-α treatment for 6 hours. RT-qPCR was used to quantify the gene expression of *CXCL8* and *CLDN1* in treated cells, and ELISA measured the secretion of IL-8 in the cell culture supernatant. Furthermore, the structure activity relationship was investigated using DataWarrior to give an overview on the different structures and their potential impact on the gene expression and IL-8 release. These findings will elucidate the role of specific structural elements of the aliphatic chain in homovanillic acid esters which contribute to their anti-inflammatory and barrier-enhancing properties.

3. Materials and Methods

3.1. Index of Materials

Table 1 List of consumables

Consumables	Producer
Disposable cannula, Sterican® Standardcannula, Gr. 2, steril	B. Braun Melsungen AG, Melsungen, DE
Disposable syringe, Injekt® Solo, sterile (2 mL)	B. Braun Melsungen AG, Melsungen, DE
Laboratory gloves, XCEED® Nitril-Schutzhandschuhe	STARLAB INTERNATIONAL GmbH, Hamburg, DE
Multichannel pipette (300 µL)	STARLAB INTERNATIONAL GmbH, Hamburg, DE
Microcentrifuge tubes, TubeOne®, RNase-free, DNase-free, DNA-free (1,5 mL)	STARLAB INTERNATIONAL GmbH, Hamburg, DE
Pasteurpipette	Carl Roth GmbH + Co. KG, Karlsruhe, DE
PCR plate, 96-Well, colorless, "Fast" Typ (Semi Sub Skirt, Low Profile, Eckschnitt A1)	Biozym Scientific GmbH, Hessisch Oldendorf, DE
PCR plate, Multiplate™ 96-Well, low profile, unskirted	Bio-Rad Laboratories, Inc., Hercules, US
Pipettetips, Filtertips, TipOne® (10 µL; 100 µL; 200 µL; 300 µL; 1000 µL)	STARLAB INTERNATIONAL GmbH, Hamburg, DE
Cloths, Kimtech® Science	Kimtech, KIMBERLY-CLARK PROFESSIONAL, Dallas, US
Reaction vessel (1,5 mL)	Carl Roth GmbH + Co. KG, Karlsruhe, DE
ROTILABO®-syringe filter, PVDF, sterile (poresize 0,22µm; Ø membrane 30mm)	Carl Roth GmbH + Co. KG, Karlsruhe, DE
Falcon tubes, steril (15 mL; 50 mL)	Sarstedt AG & Co. KG, Nümbrecht, DE
Serological pipettes, steril (5 mL; 10 mL; 25 mL; 50 mL)	Sarstedt AG & Co. KG, Nümbrecht, DE
Cell culture plates, sterile, Standard F (6-Well; 24-Well; 96-Well)	Sarstedt AG & Co. KG, Nümbrecht, DE
Cloths, Rotizell®-Tissue	Carl Roth GmbH + Co. KG, Karlsruhe, DE
Cell culture flask, steril (T75; T175)	Sarstedt AG & Co. KG, Nümbrecht, DE

Table 2 List of technical equipment and instruments

Technical equipment and instruments	Producer
C-1000 Touch ™ Thermal Cycler	Bio-Rad Laboratories, Inc., Hercules, US
CO_2 Incubator	BINDER GmbH, Tuttlingen, DE
Electric multi channel pipette, Xplorer, 8-Kanalpipette	Eppendorf AG, Hamburg, DE
PIPETBOY acu 2	INTEGRA Biosciences AG, Zizers, CH
Centrifuge 5804 R	Eppendorf AG, Hamburg, DE
Mikroliterpipette, Research plus® (0.1 – 2,5 µL; 0,5 – 10µL; 2 – 20 µL; 10 – 100 µL; 20 – 200 µL; 100 – 1000 µL)	Eppendorf AG, Hamburg, DE
Microbiological safety hood**, MSC Advantage 1.2**	Thermo Fisher Scientific Inc., Waltham, US
Microplate shaker	VWR International GmbH, Darmstadt, DE

Microscope, IT400 Trino	VWR International GmbH, Darmstadt, DE
Microvolume spectrophotometer, NanoDrop™ One/OneC Microvolume UV-Vis Spectrophotometer	Thermo Fisher Scientific Inc., Waltham, US
Microcentrifuge, Centrifuge 5418 R	Eppendorf AG, Hamburg, DE
Mikrocentrifuge, PerfectSpin Mini	**PEQLAB, VWR** International GmbH, Darmstadt, DE
Vortex	VWR International GmbH, Darmstadt, DE
Precison Balance, Entris 224I-1S	Satorius AG, Göttingen, DE
Spark® Multimode Microplatte-Reader	Tecan Group AG, Männedorf, CH
Tecan NanoQuant® plate	Tecan Group AG, Männedorf, CH
Vacuumcentrifuge, Concentrator 5301	Eppendorf AG, Hamburg, DE
Vortexer, RS-VA 10	Phoenix Instrument GmbH, Garbsen, DE
Water Treatment Plant, Reinstwassersystem, arium pro	Sartorius AG, Göttingen, DE
Waterbath, open bath steel	VWR International GmbH, Darmstadt, DE
Neubauer chamber improved (0.1mm; 0,0025 mm²)	Carl Roth GmbH + Co. KG, Karlsruhe, DE
Duranflask	Carl Roth GmbH + Co. KG, Karlsruhe, DE
Beaker	Carl Roth GmbH + Co. KG, Karlsruhe, DE

Table 3 cell line and cell culture reagents

Cell culture reagents	Producer
Capsaicin	Sigma-Aldrich, Darmstadt, DE
Capsazepine	Sigma-Aldrich, Darmstadt, DE
Dimethylsulfoxid (DMSO)	Abcam, Cambridge, UK
Dulbecco's Modified Eagle Medium (DMEM), high glucose, GlutaMAX™	Thermo Fisher Scientific Inc., Waltham, US
Erythrosin B (0.1% PBS; 0.22 µm filtriert)	Sigma-Aldrich, Darmstadt, DE
Ethanol denatured, 70%	Carl Roth GmbH + Co. KG, Karlsruhe, DE
Fetal bovine Serum (FBS)	
Filtered water	
HaCat cellline	
Keratinocyte Growth Medium 2 (0.125 ng/mL EGF; 0,004 mL/mL BPE; 0,06 mM $CaCl_2$)	PromoCell GmbH, Heidelberg, DE
Penicillin-Streptomycin, steril filtiriert (10000 Einheiten Penicillin, 10 mg/mL Streptomycin, 0,9 % NaCl)	Sigma-Aldrich, Darmstadt, DE
PBS (Phosphate-buffered saline) **Preparation:** **1710 mM NaCl (100 g/l)** **100 mM Na_2HPO_4 (14.2 g/l)** **34 mM KCl (2.5 g/l)** **18 mM KH_2PO_4 (2.4 g/l)** **10x PBS: Solve in H_2Obidest; set pH to 7.4; Fill up to 1 l with H_2Obidest; dilute to 1x PBS with H_2Obidest; autoclave, store at 4°C**	Sigma-Aldrich, Darmstadt, DE
TNF-α, recombinant human	Abcam, Cambridge, UK
TrypLE™ Express Enzym (1X), phenolrot	Thermo Fisher Scientific Inc., Waltham, US
Homovanillic acid ester	Symrise A.G.

Table 4 List of chemicals

Chemicals	Producer
Ethanol denatured, ≥ 96 %	Carl Roth GmbH + Co. KG, Karlsruhe, DE
DNase AWAY	Thermo Fisher Scientific Inc., Waltham, US
Luna® Universal qPCR Master Mix	New England Biolabs, Inc., Massachusetts, US
Nuclease-free water	Carl Roth GmbH + Co. KG, Karlsruhe, DE
RNase AWAY	Thermo Fisher Scientific Inc., Waltham, US
Thiazolyl blue **3-(4,5- dimethylthiazol-2-yl)-2,5-diphenyltetrazolium bromide** (**MTT reagent)** **(5mg/ml PBS)**	Carl Roth GmbH + Co. KG, Karlsruhe, DE
RIPA- Lysis Buffer Preparation: **10mM Tris-HCl, pH 8.0** **1mM EDTA** **0.5mM EGTA** **1% Triton X-100** **0.1% Sodium Deoxycholate (10%)** **0.1% SDS (10%)** **150mM NaCl** **Dilute with dH_2O (total volume 500 ml)**	Sigma-Aldrich, Darmstadt, DE

Table 5 List of Kits

Kits	**Producer**
Human *IL-8* ELISA Kit (ab214030)	Abcam, Cambridge, UK
LunaScriptTM RT SuperMix Kit	New England Biolabs, Inc., Massachusetts, US
Monarch® Total RNA Miniprep Kit	New England Biolabs, Inc., Massachusetts, US
Human CLDN1(Claudin 1) ELISA Kit (E-EL-H0745)	Elabscience® Bionovation Inc.
Pierce™ BCA Protein Assay Kit	Thermo Fisher Scientific Inc.

Primers

All Primers forward and reverse *(GAPDH, HRPT-1, CLDN1, CXCL8/IL-8*) were produced by Sigma-Aldrich, Darmstadt, DE

Table 6 Primer sequences

Primer	**Sequenz (5' → 3')**
GAPDH Forward Primer	AGGTCGGAGTCAACGGATTTG
GAPDH Reverse Primer	GGGGTCATTGATGGCAACAATA
HPRT1 Forward Primer	CCTGGCGTCGTGATTAGTGA
HPRT1 Reverse Primer	CGAGCAAGACGTTCAGTCCT
CXCL8/IL-8 Forward Primer	ACTGAGAGTGATTGAGAGTGGAC
CXCL8/IL-8 Reverse Primer	AACCCTCTGCACCCAGTTTTC
CLDN1 Forward Primer	TTCGTACCTGGCATTGACTGG
CLDN1 Reverse Primer	TTCGTACCTGGCATTGACTGG

Programs:
Linreg 2021.2
PRISM 9.5.1
DataWarrior v06.01.00
Chemdraw 22.2.0
Microsoft Excel 16.72
Microplate reader software (i-control™ 1.6)
BIOER Fluorescence Quantitative Detection System (V1.6.13) 2011
AI was used to rephrase some parts for a better fluency and a scientific writing style It was carefully handled and used responsibly. More details in chapter 8 “Aid Directory” of the master thesis.

3.2. Substances and Compounds

table 7 overview of the 16 homovanillic compounds (provided by Symrise) and their chemical information (Lieder et al., 2019)

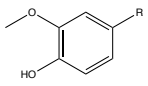

Core structure: homovanillic acid ester

Rest		Molecular formula	Molecular weight (g/mol)	sLogP
1		$C_{10}H_{12}O_4$	196.2	1.1550
2	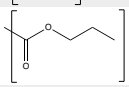	$C_{12}H_{16}O_4$	224.25	2.0157
3	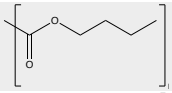	$C_{13}H_{18}O_4$	238.28	2.4701
4	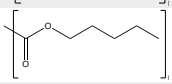	$C_{14}H_{20}O_4$	252.31	2.9245
5	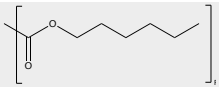	$C_{15}H_{22}O_4$	266.33	3.3789
6	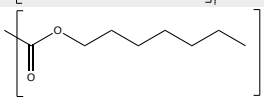	$C_{16}H_{24}O_4$	280.36	3.8333
7	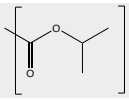	$C_{12}H_{16}O_4$	224.25	1.9206
8	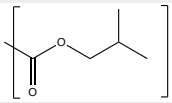	$C_{13}H_{18}O_4$	238.28	2.234
9	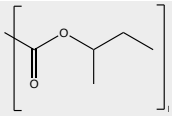	$C_{13}H_{18}O_4$	238.28	2.3750
10	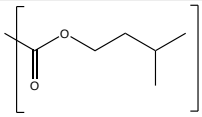	$C_{14}H_{20}O_4$	252.31	2.6884
11	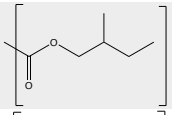	$C_{14}H_{20}O_4$	252.31	2.6884
12	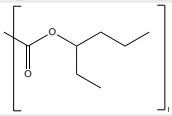	$C_{15}H_{22}O_4$	266.33	3.2838
13	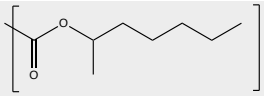	$C_{16}H_{24}O_4$	280.36	3.7382
14	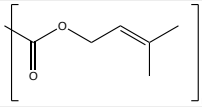	$C_{14}H_{18}O_4$	250.29	2.8243
15	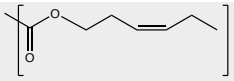	$C_{15}H_{20}O_4$	264.32	3.1267
16	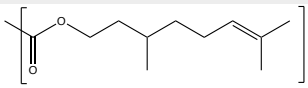	$C_{19}H_{28}O_4$	320.42	5.0656

To investigate the effects of differences in the structure of homovanillic acid esters, 16 pure homovanillic compounds, capsiate, capsaicin in a concentration of 10 µM and capsazepine (1 µM) were used for practical research. The homovanillic acid was synthesized in two steps by Symrise A.G. following Umumura et al. including the slight modifications from Lieder et al.. Guaiacol and glyoxylic acid reacted in aqueous NaOH to form mandelic acid, which was isolated via ethyl acetate extraction and distillation (yield: 50–54%). The mandelic acid was then hydrogenated using 5% palledium on carbon in acetic acid and water, followed by distillation and crystallization to yield homovanillic acid (yield: ~74%). Via an excess of the corresponding alcohol the homovanillic acid ester was formed. (Lieder et al., 2019) These substances were stored in a cool (-20°C) and dry place before usage. The compounds used, shared the same core structure and the different rests are listed in table 7.

3.3. Cell culture

HaCaT-cells were cultivated in T175 cm^2 flasks in Dulbecco`s Modified Eagle's Medium (DMEM) at 37 °C and 5 % CO_2. The medium was supplemented with 10 % fetal bovine serum (FBS) and 1 % Penicilin/Streptomycin (P/S). The final concentration of calcium in the medium was 1.8 mM and will be abbreviated hCa^{2+}-medium for simplicity and reading fluency when talking about high calcium medium. More specifically the medium contains L-alanyl-L-glutamine, sodium pyruvate (energy source), phenol red (15 mg/L) (pH indicator) and 4.5 g/L glucose (Thermofisher Scientific, 2024). Additionally, 10 % FBS was added. The serum is needed for attachment and spreading of the cells as it contains growth factors, cytokines, hormones, binding and transport proteins (Gstraunthaler & Lindl, 2021). P/S acts as an antibiotic to reduce contamination (Nygaard et al., 2015). For seeding and further experimentation Keratinocyte Growth Medium 2 (0.125 ng/mL EGF and 0.004 mg/mL BPE) was used with a calcium chloride concentration of 0.06 mM was used (Merck KGaA, 2024). The low calcium medium will be abbreviated as lCa^{2+} for simplicity.

The frozen HaCaT stocks containing 10 % DMSO were kept in liquid nitrogen (N_2). For thawing, the vials were quickly removed from the N_2 storage and thawed at 37 °C in a water bath. The cells were suspended in 9 ml DMEM medium and centrifuged at 25 °C and 120 g for 7 minutes. The medium was removed, and the cell pellet resuspended in 10 ml medium. The cell suspension was transferred to a culture flask and stored in at 37 °C and 5 % CO_2.

3.3.1. Sub-cultivation

To passage the HaCaT-cell line, first DMEM was warmed up in a water bath to 37 °C. 50 ml of hCa^{2+} Medium was prepared, adding 1 % of P/S. The used hCa^{2+} medium was aspirated from the flask with a sterile Pasteur pipette, being careful to avoid touching the cell layer. A total of 5 ml of PBS (37°C) were added to the walls of the flask, ensuring that the cells do not directly contact the PBS, removing the PBS using a Pasteur pipette. The cells were then detached from the growth surface

with TrypLE™ Express Enzyme (Wiesmann, 1999) . Adding 2.5 ml of TrypLE™ Express to the flask and distributing it evenly. TrypLE™ Express Enzyme cleaves the peptide bonds of lysine or arginine and breaks the cell-matrix connection (Wiesmann, 1999). Thereafter the flask was transferred to an incubator set at 37 °C with 5 % CO_2 for 12 minutes. After 12 minutes, the flask was removed from the incubator and firmly tapped to ensure all cells are detached. Adding 10 ml of prepared hCa^{2+} Medium to the flask to ensure that the digestion has stopped. The flask was washed thoroughly with hCa^{2+} Medium, and the cell suspension transferred to a 15 ml flacon tube. Returning the desired amount to the flask (using a new flask every fourth passage) and adding the rest of the prepared hCa^{2+} medium. The cells were incubated until 80% confluency is reached again.

3.3.1.1. Neubauer hemocytometer to determine the cell count.

To count the cells for seeding a Neubauer hemocytometer was used. The Neubauer chamber is a thick glass device with a counting grid in the center. A small amount of cell suspension was diluted 1:10 with Erytrhrosin B. The cells within the grid were counted and the mean was calculated using the following formula. (Gstraunthaler & Lindl, 2021)

$$cell\ count\ per\ ml = \frac{number\ of\ cells\ per\ square}{8} \text{ x } 10 \text{ x } 10^4$$

For clarification table 8 shows the dependency of cell density and volume of the Medium.

table 8 Dependency of cell density and volume of the Medium

Plate	Cell density per well	Surface per well [cm^2]	Medium per well [mL]
24-Well	30.000	24-Well	1
96-Well	10.000	96-Well	0.2

For counting and seeding the HaCaT-cell line, the cell suspension was first aliquoted. Making a 1:10 dilution with Erythrosin B, using 90 µl of Erythrosin B and 10 µl of cell suspension, to dye the cells. Subsequently 10 µl of the diluted suspension were pipetted on each counting surface of the Neubauer hemocytometer and the cells were counted using a microscope. To calculate the total number of cells and the counted cells were averaged. Then, the volume of the cell suspension needed for the desired treatment was calculated, suspend the determined amount of cell suspension in the appropriate volume of lCa^{2+} medium. Moreover, the cells were distributed evenly while seeding plates (96 well plate, 24 well plate). Finally, they were incubated for 4 days in an incubator set at 37 °C with 5 % CO_2.

3.4. Cytotoxicity test: MTT-Assay

The MTT test was performed to determine the cytotoxicity of the concentrations of the various substances used. Based on the reduction of the yellow, water-soluble 3-(4,5-dimethylthiazol-2-yl)-2,5-diphenyltetrazolium bromide (MTT) reagent, the cellular metabolic activity can be measured. (Stockert et al., 2018) The MTT-salt gets reduced by oxidoreductase, dehydrogenase enzymes and electron donors in viable cells. (Ghasemi et al., 2021) After decomposition of the MTT-salt a blue-violet product is formed: insoluble formazan. These formazan crystals can be dissolved in DMSO. (Stockert et al., 2018) As this reduction only takes place in metabolically active cells and the formazan crystals do not pass through the cell membrane which leads to an accumulation in the cell. The intensity of the color can be determined using a microplate reader by measuring the optical density. The absorption maximum of the formazan crystals is at a wavelength of around 570 nm. Furthermore there is a linear relationship between the level of metabolic activity and the color intensity. (Riss et al., 2004)

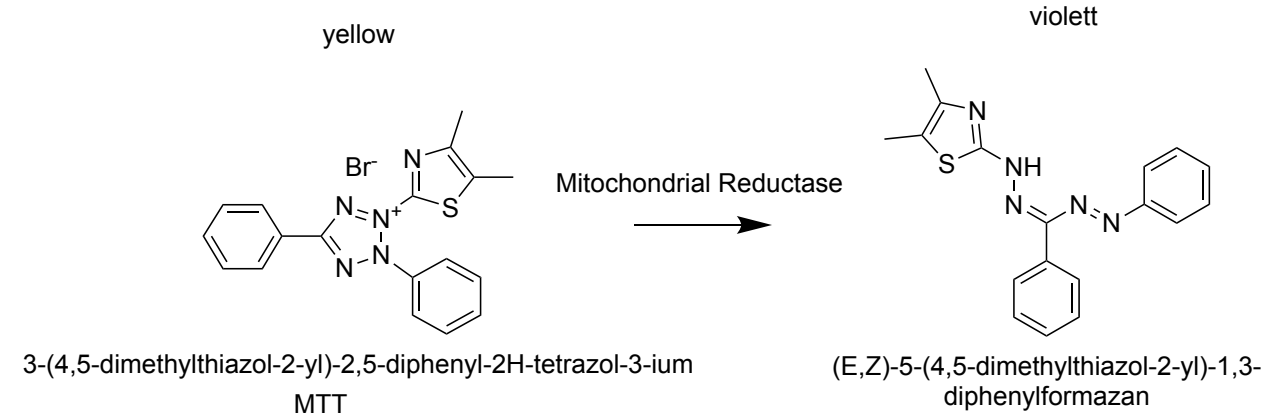

Figure 8 illustrating the MTT reaction based in the theoretical background of Ghasemi et al., 2021

In preparation of the MTT-Assay HaCaT cells were seeded in a 96-well plate under low calcium conditions. They were treated with the respective compounds at a concentration of 10 µM for 24 h or 0.1 % DMSO treatment and 0.1% ddH_2O as a control as well as capsaicin and capsiate (each 10 µM). The substances (homovanillic acid esters) were weight and dissolved in DMSO to prepare stock solutions (10 mM) for storage in a -20 °C freezer. 0.1 % dilutions of these solutions were prepared in lCa^{2+} Medium supplemented with 1 % penicillin-streptomycin (P/S). The old Medium was aspirated, and 200 µl of the prepared compound solutions were added to each well using a multichannel pipette.

For the MTT Assay, the lCa^{2+} medium was heated and supplemented with 1 % P/S (not sterile). A 1:6 dilution of the MTT stock solution was prepared with the Medium. After aspirating the old Medium, 100 µL of the prepared MTT working reagent was added into each well. The plate was then incubated for 15 minutes at 37 °C with 5 % CO_2, resulting in a color change. Subsequently, the MTT working reagent was aspirated and 150 µL of DMSO was added to each well. Optical density measurements

were obtained using a microplate reader (Spark® Tecan) at an absorption maximum of 570 nm and a reference wavelength of 650 nm.

3.5. Treatment of the HaCaT-cell line

First, the medium was prewarmed to 37°C, and the required amount for each treatment was transferred to a 50 ml Falcon tube and mixed with 0.1 % P/S. A dilution was prepared for each substance, along with 3 controls (ddH_2O with and without TNF-α and a DMSO control) to receive an end concentration of 10 µM. These dilutions were then pipetted in duplicate into a 24 well plate and incubated at 37 °C with 5 % CO_2. After 24 hours the old medium was aspirated, and the cells were treated with TNF-α (20 ng/ml). After 6 hours in the incubator at 37 °C with 5 % CO_2, the medium was decanted, and cells were lysed. The medium of the duplicates was mixed in a new 24 well plate, and 1 ml was pipetted into an Eppendorf tube and stored in a -20 °C freezer for further experiments (ELISA). The cells were mixed with 300 µl lysis buffer, and the cells were detached from the wells with the back of a tip. The 600 µl cell suspension was transferred to RNase-free Eppendorf tubes and stored at -20°C for further use (RNA isolation). To validate the previous experiments a similar treatment was performed using capsazepine (1 µM) as an antagonist of capsiate. Therefore, only selected compounds were tested also using a concentration of 10 µM with the addition of capsazepine (1 µM) using a 24 well plate. These samples were added as duplicates one with capsazepine and the other one with DMSO. Other than that, the treatment stayed the same.

3.6. RNA isolation and purification

The isolation and the purification of RNA is a crucial step in order to transcribe it into cDNA (complementary DNA) and finally to be able to analyze the respective genes. Contamination of RNase should be avoided due to the degradation of the samples. Furthermore RNA has a short half-life, therefore the RNA isolation should be well organized and stress factors such as mechanical stress, high temperature and extreme ph values avoided. (Fleige & Pfaffl, 2006)

The cells treated as previously stated (see section 3.5.) were lysed 6 hours after TNF-α treatment. For the RNA isolation the cell lysate was processed with the "Monarch® Total RNA Miniprep Kit" from New England Biolabs®. The implementation must be carried out under RNAse free conditions; therefore, all the equipment, materials and work surfaces were previously cleaned with RNase-away. Furthermore, RNAse free microreaction tubes were used and the settings for the centrifuge were as followed: room temperature (21 °C) and 16,000 x g. Under these conditions the manufactures protocol for the RNA isolation was carried out.

The cell lysate was transferred to the purification columns along with suitable collection tubes to remove gDNA and subsequent RNA elution. After centrifugation for 30 seconds, the columns were removed. The sample flow-through was mixed with an equivalent amount of ethanol (≥ 95%) by gently pipetting and the mixture was then transferred to a new column for RNA purification. Following

centrifugation for 30 seconds the flow-through was discarded. To remove any remaining gDNA, the samples were treated with RNA wash buffer (500µl), centrifuged, and the flow-through was discarded. DNase I and DNase I Reaction Buffer (ratio 1:16) and 80 µL of this mixture was applied directly to each column, followed by incubation at room temperature for 15 minutes. Next, 500 µL of Priming Buffer was pipetted onto each sample, centrifuged for 30 seconds, and the flow-through was discarded. This step was repeated with 500 µL of RNA Wash Buffer. Additionally, 500 µL of RNA Wash Buffer was pipetted onto the samples, then centrifuged for two minutes. The columns were placed on a RNase-free Eppendorf Tubes, and RNA elution was performed with 50 µL nuclease-free water. After centrifugating for 30 seconds, the samples were immediately placed on ice for further use. Next the RNA concentration as well as the quality of the RNA were determined with a Spark® Tecan microplate reader. An aliquot of the RNA of the respective sample was pipetted on a nanoquant plate. The samples were measured in duplicates and nuclease free water was used as a blank.

Wavelengths used with the Spark® Tecan were 230 nm, 260 nm, and 280 nm. Each wavelength allows for different information about the sample. Absorbance at 280 and Absorbance 230 are used for proteins as well as salts and phenol. At 260 nm nucleic acids are measured . The A260/A280 and A260/A230 ratios serve as indicators of sample purity. (Nolan et al., 2013) An A260/A280 ratio between 1.8 and 2.0 is expected for pure RNA samples, while lower values may indicate contamination, for example by proteins. The A260/A230 ratio should ideally be above 1.8; lower values can suggest residual solvents or other organic contaminants. (Arnemann, 2019)

3.7. cDNA Transcription

The conversion from RNA to the complementary DNA by reverse transcriptase is an a required step for further use in the polymerase chain reaction (Peterson & Freeman, 2009). To synthesize the cDNA the "Luna-Script RT SuperMix Kit" from New England Biolabs® was used. The reaction mixture consisted of RNA sample, the "Luna-Script RT SuperMix" and nuclease-free water. The "Luna-Script RT SuperMix" consists of a thermostable Luna Reverse Transcriptase, supporting cDNA synthesis, murine RNase inhibitor to protect the RNA from degradation, random hexamer and poly-dT primers, and blue dye as a visual indicator (New England Biolabs, 2024). The determined mean RNA concentration, divided by 500 (the required RNA in µg), yields the volume needed for the reaction mix. Subtracting 4 µl (the required volume of "Luna-Script RT SuperMix") and the volume of the RNA sample from 20 µl (total volume) leads to the amount of nuclease-free water needed. If the volume of the samples exceeded the amount required for the mixture, they were concentrated in a SpeedVac. The cDNA synthesis was then carried out in the C-1000 Touch ™ Thermal Cycler. Subsequently the synthesized cDNA was diluted 1:5 with nuclease-free water. Table 9 shows the temperature program used for the reaction:

table 9 program settings of the C-1000 Touch ™ Thermal Cycler

Cycle steps	Temperature [°C]	Time [Min]
Primer annealing	25	2
cDNA-synthesis	55	10
Enzyme deactivation	95	1
Cooling stage	4	∞

3.8. Real-time quantitative reverse transcription polymerase chain reaction

Real-time quantitative reverse transcription polymerase chain reaction (qRT-PCR) is a widely used method to identify and quantify changes in gene expression. Four main components are necessary for PCR reaction in general: primers, the DNA sample, DNA polymerase, and nucleotides. The first step of the polymerase chain reaction is the denaturation of the double-stranded DNA into two single strands at 95 °C continuing with the annealing the primers at 45-60 °C. Next, the DNA polymerase starts to synthesize the complementary DNA-Strand starting from the annealed Primer at 72 °C. This process is repeated for 40 cycles (annealing-elongation-denaturation). (Canene-Adams, 2013)

The fluorescent dye SYBR® Green was used to enable real-time quantification. It intercalates with the double-stranded DNA and emits green light after excitation proportional to the amount of double-stranded DNA in the template. The quantitative endpoint of the real-time PCR experiments occurs when the fluorescence signal exceeds a specified threshold value during the exponential phase of the cycle, known as the threshold cycle (CT). To obtain relative quantification of real-time PCR, the expression of the target gene is compared to that of the same gene in the control sample. This comparison allows for the normalization of gene expression, with *GAPDH* and *HRPT1* serving as the selected housekeeping genes (also known as reference genes) due to their constitutive expression. (Harshitha & Arunraj, 2021)

To perform real-time qPCR the following protocol was used. The diluted template cDNA, Luna Mix, primers, and nuclease-free water were thawed on ice. For housekeeping genes (*HRPT1, GAPDH*) and target genes (*CLXL8, CLDN1*), a master mix per primer was prepared for x+2 samples (usually 15 samples were treated), consisting of 11.88 µl RNase-free water, 0.66 µl primer (each forward and reverse), and 16.5 µl Luna Mix. The reaction mix was quickly vortexed and centrifuged, and then 29.7 µl were pipetted into RNase-free micro reaction tubes. 3.3 µl of cDNA template were added, along with one control per primer (Reaction Mix and nuclease-free water). The micro reaction tubes were quickly vortexed and centrifuged. 10 µl of the prepared sample mix was pipetted carefully onto a 96 well plate, which was then sealed with an adhesive film and centrifuged briefly with a plate spinner. The plate was placed into the BIOER Real time PCR instrument, and the cycling program was started. Detailed settings are provided in table 10. Since SYBR® Green is light-sensitive, all steps were performed under low light conditions.

table 10 program settings of BIOER Real Time PCR.

Cycle step	Temperatur [°C]	Time [s]	Cycles
Initiale Denaturation	95	60	1
Denaturation	95	15	40
Elongation	60	30	
Melt curve	60-95	0,3	1

3.9. Enzyme-Linked Immunosorbent Assay (ELISA)

The ELISA assay is used for quantification of target proteins in samples of cultured cells or tissue using specific antibodies. ELISA used in this master thesis was a sandwich ELISA. It was implemented to measure IL-8 in cell culture supernatants. The sandwich ELISA has a very high sensitivity due to measurement of the antigen between two layers of antibodies consisting of a capture antibody and a detection antibody. The wells are coated with the capture antibody and the sample added to the microplate, the plate gets incubated for a certain period of time (depending on the manufacturer) The unbound antibodies are removed by washing. After the washing step the detection antibodies get introduced, these antibodies are bound to an enzyme. With the addition of a substrate, the enzyme activity can be detected via a color reaction. This is proportional to the antigen present in the sample (Aydin, 2015)

The Assay „Human IL-8 ELISA Kit“ was performed according to the manufacturer's protocol (Abcam). The frozen medium supernatant was thawed, and the ELISA Kit was brought to room temperature for approximately half an hour. Samples were diluted 1:10 with “Sample Diluent NS”. For the standard curve, the IL-8 standard (“Human IL-8 Lyophilized Recombinant Protein”) was mixed with 400 µL “Sample Diluent NS” to produce a stock solution of 4000 pg/mL, gently mixed for 10 minutes on a plate shaker. A dilution series of 8 standards was prepared as shown in table 11. (Human IL-8 ELISA Kit, 2021)

*Table 11 Standard dilution for the human IL-8 ELISA (Abcam) (*Human IL-8 ELISA Kit*, 2021)*

Standard	Sample Diluent NS [µL]	Added Standard [µL]	Concentration [pg/mL]
1	375	25 stock solution	250
2	150	150 standard 1	125
3	150	150 standard 2	62,50
4	150	150 standard 3	31,25
5	150	150 standard 4	15,63
6	150	150 standard 5	7,81
7	150	150 standard 6	3,91
8 (blank)	150	-	0

The prepared standards and samples (duplicate) were applied to a "SimpleStep Pre-Coated 96-Well-Microplate", followed by the addition of a previously prepared antibody mixture (one part “Human IL-8 Capture Antibody” 10x and one part “Human IL-8 Detector Antibody” 10x diluted in eight parts “Antibody Diluent 4BI”). The plate was then incubated for 1 hour at room temperature in a microplate shaker at 400 rpm. Three washing steps were performed to remove unbound antigens and excess detection antibodies, using 350 µL wash buffer (1:10 “Wash Buffer PT” 10x and deionized water) for each wash. The plate was tapped on clean paper towels to ensure liquid removal. Subsequently, 100 µL of TMB (3,3',5,5'-tetramethylbenzidine) substrate solution (light sensitive) was pipetted into the wells, and the plate was incubated for 10 minutes on the microplate shaker at 400 rpm in the dark. The reaction was then stopped by adding 100 µLTMB stop solution per well and mixing again for 1 minute in the microplate shaker at 400 rpm, resulting in a color change from blue to yellow. Finally, the absorbance was measured at a wavelength of 450 nm. (Human IL-8 ELISA Kit, 2021)

3.10. Procedure-CLDN1 ELISA

To obtain data for CLDN1 protein abundance, a CLDN1 ELISA (Elabscience) was performed. The CLDN1 ELISA is also based on the theory of the sandwich ELISA. The Elabscience kit used has a high sensitivity (0.10 ng/ml) and high specifity (no cross reaction). The detection range lies in between of 0.16-10 ng/ml. The plate was pre-coated with an antibody specific to the human CLDN1. Subsequently, samples were added, allowing for antigen-antibody binding. Afterwards, a biotinylated detection antibody was pipetted to each well which is specific to the human CLDN1 protein and avidin-horseradish peroxidase (HRP) conjugate. Furthermore, a substrate is added to the each well to achieve an enzyme-substrate connection in order to quantify the human CLDN1 concentration through a colorimetric reaction. The intensity of the color change from blue to yellow, initiated by the addition of a stop solution, corresponded to the amount of CLDN1 detected. The absorbance is measured using the TECAN at a wavelength of 450 nm. (Elabscience, 2024)

Furthermore, all steps were similar to the once already described in chapter 3.9. Enzyme-Linked Immunosorbent Assay (ELISA), however the waiting time differed slightly. The required incubation period was 90 minutes for sample, blank and diluted standard (100 µl each). The next step consisted of using the working solution (100 µl) which needed one hour of incubation. The 350 mL wash buffer was added into each well, rinsed and repeated for three times. Afterwards the HRP working solution (100 µl) was added and the plate incubated for 30 minutes. Another wash process was performed again, 3 repetitions were used. Furthermore 90 µl of substrate reagent were added to the wells and incubated for 15 minutes under light protection. Lastly 50 µl of stop solution was added. All the incubation were performed at 37°C. (Elabscience, 2024) In order to so, the cells were treated the same as described in section 3.5.

Reagents and the dilution were prepared as described in the next paragraph following the Elabscience protocol. The wash buffer was prepared by diluting 1.3 mL of concentrated wash buffer with 28.8 mL of deionized or distilled water. To prepare the standard working solution, the standard was centrifuged at 16.900 g for 1 minute. Subsequently, 1.0 mL of the reference standard & sample diluent was added to the standard, allowing it to stand for 10 minutes while gently inverting it several times to ensure complete dissolution. Leading to a working solution with a concentration of 10 ng/mL. (Elabscience, 2024)

Serial dilutions were then performed as required, with recommended dilutions ranging from 10 ng/mL to 0 ng/mL. For dilution, 500 µL of reference standard & sample diluent was added to each of 7 microreaction tubes. Subsequently, 500 µL of the 10 ng/mL working solution was pipetted into the first tube and mixed thoroughly to obtain a 5 ng/mL working solution. This process was repeated by transferring 500 µL of solution from the previous tube to the next tube until the desired dilutions of 5 ng/mL, 2.5 ng/mL, and 0.16 ng/mL were achieved. In preparation of the biotinylated detection antibody working solution, 30 µl of concentrated detection antibody was combined with 2970 µl of diluent to receive a total volume of 3 mL, similar to the procedure for performed for the HRP conjugate working solution. (Elabscience, 2024)

Three samples were tested using different ratios, undiluted, 1:10, 1:100 and 1:1000. However, even undiluted samples exhibited absorbance levels similar to the blank (0 ng/ml to 0.16 ng/ml CLDN1 concentration).

3.10.1. BCA-Assay

Thereafter a BCA Assay was performed to quantify the protein content. The Assay was produced by thermoscientific (Pierce™ BCA Protein Assay Kit). To perform the protein quantification 9 standards were mixed in the following concentrations. (table 12) (thermoscientific, 2024).

table 12 BCA standard dilution

Vial	Volume of Diluent [µl]	Volume and Source of BCA [µl]	Final BCA concentration [µg/mL]
1	0	300 of Stock	2000
2	125	375 of Stock	1500
3	325	325 of Stock	1000
4	175	175 of vial 2	750
5	325	325 of vial 3	500
6	325	325 of vial 5	250
7	325	325 of vial 6	125
8	400	100 of vial 7	25
9	400	0	0

3.10.2. Lysis protocol

Two different lysis protocols were tested to see which one leads to a higher total protein concentration. A RIPA-Buffer (composition see chapter 3.1) was produced to lyse the cells and for the second treatment a cryogenic procedure was performed. Additionally, two replicates of each treatment were utilized. Subsequently, the absorbance was measured using the TECAN instrument to calculate the protein content. The decision to use the cryogenic method was based on its better outcomes. Further details regarding this step are provided in the following paragraph.

The collected samples underwent 3 freeze thaw steps. First of all, the sample was collected using 200 µl of PBS and scrabbing the cells of using a cell scrapper. Thereafter another 100 µl were used to rinse the well and the cell scrapper off any remaining cells. Then the cells were collected in a RNA-free micro reaction tube. The samples were prepared in duplicates therefore a total of 600 µl was collected per sample. The samples were than immediately frozen using liquid nitrogen. After that the samples were immediately defrosted in a water bath (37 °C) for approximately 3 minutes and the cell suspension was vortexed for 30 seconds to achieve a full freeze-thaw circle. These steps were repeated 3 times to ensure the complete destruction of the cell wall and therefore making it possible to measure the total protein. Moreover, the samples were centrifuged for 10 minutes at 1500 g (4 °C), and the supernatant collected to carry out the assay. The samples were stored in a freezer at -20 °C. (adapted from Overview of Cell Lysis and Protein Extraction- Thermofisher Scientific, 2025 with the help of Markus Rechl and María Fernanda Cervantes Recalde)

3.11. Structure Activity Relationship (SAR)

The structure-activity relationship provides information about the connection between the chemical structure and the biological activity. The biological effect can often be estimated from the molecular structure by using data of similar substances. (Polishchuk, 2017). The Simplified Molecular Input Line Entry System (SMILES) formula for all homovanillic acid esters tested were provided by Dr. Joachim Hans (Symrise A.G.). The SMILES formulas were introduced in Data Warrior for visualization. DataWarrior is a cheminformatics software for visualizing, analyzing, and manipulating chemical data. It provides a range of capabilities tailored for chemical data exploration and analysis (Sander et al., 2015). The structure of the 16 substances as well as the gene expression data and IL-8 release data were linked and a correlation between them was concluded. In order to so, the compounds are separated into three groups: length, ramification and double bonds. First each group was analyzed separately, and an overall conclusion was drawn about the activity. Subsequently, the fold change was calculated, using the outcome of the reaction, and dividing it with the experimental data of one of the characteristics (*CXCL8/IL-8*, *CLDN1* gene expression or IL-8 release).

3.12. Data analysis and Statistics

To evaluate the MTT test, the raw data was first blank corrected. Then the data was compared to the ddH_2O control. Outlier detection was performed using the Nalimov test at a significance level of $\alpha = 0.05$ (Rechenberg, 1982). Data points exceeding the critical value were considered statistically significant outliers and excluded from further analysis. The values are presented as percentage change to the ddH_2O control. Compound concentrations that lead to values under 70 % of the cell viability in the MTT cytotoxicity experiment were seen as toxic (ISO 10993-5, 2009).

For the analysis of the RT-qPCR, the amplification data was assessed and processed using the LinRegPCR software (version 2021.2) The initial concentration of the samples (N0), the baseline and the efficiency outliers were identified. After exporting the data, additional analyses were conducted using the determined N0 values. Initially the reference genes *GAPDH* and *HRPT1* outliers were identified. To determine the x-fold change in gene expression in respect to the mean value of the corresponding control, N0 values of a sample's triplicate were first normalized to the mean value of the corresponding sample. For every gene, the mean and the standard deviation of all samples in a treatment were calculated. The geometric mean of the reference genes in the relevant samples was used to standardize the N0 values of the corresponding sample repeats of the examined genes (*CXCL8, CLDN1*). Next, the x-fold change in gene expression was calculated as a function of the associated control's mean value. The sample means and standard deviations were calculated. The NALIMOV test was used to find outliers, which were then eliminated from the analysis ($\alpha = 0.05$).

To evaluate the ELISA data the Kit's protocol standard curve was applied (see material list). Therefore, the absorbance of the measured standards was put in context with the concentration. Subsequently a calibration curve was made using Microsoft Excel. Thereafter the concentrations of

the samples could by calculated using the formula: $y = kx + d$. Beforehand the absorbance was blank corrected compared to the control and outliers were excluded.

All experiments during this thesis were performed in 4-5 independent biological replicates and 2-4 technical replicates. The data is shown as mean ± standard deviation (SD) and complete statistical analysis was performed with PRISM 9 version 9.5.1. For every data set, a normality and lognormality test was performed using a Shapiro-Wilk-Test. Statistical significances among the compounds test concentrations and the control were determined using parametric statistical tests such as one-way ANOVA assuming an equal SD. If no equal SD could be established the Brown-Forsythe and Welch ANOVA test together with the Dunnett's T3 multiple comparisons *post hoc* test was applied. Furthermore, a student's t-test was used to calculate the significant difference of two variables. Significant difference is shown with p-values smaller than 0.05 according to the statistical standard. To investigate the correlation between the three different parameters *CXCL8* gene expression *CLDN1* gene expression and IL-8 release a Bravais-Pearson analysis was performed using DataWarrior.

4. Results

4.1. Cell viability

The aim of the present thesis was to investigate the relationship of different structural components in homovanillic acid esters and the *CLDN1* gene expression as well as the *CXCL8*/*IL-8* expression and the IL-8 release. A HaCaT cell model was used, and inflammation was simulated by treating the cells with TNF-α (20 ng/ml) for 6 hours. The cells underwent a 24-hour pre-treatment with compounds 1-16 (10 µM), as well as capsaicin (10 µM) or capsiate (10 µM). 0.1 % DMSO served as the control for the pre-treatment. For clarity, the control is depicted as a dotted line (figure 9, figure 12, figure 13, figure 14, figure 15), while the bars represent the corresponding values for each treatment. The structural groups of compounds 1-16 are categorized into three groups: compounds with varying carbon chain lengths are shaded in grey, branched compounds are shaded in black, and those with double bonds are depicted in light grey. Whereas capsaicin and capsiate are depicted in a white/dotted manner. This categorization applies consistently across all subsequent graphs. To evaluate the metabolic activity of HaCaT cells, the MTT assay was performed. This assay helps to determine the potential cytotoxicity of the homovanillic compounds, thereby excluding adverse effects on cell viability in future experiments. The controls, along with capsaicin (CAP) and capsiate (CTE), were used at the same final concentration (figure 9).

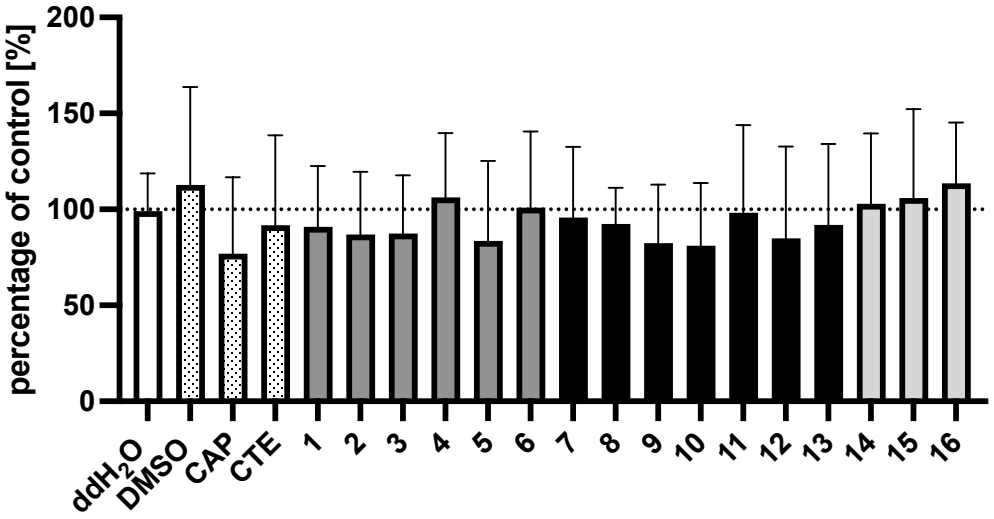

Figure 9 MTT-Assay to determine the cell-viability. HaCaT-cells were treated for 24 h with 10 µM homovanillic acid esters. Cell viability presented as percentage of the control ddH_2O.Statistics: mean ± SD, 4 technical replicates and 5 biological replicates were applied. Statistical significances were established by a Brown-Forsythe and Welch ANOVA test with Dunnett's T3 multiple comparisons post hoc test to determine differences between the samples and the control.

The concentration of 10 µM was chosen due to previous experiments form the Department of Physiological Chemistry (Cervantes Recalde et al., 2024) leading to the results that a concentration of 10 µM of capsaicin did not decrease the cell viability. Similar concentrations were also used in other studies while using HaCaT-cells. (Y. M. Lee et al., 2009; Li et al., 2007). The cell viability of capsazepine was also based on a previous study of the department which suggested that 10 µM capsazepine leads to decrease of cell viability therefore capsazepine was used at a concentration of 1 µM (Cervantes Recalde et al., 2024). Capsiate was used at a concentration of 10 µM which did

not lead to a decrease of cell viability. No significant decrease or increase in cell viability was observed after 24-hour treatment of HaCaT cells with 10 µM of compounds 1-16. Across all treatments, the average cell viability was between 81.14 % and 113.66%. The cut point value being 70 %, indicating cytotoxic effects according to ISO 10993-5, 2009. Therefore, no adverse effects on the cell viability are seen after a 24h treatment of HaCaT cells with the tested compounds.

4.2. CLDN1 protein ELISA

To determine whether the increase in *CLDN1* expression translated into elevated CLDN1 protein levels within the cells, a CLDN1 ELISA was employed. This assay quantitatively measures human claudin-1 concentration. Despite the high total protein concentration in the samples, the CLDN1 protein could not be effectively quantified with the use of the selected kit, because the absorbance of the sample was below the detection limit of the lowest standard concentration (0.16 ng/ml) (Elabscience, 2024). The absorbance values for the standards, control, and **R16**, along with their corresponding concentrations (ng/ml), are presented in table 13.

Table 13 depicts the standard curve (concentration and Absorbance) (one replicate) and the mean value of the DMSO-control and R16 Absorbance (2 replicates undiluted)

	Concentration [ng/ml]	**Absorbance**
S1	5	1.4461
S2	2.5	0.9454
S3	0.16	0.149
Blank	0	0.0792
DMSO-Control		0.10925
R16		0.09605

The absorbance value of **R16** falls between the blank and the lowest standard concentration. Specifically, the absorbance of the sample was measured at 0.096 Abs., which is below the lowest standard value of 0.149 Abs.. This suggests that the expression of claudin-1 protein in the treated cells is significantly reduced, implying that CLDN1 protein levels in the sample were lower than the limit of detection. Further concentration of the samples was not performed due to time constraints, and the experiment was not repeated with adjusted conditions.

4.3. *CXCL8*/ *IL-8* and *CLDN1* Gene Expression as well as IL-8 Release

The RT-qPCR and ELISA data are presented following the treatment of HaCaT cells for 24 hours with 10 µM homovanillic acid esters, followed by an additional 6-hour TNF-α (20ng/ml) treatment. The fold change in the presented data is relative to the solvent control (0.1% DMSO and TNF-α). These experiments aimed to identify and quantify alterations in the gene expression of *CXCL8* and *CLDN1*, as well as IL-8 release, with a particular focus on the interaction between IL-8 release and *CLDN1* gene expression in keratinocytes treated with homovanillic acid esters. The table below presents the chemical structures relevant to this chapter, providing a readily accessible reference to support clarity and facilitate interpretation of the following findings.

Table 14 Structures of the relevant homovanillic acid esters

Homovanillic acid ester	Structure
R10	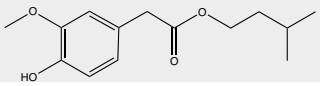
R3	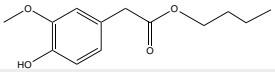
R5	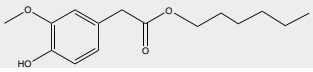
R7	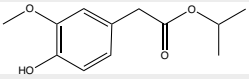
R12	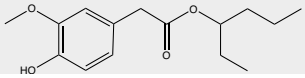
R15	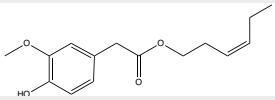
R16	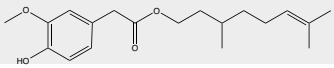

The subsequent graphs depict the *CXCL8* gene expression, with homovanillic acid esters displayed separately from the controls in the diagrams. The effects of the compounds on *CXCL8* gene expression were compared to the DMSO and TNF-α control groups, and the results are shown as fold changes relative to the control.

Figure 10 illustrates the results of the *IL-8*/*CXCL8* expression measured by RT-qPCR. Observations of capsaicin and capsiate showed no statistically significant changes. Similarly, compounds in the "no ramification" and "double bond" groups exhibited no significant differences in *CXCL8* expression compared to the control. However, one compound in the "ramification" group demonstrated a significant difference from the control. **R10**, characterized by branching, notably affects *CXCL8* gene expression in HaCaT cells. This homovanillic acid ester exhibited a fold change of 2.99 ± 1.58 after a 24-hour pretreatment followed by a 6-hour TNF-α treatment. In contrast, all other homovanillic acid esters showed no significant changes.

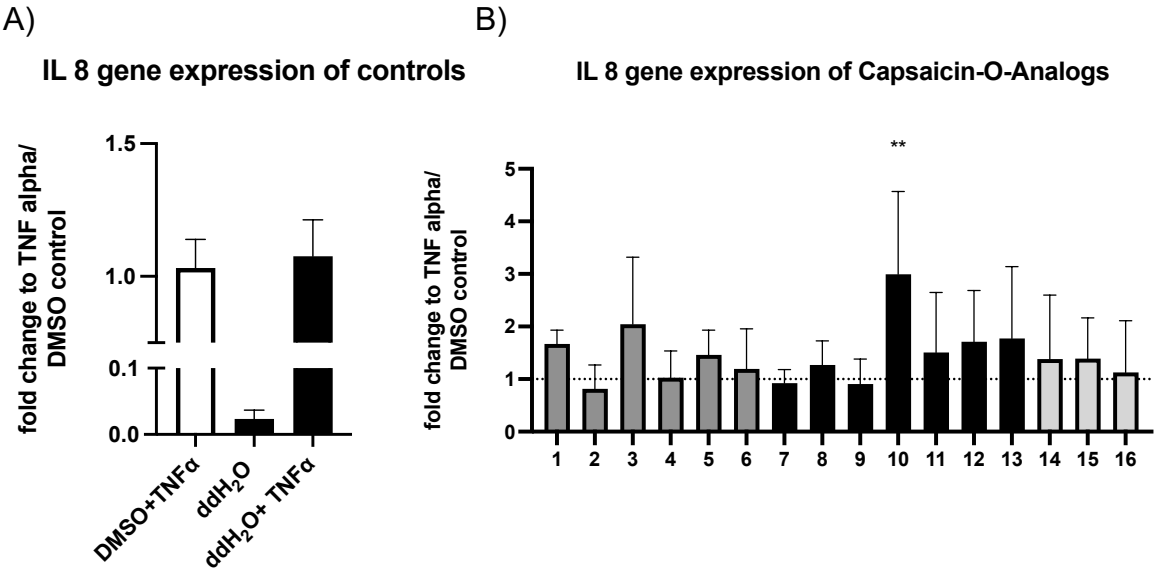

*Figure 10 24 h treatment of 10 µM homovanillic acid esters before the incubation with 20 ng/ml TNF-α for 6 h. IL 8 gene expression presented as fold change of the control (0.1 % DMSO). Statistics: mean ± SD,3 technical replicates and 5 biological replicates were applied Statistical significances were established by a Brown-Forsythe and Welch ANOVA to determine differences between the samples and the DMSO control (**p<0.01 and ****p<0.0001). GREY: no ramifications, BLACK: ramifications, LIGHT GREY: double bonds.*

The results of the *CLDN1* gene expression follows a trend that the length of the carbon chain plays an important role on the impact of inflammation and the barrier integrity in keratinocytes (see section 2.5.). These results are depicted in the diagrams (figure 11) below. High significance can be observed for **R3** and **R5**, with a carbon sight chain of four and six carbons. These two homovanillic compounds express a fold change of 2.42 ± 1.07 and 2.06 ± 0.32 Branching also seems to be important for the *CLDN1* gene expression this is especially true for **R7, R10** and **R12** . Here a fold change of 0.62 ± 0.21 for **R7**, 2.16± 0.80 for **R10** and 1.69 ± 0.67 for **R12** can be observed. The significant effect of substance **15** on the *CLDN1* gene expression would be a combination of the two characteristics length and double bond, with a carbon side chain of six carbons and a double bond at the gamma carbon. The fold change of R15 being 2.26 ± 0.89.

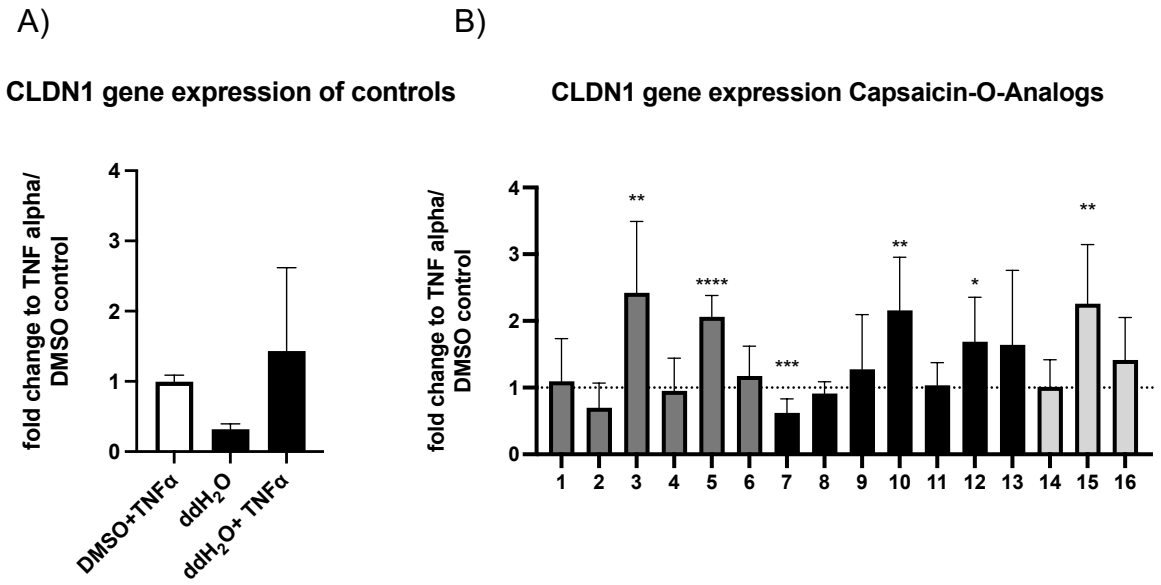

*Figure 11 24 h treatment of 10 µM homovanillic acid esters before the incubation with 20 ng/ml TNF-α for 6 h. CLDN 1 gene expression presented as fold change of the control (0.1 % DMSO). Statistics: mean ± SD, 3 technical replicates and 5 biological replicates were applied. Statistical significances were established by a Brown-Forsythe and Welch ANOVA to determine differences between the samples and the DMSO control (*p<0.05, **p<0.01 ***p<0.001 and ****p<0.0001)). GREY: no ramifications, BLACK: ramifications, LIGHT GREY: double bonds.*

R5, R15 and **R16** do follow this observation. The structure of the compound's rest can be described as followed: **R5** is part of the "no ramification group" whereas **R15** and **R16** are part of the "double bond group". CTE (1.30 ± 0.16), **R5** (0.71± 0.19) and **R16** (0.59 ± 0.20) even show a significant decrease in the IL-8 release. No significance was noted for the other compounds tested (figure 12)

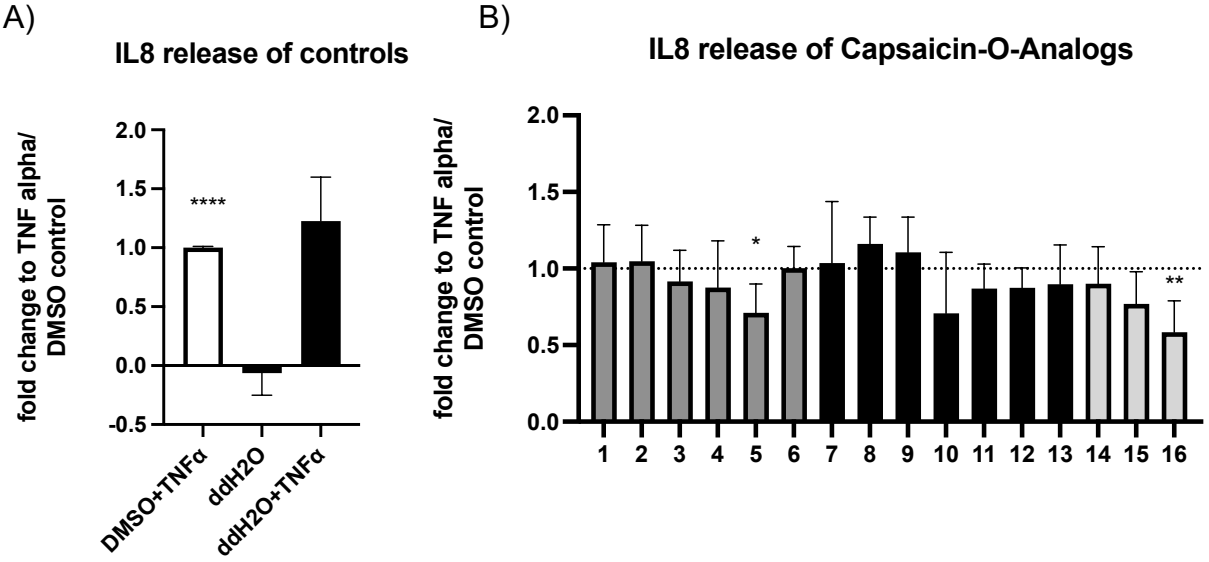

*Figure 12 24 h treatment of 10 µM homovanillic acid esters before the incubation with 20 ng/ml TNF-α for 6 h. IL 8 release presented as fold change of the control (0.1 % DMSO). Statistics: mean ± SD, 2 technical replicates and 5 biological replicates were applied. Statistical significances were established by an Ordinary one-Way Anova to determine differences between the samples and the control (*p<0.05, **p<0.01 and ****p<0.0001).*

After analyzing the data of the 16 compounds of interest, three compounds were selected based on their *CLDN1* increase compared to the control and the subsequent decrease in the IL-8 release. These three compounds are **R5**, **R15**, and **R16**. *CLDN1* gene expression was increased during the treatment with **R5** and **R15** whereas **R16** didn't show any significance. The *CXCL8* gene expression for all three compounds didn't show any significant effect. However, homovanillic acid ester **R5** exhibits a fold change of 0.71 ± 0.19, **R15** shows a fold change of 0.77 ± 0.2105 and **R16** a fold change of 0.59 ± 0.20 in the IL-8 release experiment. All three have a specific number of carbons, starting from six carbons in the aliphatic side chain (R**5,R15**) and going up to eight carbons (R**16**). **R15** also exhibits a double bond at the gamma carbon, **R16** at the êta position of the carbon chain. Especially these compounds are structurally the most similar to capsaicin. Figure 13 gives a good overview of the explained results. Here, only the three selected compounds are depicted, showing their impact on the gene expressions and the IL-8 release.

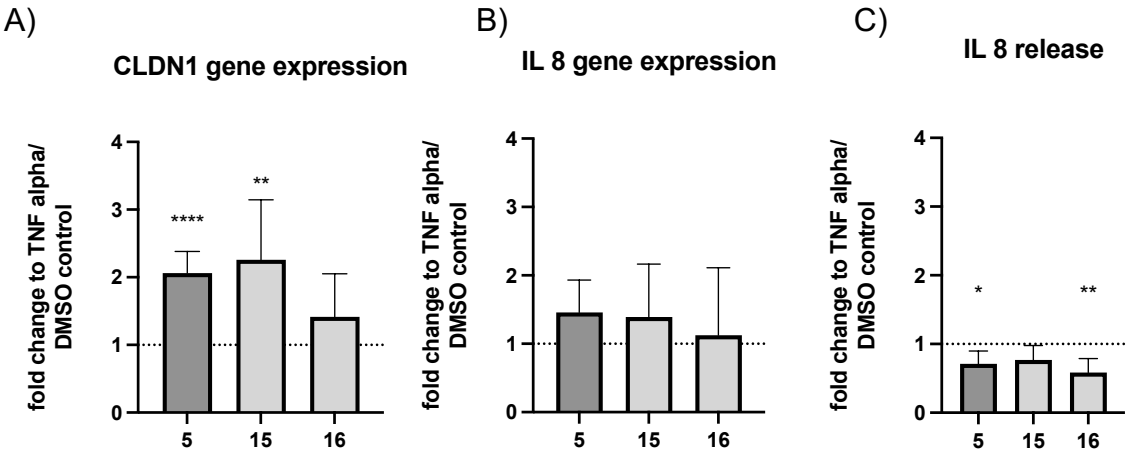

*Figure 13: 24 h treatment of 10 µM homovanillic acid esters before the incubation with 20 ng/ml TNF-α for 6 h. IL 8 and CLDN1 gene expression presented as fold change of the control (0.1 % DMSO). (a) Statistics: mean ± SD, 3 technical replicates and 5 biological replicates were applied Statistical significances were established by a Brown-Forsythe and Welch ANOVA to determine differences between the samples and the DMSO control (**p<0.01 and ****p<0.0001). (b) Statistics: mean ± SD, 2 technical replicates and 5 biological replicates were applied. Statistical significances were established by an Ordinary One-Way Anova to determine differences between the samples and the control (*p<0.05, **p<0.01). (c)*

4.4. Evaluation of TRPV1 channel involvement of compounds 5,15 and 16

Additional experiments using capsazepine (1 µM), a TRPV1 antagonist (Gonzalez-Reyes et al., 2013; Ilie et al., 2019), were conducted to determine whether the effects of homovanillic compounds (R5, R15, and R16) on *CLDN1* and *CXCL8* gene expression and IL-8 release involve TRPV1 activation. Capsiate, a non-pungent capsaicin analog with reduced anti-inflammatory efficacy due to its unstable ester bond (Iida et al., 2003), was included as a control. TRPV1 is known to modulate inflammation and barrier function (Nguyen & Soulika, 2019; Gupta et al., 2022; Chen et al., 2019).

In this experiment, two groups were compared to analyze the involvement of TRPV1. Both groups were treated with the specific compound; however, one group additionally received capsazepine (1 µM). The group (not treated with CAPSZ) was normalized to a baseline value of 1. The effects of capsiate are shown in figures 14A, 14B, and 14C, representing *CXCL8* gene expression, *CLDN1* gene expression, and IL-8 protein release, respectively. Notably, a statistically significant difference compared to the control was observed only for IL-8 release, with a modest fold change of 1.10 ± 0.13. This slight increase does not reflect an inhibitory effect of capsazepine. (figure 14)

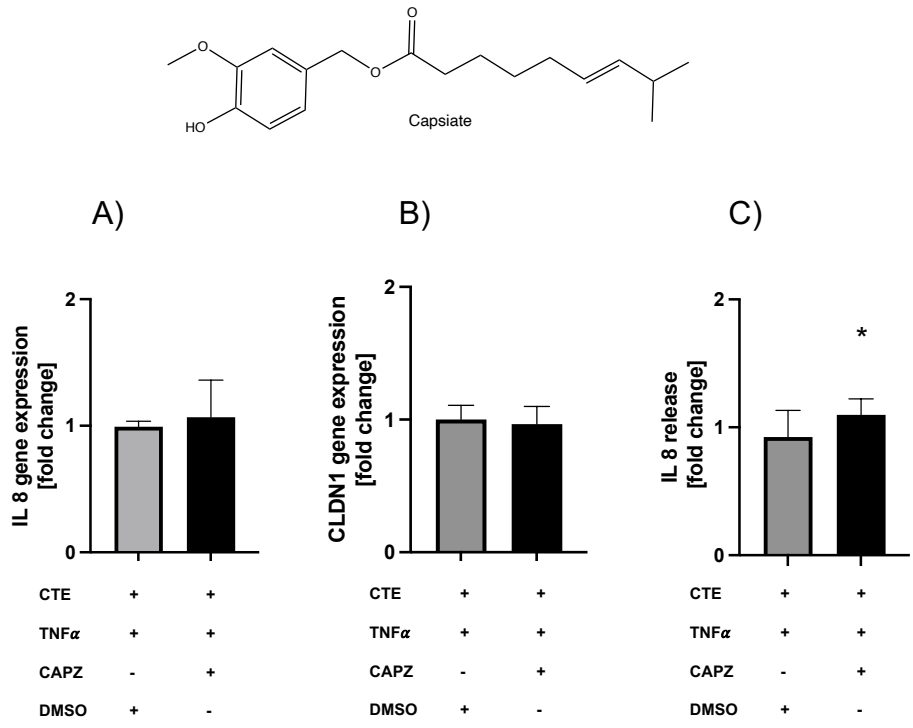

*Figure 14 HaCaT cells pretreated with 10 µM homovanillic acid esters and 1µM capsazepine for 24 h before the incubation with 20 ng/ml TNF-α for 6 h showing the structure of capsiate. Data is presented as comparison between the treatment with and without capsazepine. IL-8/CXCL8 gene expression (a) CLDN1 (b) Statistics: mean ± SD, 3 technical replicates and 4 biological replicates were applied. IL 8 release (c) Statistics: mean ± SD, 2 technical replicates and 3 biological replicates were applied. Statistical significances were established by an unpaired t-Test. (*p< 0.5).*

R5 exhibits notable effects on the gene expression of both genes (*CLDN1* and *CXCL8*) when comparing results with and without the addition of capsazepine. (figure 15). Since both capsazepine and the compounds under investigation are presumed to interact with TRPV1, the possibility that R5 may also influence this channel cannot be excluded, although involvement of additional pathways cannot be ruled out. Upon co-treatment with capsazepine, *CXCL8* gene expression showed a fold change of 0.84 ± 0.13 (figure 15A), and *CLDN1* gene expression was 1.33 ± 0.54 (figure 15B) The subsequent data also revealed no significant impact on IL-8 release (figure 15C) only an effect on the protein of tight junctions and a decrease in the *CXCL8* gene expression was observed.

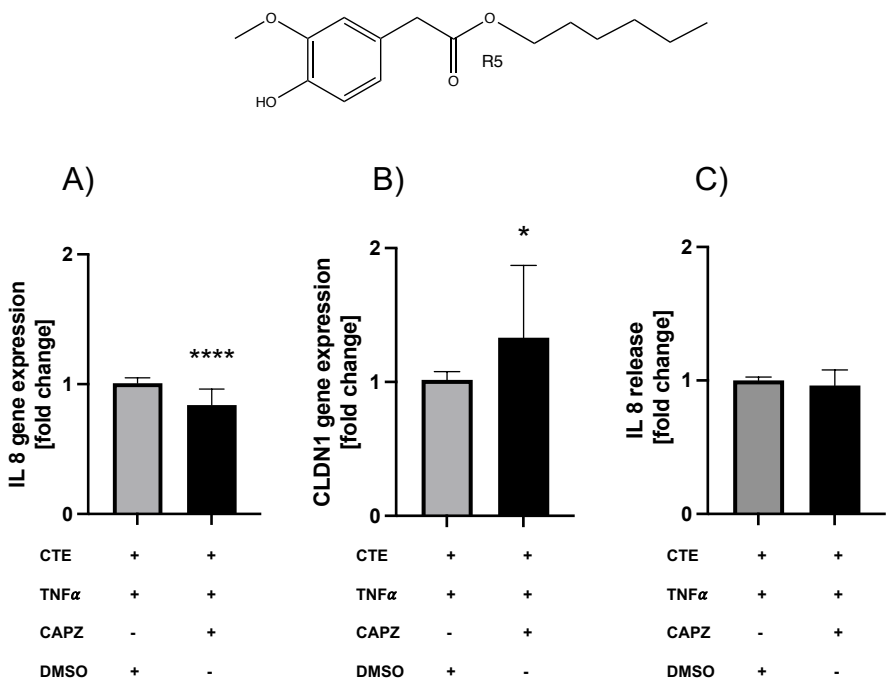

*Figure 15 HaCaT cells pretreated with 10 µM homovanillic acid esters and 1 µM capsazepine for 24 h before the incubation with 20 ng/ml TNF-α for 6 h showing the structure of R5. Data is presented as comparison between the treatment with and without capsazepine. IL-8/CXCL8 gene expression (a) CLDN1 (b) Statistics: mean ± SD, 3 technical replicates and 4 biological replicates were applied. IL 8 release (c) Statistics: mean ± SD, 2 technical replicates and 3 biological replicates were applied. Statistical significances were established by an unpaired t-Test. (*p< 0.5 ****p<0.0001).*

Analysis of the R15 data revealed a significant difference in *CLDN1* gene expression upon co-treatment with capsazepine, with a fold change of 1.30 ± 0.18 compared to keratinocytes treated with R15 alone (Figure 16B). No significant changes were observed in *CXCL8* gene expression (Figure 16A) or in IL-8 protein release (Figure 16C). While R15 and capsazepine may both interact with TRPV1, the data do not provide direct evidence that R15 acts specifically through this channel.

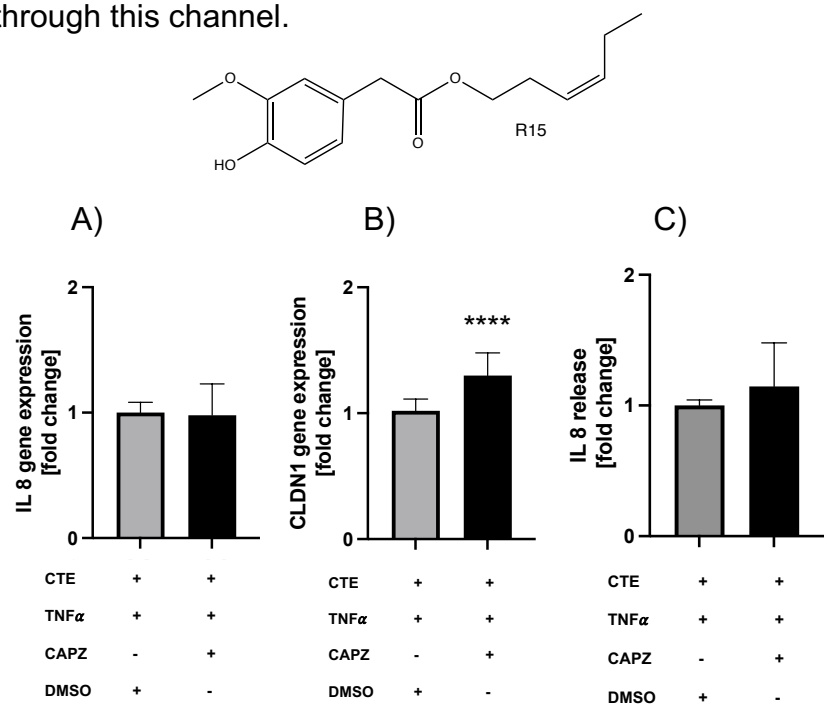

*Figure 16 HaCaT cells pretreated with 10 µM homovanillic acid esters and 1µM capsazepine for 24 h before the incubation with 20 ng/ml TNF-α for 6 h showing the structure of R15. Data is presented as comparison between the treatment with and without capsazepine.IL-8/ CXCL8 gene expression (a) CLDN1 (b) Statistics: mean ± SD, 3 technical replicates and 4 biological replicates were applied. IL 8 release (c) Statistics: mean ± SD, 2 technical replicates and 3 biological replicates were applied. Statistical significances were established by an unpaired t-Test. (****p<0.0001).*

Regarding **R16** only the *CXCL8* gene expression was significantly affected with a fold change of 0.90 ± 0.10, leading to a downregulation of the gene. The *CLDN1* gene expression as well as the IL-8 release, during this experiment, does not seem to be affected by **R16**.

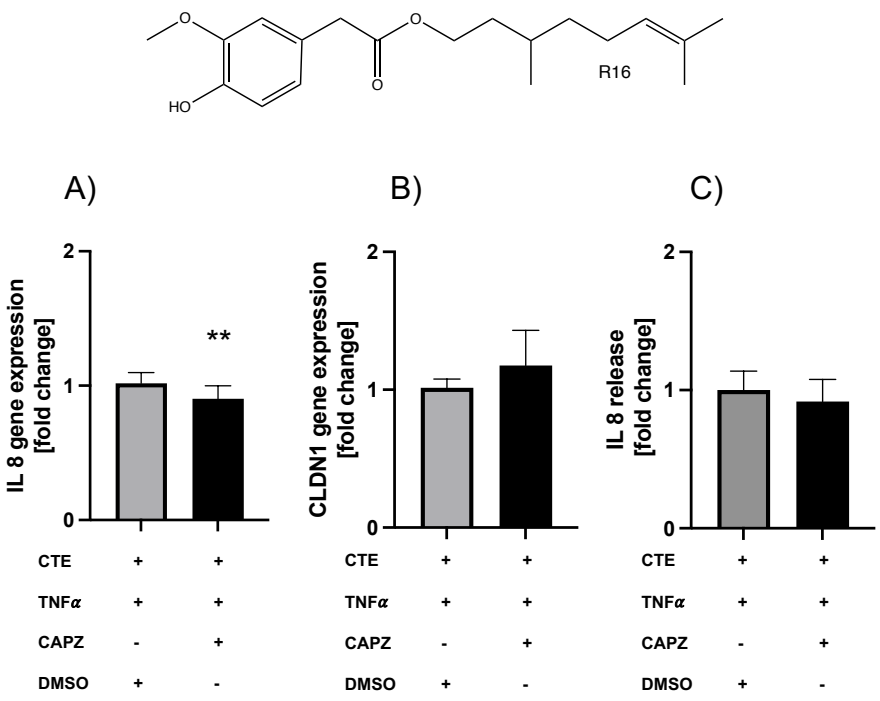

*Figure 17 HaCaT cells pretreated with 10 µM homovanillic acid esters and 1 µM capsazepine for 24 h before the incubation with 20 ng/ml TNF-α for 6 h showing the structure of R16. .Data is presented as comparison between the treatment with and without capsazepine. IL-8/ CXCL8 gene expression (a) CLDN1 (b) Statistics: mean ± SD, 3 technical replicates and 4 biological replicates were applied. IL 8 release (c) Statistics: mean ± SD, 2 technical replicates and 3 biological replicates were applied. Statistical significances were established by an unpaired t-Test. (**p<0.01).*

4.5. Structure -activity relationship (SAR) analysis

To investigate whether characteristic features of the homovanillic acid ester structure influence the differential gene expression of *CXCL8* and *CLDN1*, as well as IL-8 protein release, a structure-activity relationship (SAR) analysis was conducted. This analysis was based on the results of a 24-hour treatment with homovanillic acid esters (10 µM) followed by a 6-hour stimulation with TNF-α (20 ng/ml). The structural features of the 16 tested compounds were linked to their respective gene expression and IL-8 release data, allowing to identify potential relationships. Each compound group was analyzed independently, and overarching conclusions were subsequently drawn regarding their bioactivity. This data analysis aims to pinpoint key structural elements in homovanillic acid esters that could affect inflammation and barrier integrity of keratinocytes when used at a concentration of 10 µM. Using DataWarrior, variations in biological activity were evaluated in relation to the structural differences of the compounds. Notably, a significant negative correlation (r = -0.527) was identified between the reduction in IL-8 release and the expression of the *CLDN1* gene, as determined by Bravais-Pearson analysis. All technical replicates are plotted as datapoints for the IL-8 release and the *CLDN1* gene expression were listed as DELTA_IL-8 release and DELTA_CLDN1 Expression Fold change and plotted against each other. This is also the case for the graphs showing correlations with their respective parameters. These findings could provide valuable insights into the interplay between inflammation and barrier function in keratinocytes. (figure 18).

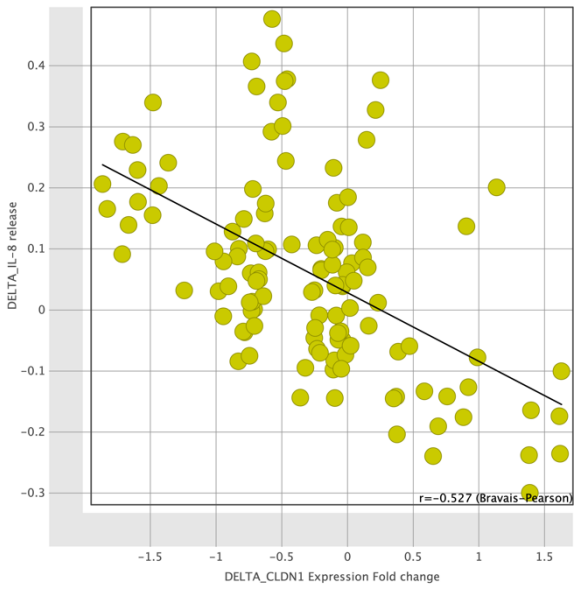

Figure 18 correlation between IL-8 release and CLDN1 gene expression, calculated from fold changes in experimental data (SMILE_1) and deviations from predicted values (SMILE_2). Each compound (n=16) can adopt multiple structural formations (1–15 variants per molecule), potentially influencing the observed response. The graph shows all technical replicates for all compounds which make up for 121 datapoints in the graph. The figure was made by DataWarrior. Statistical analysis done via Bravais-Pearson with a r-value of -0.527

The influence of the side chain length was examined using a selection of 16 compounds featuring saturated/ unsaturated, branched/non-branched side chains ranging from C1 to C10. Chain lengths exceeding C10 were avoided due to their tendency towards low water solubility and diminishing bioavailability which makes them unsuitable for testing (Silverman & Holladay, 2014). The chain length of eight carbons falls within the optimal range for balancing lipophilicity and water solubility, crucial for bioavailability and cell membrane penetration (Silverman & Holladay, 2014). To get more insight into this correlations, specific examples are provided in the next paragraphs. As outlined in the SAR chapter of the Methods, the compounds were categorized based on chain length, ramifications, and double bonds.

Regarding the carbon chain, alterations were observed in length affecting IL-8 release and *CLDN1* gene expression, particularly evident in **R2**, **R5**, and **R6**, especially for shorter carbon chains. In general, positive outcomes can be demonstrated with a reduction of 1-3 carbons in the compound tail with the following compounds. In the IL-8 release **R2** exhibits a fold change to the TNF-α /DMSO control of 1.05 ± 0.24 and **R1** a fold change of 1.04 ± 0.25, respectively. Whereas the *CLDN1* gene expression slightly increases when the carbon side chain of **R2** is decreased by two carbons. Rather similar changes can be detected in the IL-8 release and *CLDN1* gene expression when the carbon chain was one carbon longer (**R2-R3**). Additionally, **R5** shows similar results in IL-8 release when comparing the experimental data and the computationally obtained data, however the *CLDN1* gene expression was increased by approximately 0.25 %. This could be observed when the carbon side chain was shortened by two carbons (**R5**-**R3**). **R6** exhibits a slight inhibitory effect on the IL-8 release and an increase barrier-promoting activities, when branching, as in **R7** was observed**.** Furthermore, shortening the carbon chain by three units resulted in a reduced IL-8 release, as indicated by the fold change relative to the TNF-α/DMSO control: **R6** shows a fold change of 1.00 ± 0.14, while **R3** decreases to 0.92 ± 0.2022. Similarly, *CLDN1* gene expression shows a fold change of 1.17 ± 0.45 for **R6** and increases to 2.42 ± 1.07 for **R3.** The structural modification from **R6** to **R5** and **R4** resulted in a decrease in IL-8 release, accompanied by an increase in *CLDN1* gene expression—exceeding a twofold change compared to the experimental control. (figure 19)

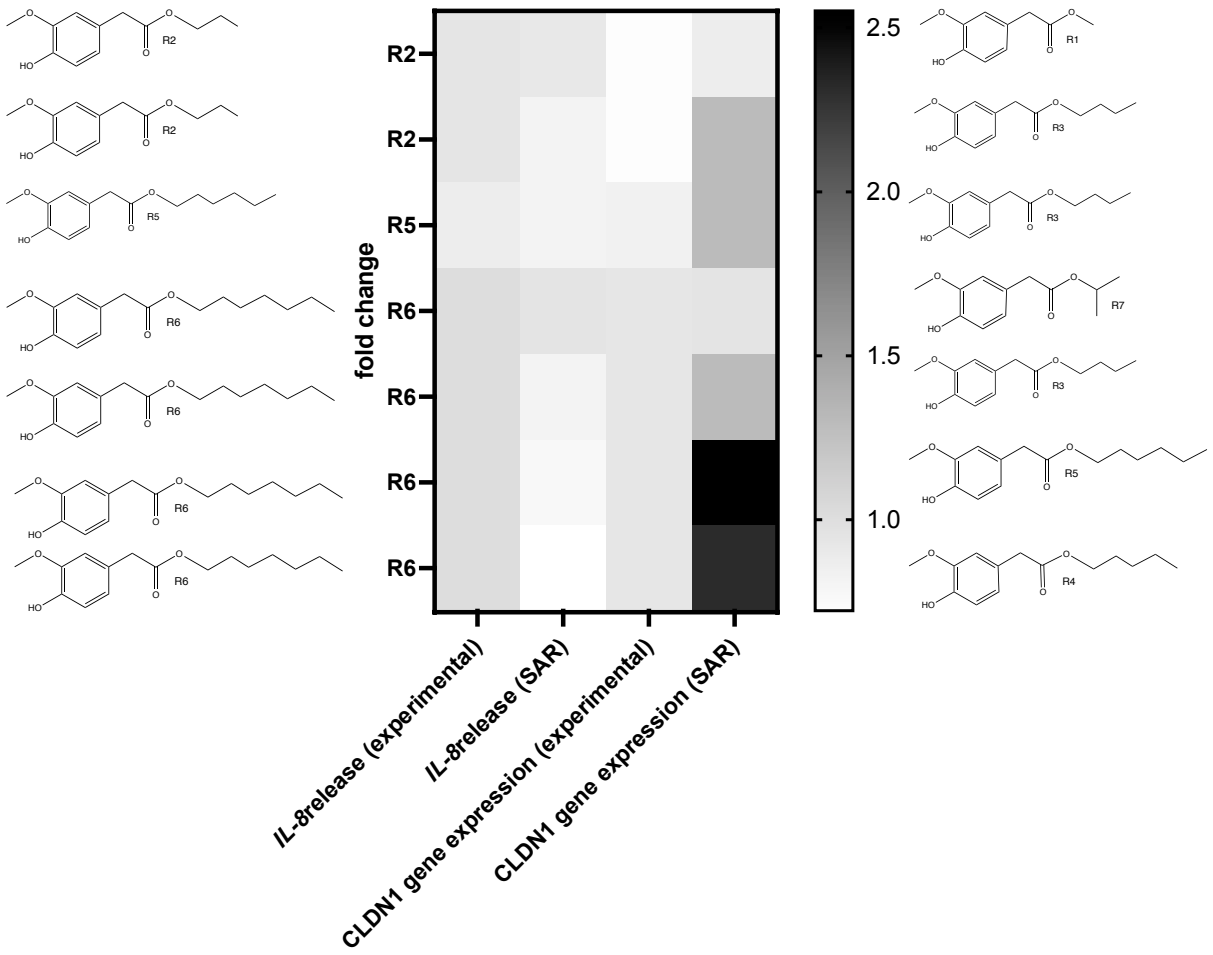

Figure 19 diagram showing the difference of the experimental data and the computationally obtained data of the length group. Comparison of fold change IL-8 release (experimental) IL-8 release (SAR) as well as CLDN1 gene expression (experimental) and CLDN1 gene expression (SAR). This figure also shows the starting structure (left) and the obtained structure (right) giving inside in the possible change and the effect on the IL-8 release and the CLDN1 gene expression, serving as the visualization of the SAR-data.

The impact of branching in the alkyl chain was evaluated using the next set of compounds. Branching typically increases molecular volume, potentially reducing lipophilicity and introducing new stereogenic centers, thus influencing the bioactivity of the compounds. (Silverman & Holladay, 2014). Among the ramification group, several compounds, including **R7**, **R10**, **R11**, **R12**, and **R13**, exhibit the effects of an increase in *CLDN1* gene expression and a decrease in IL-8 release, when branches were minimized, favoring an open chain structure. Additionally, a double bond in the side chain amplified the effect on *CLDN1* gene expression and consequently reduced IL-8 release (**R15**). Changing the side chain to an open configuration with a variation of four-five carbons (**R3-R4**) demonstrates a notable impact. To provide a more precise assessment, changing the side chain to an open configuration with a variation of four-five carbons (**R3-R4**) and the formation of a double bond (**R15)** demonstrates the highest effect towards an increase in the *CLDN1* gene expression. Starting with **R7**, the data demonstrate that an open side chain of four carbons results in a more pronounced effect. Specifically, a decrease in IL-8 release and an higher increase in *CLDN1* gene expression. **R10** demonstrates a reduction of the IL-8 release and an increase in the *CLDN1* gene expression if a double bond is formed. Furthermore, similar results can be observed if the side chain has open chain formation with five carbons. **R11** exhibits a reduction on the IL-8 release and a higher impact on the *CLDN1* gene expression when the structure is converted to **R3**, **R15** and **R4**. Most promising in terms of barrier-promoting properties, is the transition from **R11** to **R15 which** shows a notable shift: IL-8 release decreases, with fold changes relative to the TNF-α/DMSO control of 0.87 ± 0.16 for **R11** and 0.77 ± 0.21 for **R15**. Additionally, *CLDN1* gene expression increases from a fold change of 1.04 ± 0.34 for **R11** to 2.26± 0.89 for **R15**. Whereas **R12** shows also slight indications of a decrease in IL-8 release and an increase in the *CLDN1* gene expression outcome if the structure change shows an open side chain formation or an unsaturation. **R13** shows a similar trend, particularly when the structure is modified to **R15** or **R4**, featuring a saturated end group and a six-carbon side chain (**R15**) or an open side chain structure with five carbons (**R4**). Furthermore, it can be noted that the formation of **R15** and **R4** from the compounds **R10**, **R11**, **R12**, and **R13** leads to favorable conditions- an increase in the *CLDN1* gene expression and a decrease in IL-8 release.

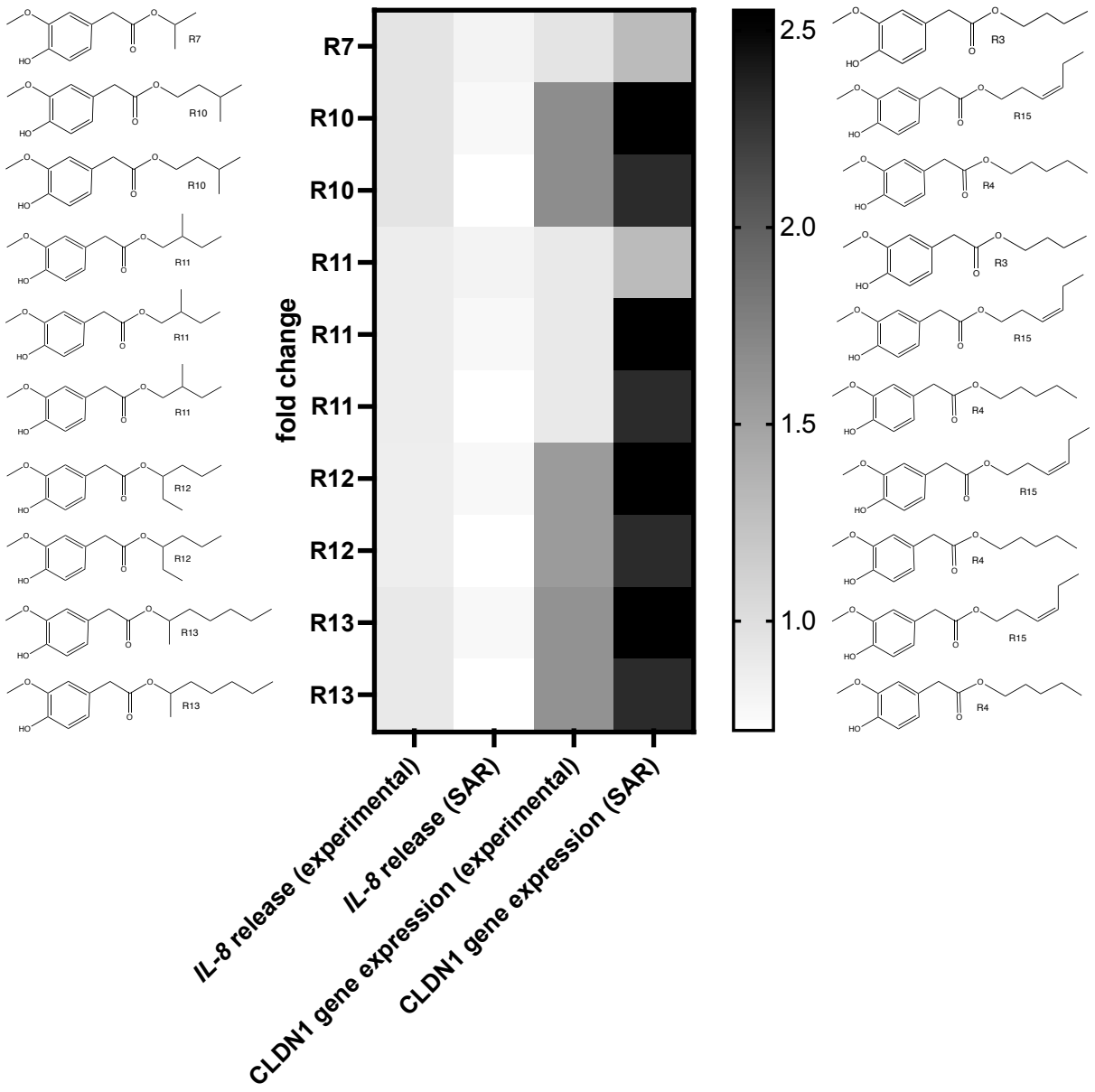

Figure 20 diagram showing the difference of the experimental data and the computationally obtained data of the ramification group. Comparison of fold change IL-8 release (experimental) IL-8 release (SAR) as well as CLDN1 gene expression (experimental) and CLDN1 gene expression SAR. This figure also shows the starting structure (left) and the obtained structure (right) giving inside in the possible change and the effect on the IL-8 release and the CLDN1 gene expression, serving as the visualization of the SAR-data.

Lastly, the impact of unsaturation in the in the side chain was explored. Double bonds generally decrease flexibility and increase rigidity (Silverman & Holladay, 2014) Within this group, two homovanillic compounds, namely **R15** and **R16**, showed an effect on *CLDN1* expression and IL-8 release during *in vitro* testing. Among the compounds featuring double bonds, only **R14** displayed enhanced effects following rearrangement of the side chain, underlining the importance of chain length in this context (SAR-Analysis). At least five carbons in this group seem to have the most impact on the two parameters: IL-8 release and *CLDN1* gene expression. A branched side chain to an open side chain of seven carbons doubled the impact on the *CLDN1* gene expression. Switching the double bond from the beta carbon to the gamma carbon and eliminating the methyl group at the gamma carbon to form **R15** led to an increase in the CLDN1 gene expression and a decrease in IL-8 release. The fold change in IL-8 release relative to the TNF-α/DMSO control decreases from 0.90 ± 0.24 for **R14** to 0.77 ± 0.21 for **R15**. Notably, *CLDN1* gene expression is markedly affected, nearly doubling—from a fold change of 1.01 ± 0.41 to 2.26 ± 0.89 from **R14** to **R15**, respectively. A change to five carbons (**R4**) in the side chain led to similar outcomes in the IL-8 release and the *CLDN1* gene expression.

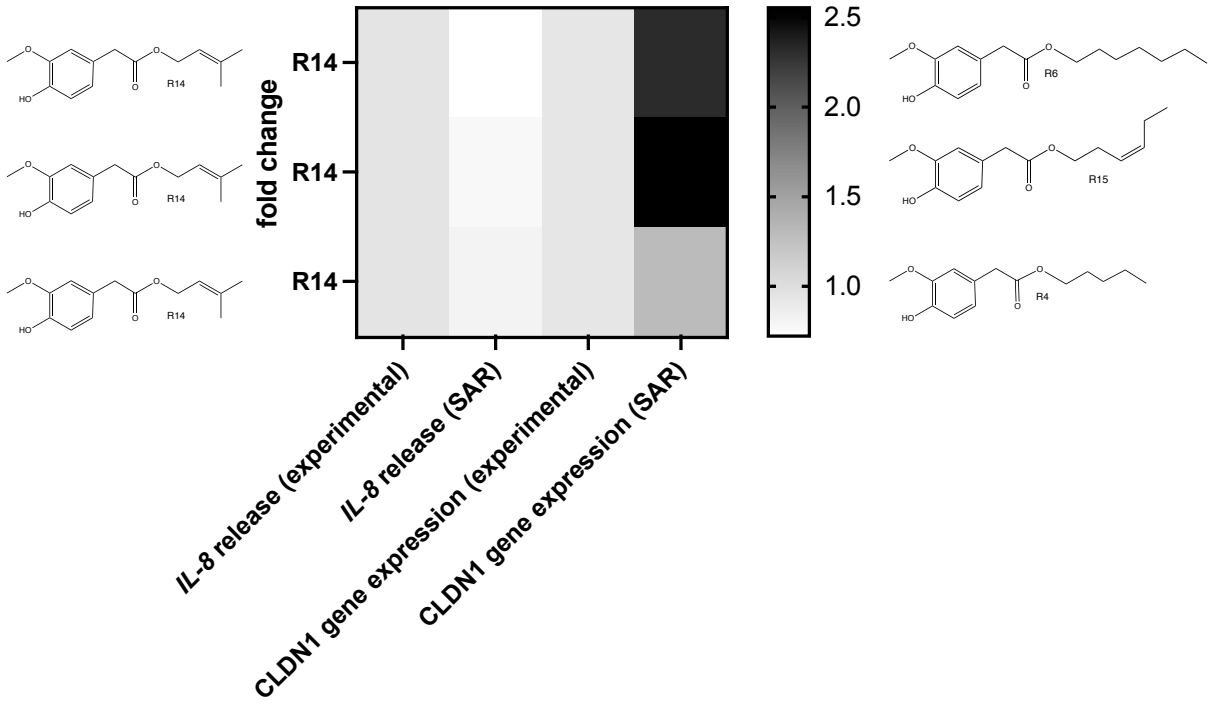

Figure 21 diagram showing the difference of the experimental data and the computationally obtained data of the double bond group. Comparison of fold change IL-8 release (experimental) IL-8 release (SAR) as well as CLDN1 gene expression (experimental) and CLDN1 gene expression (SAR). This figure also shows the starting structure (left) and the obtained structure (right) giving inside in the possible change and the effect on the IL-8 release and the CLDN1 gene expression, serving as the visualization of the SAR-data.

Considering the correlation between the *CLDN1* gene expression and *CXCL8* gene expression it can be observed that here a positive “r” of 0.716 was computed via Bravais-Pearson in DataWarrior.

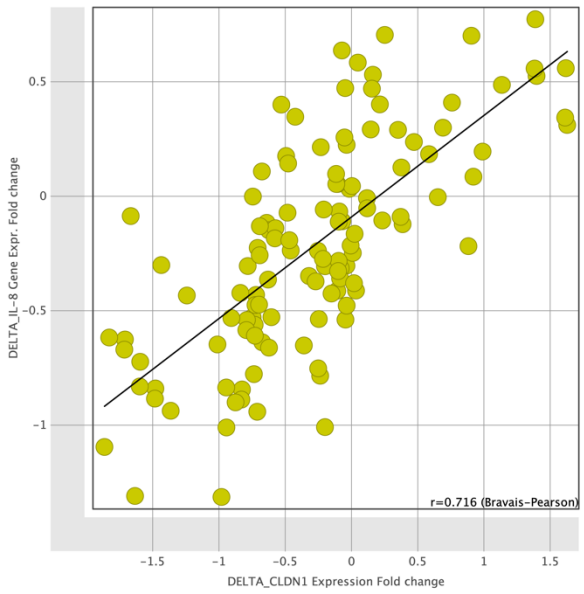

Figure 22 correlation between CXCL8/ IL-8 gene expression and CLDN1 gene expression, calculated from fold changes in experimental data (SMILE_1) and deviations from predicted values (SMILE_2). Each compound (n=16) can adopt multiple structural formations (1–15 variants per molecule), potentially influencing the observed response. The graph shows all technical replicates for all compounds which make up for 121 datapoints in the graph. The figure was made by DataWarrior. Statistical analysis done via Bravais-Pearson with a r-value of 0.716.

When focusing on the “chain length group” a trend can be observed. The transition to **R7** has an effect on the *CLDN1* gene expression and *CXCL8* gene expression, which means an upregulation of the first gene and a downregulation of the second. This is especially the case for **R2**, **R5** and **R6**. **R7** has a methyl group near the ester bond, which could suggest, only in the context of the simultaneous downregulation of *CXCL8* gene expression and an upregulation of *CLDN1* gene expression, that ramification could result in decreased inflammatory cytokine release accompanied by an upregulation of TJ (tight junction) protein. Even though the previous SAR Data analyses stated otherwise. These findings are depicted in figure 23.

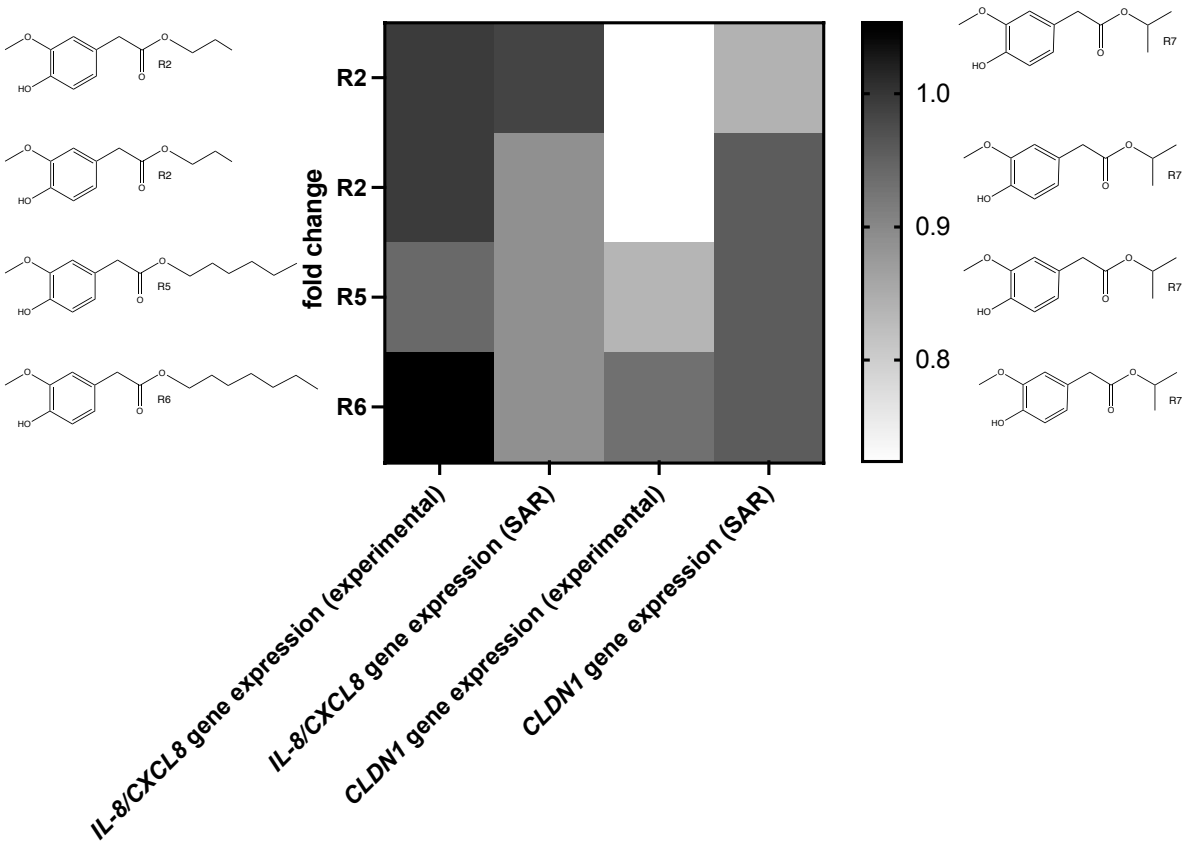

Figure 23 diagram showing the difference of the experimental data and the computationally obtained data of the length group. Comparison of fold change CXCL8 gene expression(experimental) CXCL8 gene expression (SAR) as well as CLDN1 gene expression (experimental) and CLDN1 gene expression (SAR). This figure also shows the starting structure (left) and the obtained structure (right) giving inside in the possible change and the effect on the CXCL8 gene and the CLDN1 gene, serving as the visualization of the SAR-data.

Furthermore, in the context of gene expression and the ramification group it can be noted that only the changes of two compounds led to an increase in *CLDN1* gene expression and a decrease in *CXCL8* gene expression. These being **R10** and **R11**. Both showed an impact on these parameters when changed to compounds without ramification or double bonds. The only exception being the change from **R11** to **R7**. The fold changes of these outcomes are depicted in figure 24. Again, an open side chain seems to be favored starting from at least four carbons to seven carbons.

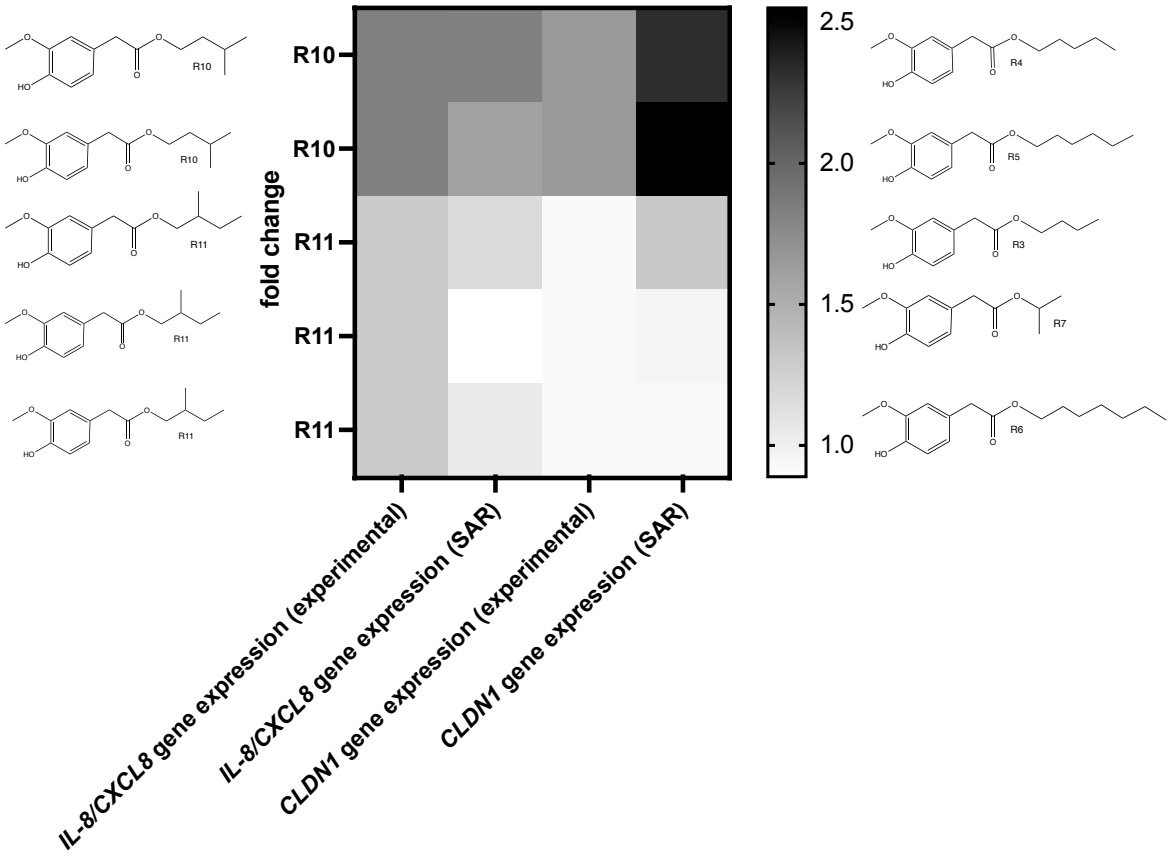

Figure 24 diagram showing the difference of the experimental data and the computationally obtained data of the ramification group. Comparison of fold change CXCL8 gene expression(experimental) CXCL8 gene expression (SAR) as well as CLDN1 gene expression (experimental) and CLDN1 gene expression (SAR). This figure also shows the starting structure (left) and the obtained structure (right) giving inside in the possible change and the effect on the CXCL8 gene and the CLDN1 gene, serving as the visualization of the SAR-data.

Lastly **R14** is the only compound in the double group and its changes to **R3** and **R7** seems the have a stronger effect on the *CLDN1* gene expression and the downregulation of *CXCL8* gene expression.

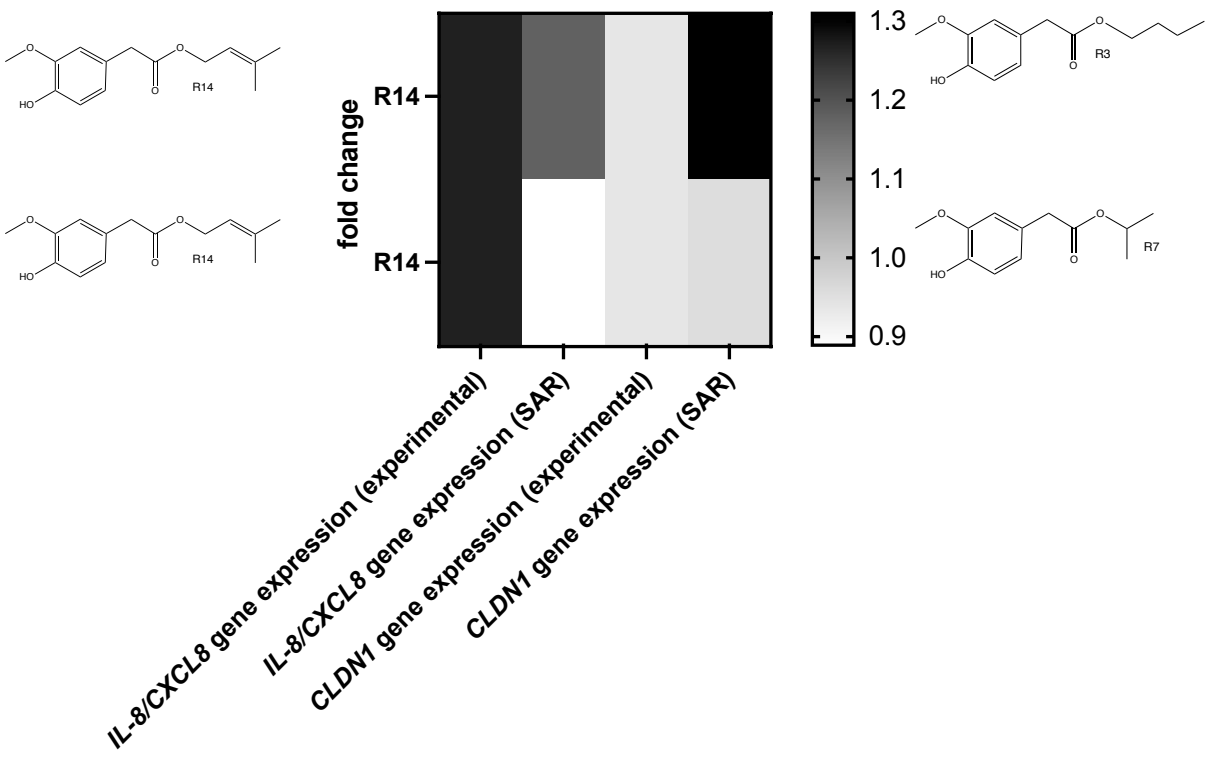

Figure 25 diagram showing the difference of the experimental data and the computationally obtained data of the double bond group. Comparison of fold change CXCL8 gene expression(experimental) CXCL8 gene expression (SAR) as well as CLDN1 gene expression (experimental) and CLDN1 gene expression (SAR). This figure also shows the starting structure (left) and the obtained structure (right) giving inside in the possible change and the effect on the CXCL8 gene and the CLDN1 gene, serving as the visualization of the SAR-data.

All the data together suggests that the change to **R7** with aliphatic side chain of two carbons and a methyl group on the alpha carbon led to a more profound change in the upregulation of *CLDN1* with the simultaneous downregulation of *CXCL8*. Furthermore, it can be noted that in the "length group" a side chain of at least four carbons up to seven carbons, seems necessary to achieve higher *CLDN1* gene expression and values accompanied by downregulation of IL-8 release. This finding correlates with the previous SAR analyses concerning the interplay of *CLDN1* gene expression and IL-8 release.

Looking at the correlation of the *CXCL8* gene expression and the IL-8 release only a very small “r” was observed, which suggests that the interplay with these two parameters is rather small. “r” has a value of -0.23 using a Bravais-Pearson evaluation in DataWarrior. This is showcased in the figure below.

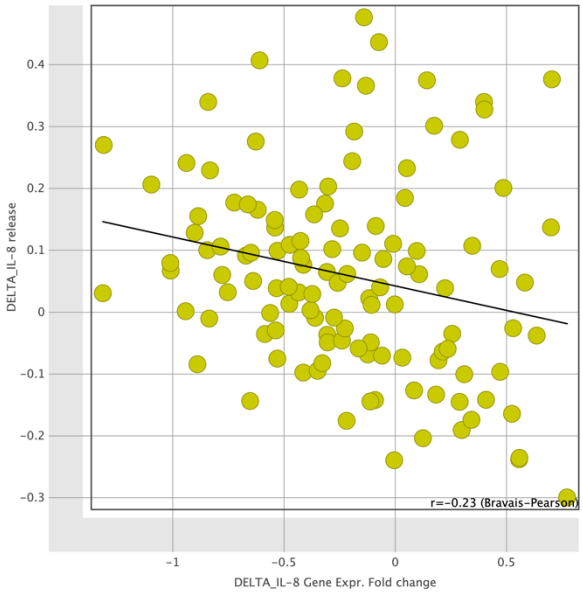

Figure 26 correlation between delta IL-8 release and delta CXCL8/ IL-8 gene expression, calculated from fold changes in experimental data (SMILE_1) and deviations from predicted values (SMILE_2). Each compound (n=16) can adopt multiple structural formations (1–15 variants per molecule), potentially influencing the observed response. The graph shows all technical replicates for all compounds which make up for 121 datapoints in the graph. The figure was made by DataWarrior. Statistical analysis done via Bravais-Pearson with a r-value of -0.23.

5. Discussion

The hypothesis underlying this study states that specific structural elements of the aliphatic chain of homovanillic acid esters are associated with the anti-inflammatory and barrier-promoting properties of capsaicin in human keratinocytes. To address this hypothesis, HaCaT cells were utilized and cultured accordingly as described in chapter 3.3. cell culture. A suitable concentration of the compounds was determined using a MTT assay. Subsequently, HaCaT cells were pre-treated with a concentration of 10 µM of each 16 compounds for 24 hours, followed by treatment with 20 ng/mL TNF-α for an additional 6 hours. Afterward, RT-qPCR was used to determine the gene expression of *CXCL8*/*IL-8*, *CLDN1*. Additionally, the amount of IL-8 secreted by the cells in the supernatant of the cell culture medium was measured using ELISA. The participation of the TRPV1 channel was further examined using capsazepine as an antagonist of the TRPV1 receptor. Lastly, it was investigated if this effect can be predicted with the structure by employing a structure-activity relationship using DataWarrior.

The screening revealed that three out of the 16 tested compounds affected the expression of essential TJ protein CLDN1 and the release of the pro-inflammatory cytokine IL-8. These three compounds are **R5**, **R15** and **R16**. A significant effect was shown for **R5**, **R15** on the *CLDN1* gene expression and the IL-8 release was significantly decreased for **R5** and **16.** All three compounds follow a trend of simultaneous increase in the *CLDN1* gene expression and a decrease in the IL-8-release. The structures below show a comparison of capsaicin and capsiate to these three compounds, highlighting their similarities.

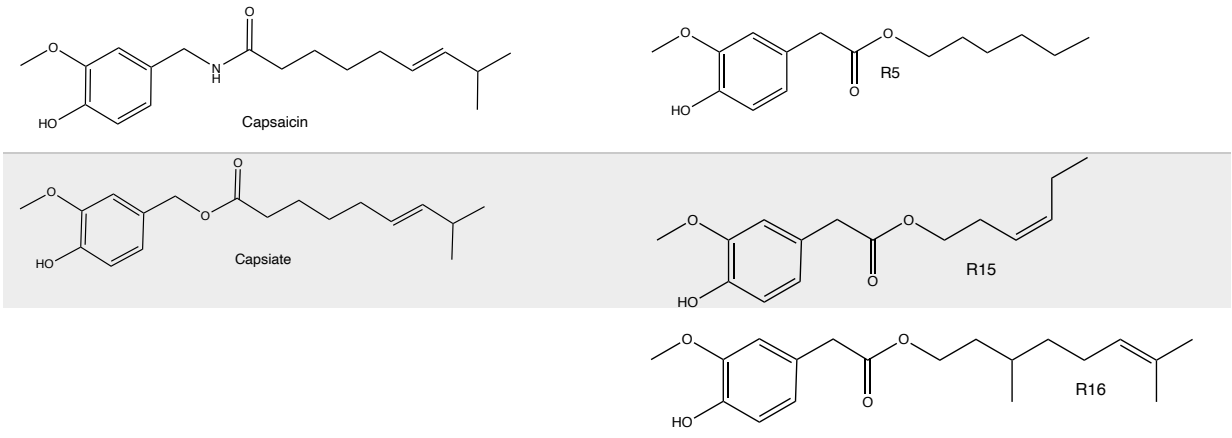

Figure 27 showing the comparison of capsaicin and capsiate with the selected homovanillic acid esters

The upregulation of *CLDN1* suggests that these compounds may reinforce barrier integrity, which could influence inflammatory responses by reducing permeability and preventing the infiltration of immune cells. (Tokumasu et al., 2016) Tokumasu et al., 2016 suggested that an increase in *CLDN1* gene expression in the skin has a positive effect, especially in enhancing skin barrier function. Due to its importance to the tight junctions, is essential for maintaining the integrity of the epidermal

barrier and homeostasis of the skin. Higher levels of *CLDN1* also show a correlation with reduced features of atopic dermatitis. (Tokumasu et al., 2016) A significant decrease in the claudin expression can also be demonstrated when talking about the inflammatory skin disease rosacea, which suggests that a downregulation of the barrier promoting gene is linked to an impaired skin barrier (Deng et al., 2019)

The decrease in IL-8 release, as observed in this study, can have several positive effects, in the context of inflammatory skin conditions. IL-8 (pro-inflammatory cytokine) plays a role in attracting neutrophils and inducing inflammation. Therefore, reducing its levels can improve skin health in various dermatological conditions. (Qazi et al., 2011) Chronic inflammatory skin disease, like psoriasis could be treated by neutralizing IL-8 leading to a reduction of inflammation and a relief in the associated symptoms. (George Qing Wei Ye, 2006) Neutralization of IL-8 also inhibits of Epidermal Growth Factor Receptor (EGFR) which is of particular interest in cancer research (Bangsgaard et al., 2012). Also other skin conditions could be positively affected when reducing IL-8, for example an improved skin appearance of patients suffering from rosacea (George et al., 2023). In atopic dermatitis, lower levels of IL-8 in the *stratum corneum* are associated with reduced skin inflammation, therefore its positive therapeutic response was assumed (Murata et al., 2021). However, it must be noted that, while the decrease of IL-8 levels can have anti-inflammatory effects, it is important to consider that IL-8 also plays a role in immune defense. Therefore, suppressing IL-8 may impair the skin's ability to respond to infections. A careful balance must be kept. (Qazi et al., 2011)

The receptor TRPV1 plays an important role during inflammation but is also known for its role in pain perception and thermosensation (Ilie et al., 2019). It has various chemical agonists such as capsaicin (Diver et al., 2022). In the context of this study, TRPV1's role in inflammation and barrier integrity is of particular interest. Additionally, capsaicin is known to modulate inflammatory responses by desensitizing nociceptive neurons and inhibiting pro-inflammatory cytokine production. (Ilie et al., 2019) Structural features like the ones in capsaicin contribute to TRPV1 activation through specific electrostatic, hydrogen-bonding, steric, and hydrophobic interactions, which can stabilize the receptor (Chen et al., 2019).

Capsaicin, as an agonist of TRPV1, can activate the receptor through the presence of a vanillyl moiety (Head of the structure, which is also present in all the 16 analogues). Furthermore, the hydrophobic tail of capsaicin enhances its affinity for the TRPV1 channel, promoting effective interaction and activation. (Caballero, 2022) While capsaicin is a potent activator of TRPV1, other compounds with similar structural features can either mimic or inhibit its effects (Chen et al., 2019). Three compounds of this study show that they could potentially mimic capsaicin’s behavior. **R5** and **R15** show a side chain of six carbons whereas **R16** has the same length as capsaicin/capsiate of

eight carbons. Therefore, it might be concluded that a carbon length of preferably six carbons leads to increases in CLDN1 expression and the downregulation of IL-8 release. Also, the double bonds seem to make an impact as two of three compounds (from the double bond group) also show this effect.

To determine whether TRPV1 affected *CLDN1* gene expression and IL-8 release, experiments were conducted using three selected compounds, with capsazepine serving as an antagonist to block TRPV1 receptor activity (Gonzalez-Reyes et al., 2013). If TRPV1 were solely responsible for the effect, the addition of capsazepine would be expected to completely abolish or significantly reduce the response. However, the results indicate that capsazepine did not fully block the effects, suggesting that additional mechanisms or receptors are involved. Compound **R5** exhibits notable effects on the gene expression of both genes when comparing results with and without the addition of capsazepine, leading to a decrease in the *CLXL8* gene expression and an increase in *CLDN1* gene expression. Analysing the data of **R15,** an impact regarding the *CLDN1* gene expression can be demonstrated. This could suggest that **R15** indeed affects the *CLDN1* gene expression, however it does not directly show whether **R15** is affecting TRPV1. Regarding **R16** only the *CXCL8* gene expression was significantly affected. The observed impact on *CXCL8* gene expression suggests that **R16** may influence the transcriptional regulation of *CXCL8,* also leading to a downregulation of the gene as for **R5** during these experiments using capsazepine as an antagonist. In all of these three compounds no impact on the IL-8 release was noted only the gene expression seems to be affected.

One possible explanation of these results might be that these compounds may act through multiple pathways or that TRPV1 was not involved at all. TRPV1 may not be the primary target of these three compounds, and the response could originate from another ion channel or receptor that capsazepine does not inhibit. Therefore, it might be suggested that these three compounds (**R5**, **R15** and **R16**) exert their effect through a broader mechanism of action beyond TRPV1 activation. One possibility could be the mitogen-activated protein kinases (MAPK) signaling pathway which is affected during inflammation in keratinocytes (Di Meo et al., 2025). NF-kB signaling pathway could also be involved, which leads to the activation of proinflammatory cytokines and matrix metalloproteinases (MMPs) in keratinocytes (S. Han et al., 2018). Alternative pathways, such as those mediated by other transient receptor potential (TRP) channels, may also play a role (McKnight et al., 2022). Additionally, the possibility that TRPV1 activation occurs in conjunction with other signaling cascades rather than as an isolated event further supports the hypothesis that these compounds exert their effects through different mechanism of action (Xu et al., 2022).

Furthermore, a correlation could be identified between the reduction in IL-8 release and the expression of the *CLDN1* gene with a negative correlation of -0.527, determined through Bravais-Pearson analysis, suggesting an inverse relationship between IL-8 release and *CLDN1* gene expression. Moreover, this correlation supports the hypothesis proposed by the RT-q PCR and ELISA experiments, which already suggested that there might be an inverse relationship between IL-8 release and the *CLDN1* gene expression. The expression of *CLDN1*, key component of tight junctions and therefore important for barrier integrity, increases, the release of IL-8, a pro-inflammatory cytokine, tends to decrease. A " r " of -0,527 in biological systems can be seen as achievable, and it is acceptable to assume such correlations due to the complex interactions of compounds and biological system (A. Gupta et al., 2024).

To further underline these findings the structure-activity relationship was taken into consideration. A structure of six carbons and a double bond in the side chain leads to an increase in *CLDN1* gene expression and a decrease in the IL-8 release, which goes along with the previous observations suggesting that the structure of **R15** has a strong impact on the release of pro-inflammatory cytokines like IL-8 or the expression of TJ proteins like CLDN1 for both experimental analyses and structure-activity relationships. This structure shows no branching and possesses only one double bond at the gamma carbon and a side chain length of six carbons. To come to this conclusion all 16 analogues were analyzed, and the outcome taken into consideration.

The SAR data also highlights that the emergence of branching may induce steric hindrance (Silverman & Holladay, 2014). This becomes apparent as the relocation of methyl side chain branching to a non-branched compound consistently results in increased gene expression of *CLDN1* showing a tendency towards tight junction formation, essential for barrier function and a simultaneous decrease in IL-8 release. This is also true for the formation of compounds without a double bond. The observation was made that even the compounds **R1**, **R3**, **R4**, **R5**, **R6** (only difference in length) had more impact on these parameters then the appearance of branching. This is especially true for branching near the functional group of the compound, suggesting that the steric hindrance is too strong for the compound to bind to a receptor. However, there is one case were branching led to the decrease IL-8 release and an increase in *CLDN1* gene expression, the structural change from **R6** to **R7**.

Furthermore, while **R4** exhibits promising outcomes in structure-activity relationships, the data in the experimental analyses is less remarkable. Structurally, **R4** has a side chain of 5 carbons. **R4** shows a decrease in the IL-8 release and an increase in *CLDN1* gene expression during the SAR and is therefore the most prominent structure in the "length group". Considering these aspects, a carbon chain length of at least five carbons in the side chain may contribute to these effects. Moreover, **R4** and **R15** share strong similarities with capsaicin in terms of length and/or double bond configuration.

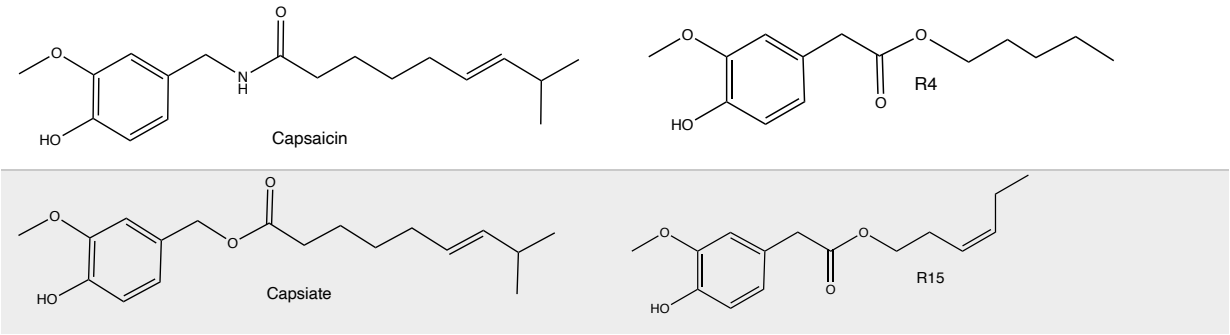

Figure 28 showing the comparison of capsaicin and capsiate with R4 and R15

The correlation of the downregulation of the *CXCL8* gene expression and the upregulation of the *CLDN1* gene expression was also analyzed. Here it can be seen that in all of the three groups: length ramification and double bonds, one change seems to be the most prominent, this being **R7** with a methyl group at the alpha carbon and an aliphatic side chain of two carbons. However, it seems like, an open aliphatic side chain varying in length led to a decrease in *CXCL8* gene expression and an increase in *CDLN1* gene expression. A side chain of at least four carbons seems to be necessary in order to achieve these outcomes. Furthermore, the high correlation index of "r" = 0.716 also asserts the claim that these two parameters indeed correlate with each other. This would also further embed the notion that some compounds and their changes in the aliphatic tail may lead to healthier skin barrier and have anti-inflammatory properties.

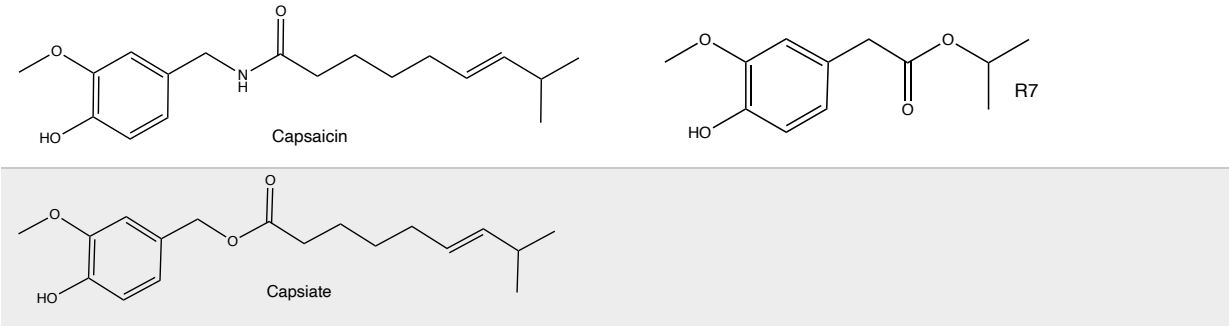

Figure 29 showing the comparison of capsaicin and capsiate with R7

The results of the *CXCL8* gene expression were analyzed separately due to the absence of any observed correlation in the experimental data and due the fact that the SAR data also showed a very small correlation between the *CXCL8* gene expression, and the IL-8 release. The same order and grouping were kept also for these analyses. **R6** was the only compound of the "length group" with a downregulation of the *CXCL8* gene expression coupled with decrease in the IL-8 release, if the side chain was either elongated shortened or branched. Furthermore, four compounds of the branching group suggested favorable results when being altered: **R10**, **R11**, **R12** and **R13**. No correlation can be found suggesting that any specific alteration of the three (length, branching double bond) led to a downregulation of the *CXCL8* gene expression coupled with decrease in the IL-8 release, because all of them showed an effect this is especially true for **R10**. **R13** seems to decrease *CXCL8* gene expression, and the IL-8 release when the ramification is being kept (different formation) No branching int the case of **R11** and **R12** seems to lead to the same outcomes. Considering the double

bonds **R14** showed an effect on the *CXCL8* gene expression and IL-8 release when changes in the structure occurred. A change to a saturated side chain without branching suggested a decrease in these two parameters. Moreover, a trend can be acknowledged, a change in length leads to overall decrease in inflammation considering the *CXCL8* gene expression and the release of the cytokine. Even though the steric hindrance gets increased when introducing a methyl or ethylgroup in the side chain (Silverman & Holladay, 2014), the SAR data suggested this could also in some cases (**R6**, **R10**) lead to a decrease in the transcriptional activities of *IL-8* as well as the release of the protein. No considerable overlap can be seen with the previous experimental data and the analyses of the structure activity relationship.

All the data together analyzed by DataWarrior including the increase in *CLDN1* gene expression, decrease in *CXCL8* gene expression and the IL-8 release suggests that an open side chain with four to six carbons is the most promising structure of the homovanillic compounds. Furthermore, an unsaturated side chain also seems to have a strong effect on the increase in *CLDN1* gene expression and the decrease in IL-8 release. Also considering the experimental data the structure of six carbons and a double bond at the gamma carbon shows this effect on these two parameters throughout the study design. This structure shows a close similarity to capsaicin or capsiate, just with a shorter carbon side chain, suggesting that a carbon chain of six carbons already leads to an increase in *CLDN1* gene expression and a decrease in IL-8 release. However, the effects on other inflammatory pathways must be explored in order to fully elucidated the mechanism of action. These findings can be further used to develop compounds with these characteristics.

6. Conclusion and Outlook

This study provides insights into the potential anti-inflammatory and barrier-promoting effects of homovanillic compounds, highlighting their interaction with TRPV1. The observed correlation between increased *CLDN1* expression and decreased IL-8 release suggests a promising mechanism that could be further used for therapeutic interventions in inflammatory skin disorders. A long aliphatic side chain of four to six carbons (without ramifications or double bonds) has a generally strong impact on the upregulation of *CLDN1* gene expression. Furthermore, a side chain of six carbons a double bond at the gamma carbon leads to an upregulation of the *CLDN1* gene expression and downregulation of the IL8 release in the experimental setting and during the SAR Analyses. This structure led to a significant increase in the *CLDN1* gene expression the basal keratinocytes and a subsequent decrease of the pro- inflammatory cytokine IL-8. Therefore, being the most prominent structure out of all the 16 homovanillic acid esters.

In the context of TRPV1 involvement, the findings suggested that this receptor was not solely responsible for the effect. A side chain of six carbons with ramification and double bonds exhibits notable effects on the gene expression of both genes when comparing results with and without the addition of capsazepine. Analysing the data of the saturated structure with six carbons in the side chain, an impact regarding the *CLDN1* gene expression can be demonstrated. Regarding the compound with eight carbons, ramifications and a double bond in the side chain, only the *CXCL8* gene expression was significantly reduced. These compounds show an aliphatic side chain of at least six carbons, **R15** the additional double bond and **R16** double bond and ramification. These findings were published at “Frontiers in Pharmacology” under the title “Role of homo-vanillic acid esters in the regulation of skin inflammatory pathways and their effect on tight junction protein expression” by Cervantes Recalde et al., 2025.

However, there are several limitations to consider. While the study demonstrates a relationship between TRPV1 and inflammatory processes, it does not conclusively establish TRPV1 as the primary target of these 16 homovanillic acid esters. The incomplete inhibition by capsazepine suggests the involvement of other receptors or signaling pathways. This however must be further investigated. The use of HaCaT cells, provides a useful model for studying skin inflammation but it those not fully replicate the complexity of *in vivo* skin responses. New Approach Methodologies (NAMs) could be employed to reduce animal testing and to further investigate the mechanism of action. Additionally, the time points and concentrations used in the experiments may not capture the full spectrum of gene expression changes over longer durations. The structure-activity relationship (SAR) analysis requires additional validation. The predictive modeling using DataWarrior suggests structural features that may influence bioactivity, but further experimental studies are needed to confirm these findings in a broader biological context.

In conclusion, this study provides some new insights of homovanillic compounds in modulating inflammation and barrier integrity. However, additional research is necessary to fully elucidate their mechanisms of action. Further exploration of alternative pathways, validation through NAMs, and optimization of experimental conditions will be essential to use these findings for therapeutic applications.

7. References

Arda, O., Göksügür, N., & Tüzün, Y. (2014). Basic histological structure and functions of facial skin. *Clinics in Dermatology*, *32*(1), 3–13. https://doi.org/10.1016/j.clindermatol.2013.05.021

Arnemann, J. (2019). DNA-/RNA-Konzentrationsbestimmung. In A. M. Gressner & T. Arndt (Eds.), *Lexikon der Medizinischen Laboratoriumsdiagnostik* (pp. 719–719). Springer Berlin Heidelberg. https://doi.org/10.1007/978-3-662-48986-4_3464

Aydin, S. (2015). A short history, principles, and types of ELISA, and our laboratory experience with peptide/protein analyses using ELISA. *Peptides*, *72*, 4–15. https://doi.org/10.1016/j.peptides.2015.04.012

Aza-González, C., Núñez-Palenius, H. G., & Ochoa-Alejo, N. (2011). Molecular biology of capsaicinoid biosynthesis in chili pepper (Capsicum spp.). *Plant Cell Reports*, *30*(5), 695–706. https://doi.org/10.1007/s00299-010-0968-8

Bagood, M. D., & Isseroff, R. R. (2021). TRPV1: Role in Skin and Skin Diseases and Potential Target for Improving Wound Healing. *International Journal of Molecular Sciences*, *22*(11), 6135. https://doi.org/10.3390/ijms22116135

Bangsgaard, N., Houtkamp, M., Schuurhuis, D. H., Parren, P. W. H. I., Baadsgaard, O., Niessen, H. W. M., & Skov, L. (2012). Neutralization of IL-8 Prevents the Induction of Dermatologic Adverse Events Associated with the Inhibition of Epidermal Growth Factor Receptor. *PLoS ONE*, *7*(6), e39706. https://doi.org/10.1371/journal.pone.0039706

Baroni, A., Buommino, E., De Gregorio, V., Ruocco, E., Ruocco, V., & Wolf, R. (2012). Structure and function of the epidermis related to barrier properties. *Clinics in Dermatology*, *30*(3), 257–262. https://doi.org/10.1016/j.clindermatol.2011.08.007

Basharat, S., Gilani, S. A., Iftikhar, F., Murtaza, M. A., Basharat, A., Sattar, A., Qamar, M. M., & Ali, M. (2020). Capsaicin: Plants of the Genus ***Capsicum*** and Positive Effect of Oriental Spice on Skin Health. *Skin Pharmacology and Physiology*, *33*(6), 331–341. https://doi.org/10.1159/000512196

Caballero, J. (2022). A new era for the design of TRPV1 antagonists and agonists with the use of structural information and molecular docking of capsaicin-like compounds. *Journal of Enzyme Inhibition and Medicinal Chemistry*, *37*(1), 2169–2178. https://doi.org/10.1080/14756366.2022.2110089

Canene-Adams, K. (2013). General PCR. In *Methods in Enzymology* (Vol. 529, pp. 291–298). Elsevier. https://doi.org/10.1016/B978-0-12-418687-3.00024-0

Cao, C., Xiao, Z., Wu, Y., & Ge, C. (2020). Diet and Skin Aging—From the Perspective of Food Nutrition. *Nutrients*, *12*(3), 870. https://doi.org/10.3390/nu12030870

Cao, E., Liao, M., Cheng, Y., & Julius, D. (2013). TRPV1 structures in distinct conformations reveal activation mechanisms. *Nature*, *504*(7478), 113–118. https://doi.org/10.1038/nature12823

Castillo, E., López-González, I., De Regil-Hernández, R., Reyes-Duarte, D., Sánchez-Herrera, D., López-Munguía, A., & Darszon, A. (2007). Enzymatic synthesis of capsaicin analogs and their effect on the T-type Ca2+ channels. *Biochemical and Biophysical Research Communications*, *356*(2), 424–430. https://doi.org/10.1016/j.bbrc.2007.02.144

Cervantes Recalde, M. F., Schmidt, J., Girardi, C., Massironi, M., Rechl, M. L., Hans, J., Stuhlmann, D., Somoza, V., & Lieder, B. (2024). Capsaicin attenuates the effect of inflammatory cytokines in a HaCaT cell model for basal keratinocytes. *Frontiers in Pharmacology*, *15*, 1474898. https://doi.org/10.3389/fphar.2024.1474898

Cervantes Recalde, M. F., Bogensperger, E. Z., Hans, J., Stuhlmann, D., Somoza, V., & Lieder, B. (2025). Role of homovanillic acid esters in the regulation of skin inflammatory pathways and their effect on tight junction protein expression. *Frontiers in Pharmacology*, *16*, 1629941. https://doi.org/10.3389/fphar.2025.1629941

Chen, K., Feng, L., Feng, S., Yan, Y., Ge, Z., Li, Z., & Chen, Z. (2019). Multiple quantitative structure–pungency correlations of capsaicinoids. *Food Chemistry*, *283*, 611–620. https://doi.org/10.1016/j.foodchem.2019.01.078

Chéret, J., Lebonvallet, N., Carré, J., Misery, L., & Le Gall-Ianotto, C. (2013). Role of neuropeptides, neurotrophins, and neurohormones in skin wound healing. *Wound Repair and Regeneration*, *21*(6), 772–788. https://doi.org/10.1111/wrr.12101

Colombo, I., Sangiovanni, E., Maggio, R., Mattozzi, C., Zava, S., Corbett, Y., Fumagalli, M., Carlino, C., Corsetto, P. A., Scaccabarozzi, D., Calvieri, S., Gismondi, A., Taramelli, D., & Dell'Agli, M. (2017). HaCaT Cells as a Reliable In Vitro Differentiation Model to Dissect the Inflammatory/Repair Response of Human Keratinocytes. *Mediators of Inflammation*, *2017*, 1–12. https://doi.org/10.1155/2017/7435621

De Cesaris, P., Starace, D., Riccioli, A., Padula, F., Filippini, A., & Ziparo, E. (1998). Tumor Necrosis Factor-α Induces Interleukin-6 Production and Integrin Ligand Expression by Distinct Transduction Pathways. *Journal of Biological Chemistry*, *273*(13), 7566–7571. https://doi.org/10.1074/jbc.273.13.7566

Denda, M., Sokabe, T., Fukumi-Tominaga, T., & Tominaga, M. (2007). Effects of Skin Surface Temperature on Epidermal Permeability Barrier Homeostasis. *Journal of Investigative Dermatology*, *127*(3), 654–659. https://doi.org/10.1038/sj.jid.5700590

Deng, Z., Chen, M., Xie, H., Jian, D., Xu, S., Peng, Q., Sha, K., Liu, Y., Zhang, Y., Shi, W., & Li, J. (2019). Claudin reduction may relate to an impaired skin barrier in rosacea. *The Journal of Dermatology*, *46*(4), 314–321. https://doi.org/10.1111/1346-8138.14792

Di Meo, C., Tortolani, D., Standoli, S., Ciaramellano, F., Angelucci, B. C., Tisi, A., Kadhim, S., Hsu, E., Rapino, C., & Maccarrone, M. (2025). Cannabinol modulates the endocannabinoid system and shows TRPV1 -mediated anti-inflammatory properties in human keratinocytes. *BioFactors*, *51*(1), e2122. https://doi.org/10.1002/biof.2122

Diver, M. M., Lin King, J. V., Julius, D., & Cheng, Y. (2022). Sensory TRP Channels in Three Dimensions. *Annual Review of Biochemistry*, *91*(1), 629–649. https://doi.org/10.1146/annurev-biochem-032620-105738

Domene, C., Darré, L., Oakes, V., & Gonzalez-Resines, S. (2022). A Potential Route of Capsaicin to Its Binding Site in the TRPV1 Ion Channel. *Journal of Chemical Information and Modeling*, *62*(10), 2481–2489. https://doi.org/10.1021/acs.jcim.1c01441

Elabscience. (2024, December 31). *Claudin 1 ELISA Kit*. https://789.bio/ea/H8irXL

Feng, J., Xu, Y., Wei, Z., Xia, Y., Zhang, H., Shen, C., Wang, P., Yan, W., Fang, D., & Fang, Y. (2022). Capsaicin inhibits migration and invasion via inhibiting epithelial-mesenchymal transition in esophageal squamous cell carcinoma by up-regulation of claudin-3 expression. *Journal of Functional Foods*, *89*, 104934. https://doi.org/10.1016/j.jff.2022.104934

Fleige, S., & Pfaffl, M. W. (2006). RNA integrity and the effect on the real-time qRT-PCR performance. *Molecular Aspects of Medicine*, *27*(2–3), 126–139. https://doi.org/10.1016/j.mam.2005.12.003

George Qing Wei Ye. (2006). *Topical treatment of psoriasis using neutralizing antibodies to interleukin-8* (YES Biotech Laboratories Ltd. Patent No. 7147854). https://patentimages.storage.googleapis.com/ed/3f/f3/992352f24ae82b/US7147854.pdf

George, R., Gallo, R. L., Cohen, J. L., Brown, M., Okeke, C. A. V., & Byrd, A. S. (2023). Reduction of Erythema in Moderate-Severe Rosacea by a Low Molecular Weight Heparan Sulfate Analog (HSA). *Journal of Drugs in Dermatology*, *22*(6), 546–553. https://doi.org/10.36849/JDD.7494

Ghasemi, M., Turnbull, T., Sebastian, S., & Kempson, I. (2021). The MTT Assay: Utility, Limitations, Pitfalls, and Interpretation in Bulk and Single-Cell Analysis. *International Journal of Molecular Sciences*, *22*(23), 12827. https://doi.org/10.3390/ijms222312827

Gouin, O., L'Herondelle, K., Lebonvallet, N., Le Gall-Ianotto, C., Sakka, M., Buhé, V., Plée-Gautier, E., Carré, J.-L., Lefeuvre, L., Misery, L., & Le Garrec, R. (2017). TRPV1 and TRPA1 in cutaneous neurogenic and chronic inflammation: Pro-inflammatory response induced by their activation and their sensitization. *Protein & Cell*, *8*(9), 644–661. https://doi.org/10.1007/s13238-017-0395-5

Graham, D. M., Huang, L., Robinson, K. R., & Messerli, M. A. (2013). Epidermal keratinocyte polarity and motility require Ca2+ influx through TRPV1. *Journal of Cell Science*, jcs.122192. https://doi.org/10.1242/jcs.122192

Gstraunthaler, G., & Lindl, T. (2021). *Zell- und Gewebekultur: Allgemeine Grundlagen und spezielle Anwendungen*. Springer Berlin Heidelberg. https://doi.org/10.1007/978-3-662-62606-1

Günzel, D., & Yu, A. S. L. (2013). Claudins and the Modulation of Tight Junction Permeability. *Physiological Reviews*, *93*(2), 525–569. https://doi.org/10.1152/physrev.00019.2012

Guo, R., Qiu, H., Li, H., Ma, D., Guan, Y., & Wang, Y. (2023). The Preemptive Analgesic Effect of Capsaicin Involves Attenuations of Epidermal Keratinocytes Proliferation and Expression of Pro-Inflammatory Mediators After Plantar Incision in Rats. *Journal of Pain Research*, *Volume 16*, 141–149. https://doi.org/10.2147/JPR.S395065

Gupta, A., Stead, T. S., & Ganti, L. (2024). Determining a Meaningful R-squared Value in Clinical Medicine. *Academic Medicine & Surgery*. https://doi.org/10.62186/001c.125154

Gupta, R., Kapoor, B., Gulati, M., Kumar, B., Gupta, M., Singh, S. K., & Awasthi, A. (2022). Sweet pepper and its principle constituent capsiate: Functional properties and health benefits. *Critical Reviews in Food Science and Nutrition*, *62*(26), 7370–7394. https://doi.org/10.1080/10408398.2021.1913989

Gupta, R., Kapoor, B., Gulati, M., Singh, S. K., & Saxena, D. (2021). The two faces of capsiate: Nutraceutical and therapeutic potential. *Trends in Food Science & Technology*, *110*, 332–348. https://doi.org/10.1016/j.tifs.2021.02.012

Han, K., Jeong, H.-J., Sung, J., Keum, Y. S., Cho, M.-C., Kim, J.-H., Kwon, J.-K., Kim, B.-D., & Kang, B.-C. (2013). Biosynthesis of capsinoid is controlled by the Pun1 locus in pepper. *Molecular Breeding*, *31*(3), 537–548. https://doi.org/10.1007/s11032-012-9811-y

Han, S., Kang, S. M., Oh, J., Lee, D. H., & Chung, J. H. (2018). Src kinase mediates UV -induced TRPV 1 trafficking into cell membrane in HaCaT keratinocytes. *Photodermatology, Photoimmunology & Photomedicine*, *34*(3), 214–216. https://doi.org/10.1111/phpp.12363

Harshitha, R., & Arunraj, D. R. (2021). Real-time quantitative PCR: A tool for absolute and relative quantification. *Biochemistry and Molecular Biology Education*, *49*(5), 800–812. https://doi.org/10.1002/bmb.21552

He, G.-J., Ye, X.-L., Mou, X., Chen, Z., & Li, X.-G. (2009). Synthesis and antinociceptive activity of capsinoid derivatives. *European Journal of Medicinal Chemistry*, *44*(8), 3345–3349. https://doi.org/10.1016/j.ejmech.2009.02.017

Hellmich, U. A., & Gaudet, R. (2014). Structural biology of TRP channels. *Handbook of Experimental Pharmacology*, *223*, 963–990. https://doi.org/10.1007/978-3-319-05161-1_10

Human IL-8 ELISA Kit. (2021). Human IL-8 ELISA Kit. https://www.abcam.com/ps/products/214/ab214030/documents/Human-IL-8-ELISA-kit-protocol-book-v2-ab214030%20(website).pdf

Idriss, H. T., & Naismith, J. H. (2000). TNF? And the TNF receptor superfamily: Structure-function relationship(s). *Microscopy Research and Technique*, *50*(3), 184–195. https://doi.org/10.1002/1097-0029(20000801)50:3<184::AID-JEMT2>3.0.CO;2-H

Iida, T., Moriyama, T., Kobata, K., Morita, A., Murayama, N., Hashizume, S., Fushiki, T., Yazawa, S., Watanabe, T., & Tominaga, M. (2003). TRPV1 activation and induction of nociceptive response by a non-pungent capsaicin-like compound, capsiate. *Neuropharmacology*, *44*(7), 958–967. https://doi.org/10.1016/S0028-3908(03)00100-X

Ilie, M., Caruntu, C., Tampa, M., Georgescu, S.-R., Matei, C., Negrei, C., Ion, R.-M., Constantin, C., Neagu, M., & Boda, D. (2019). Capsaicin: Physicochemical properties, cutaneous reactions and potential applications in painful and inflammatory conditions (Review). *Experimental and Therapeutic Medicine*. https://doi.org/10.3892/etm.2019.7513

ISO 10993-5. (2009). "Biological evaluation of medical devices –: Part 5: Tests for in vitro cytotoxicity". *International Organization for Standardization. Genf, Schweiz.*

Kaiser, M., Burek, M., Britz, S., Lankamp, F., Ketelhut, S., Kemper, B., Förster, C., Gorzelanny, C., & Goycoolea, F. M. (2018). The Influence of Capsaicin on the Integrity of Microvascular Endothelial Cell Monolayers. *International Journal of Molecular Sciences*, *20*(1), 122. https://doi.org/10.3390/ijms20010122

Khavkin, J., & Ellis, D. A. F. (2011). Aging Skin: Histology, Physiology, and Pathology. *Facial Plastic Surgery Clinics of North America*, *19*(2), 229–234. https://doi.org/10.1016/j.fsc.2011.04.003

Lee, E.-J., Jeon, M.-S., Kim, B.-D., Kim, J.-H., Kwon, Y.-G., Lee, H., Lee, Y. S., Yang, J.-H., & Kim, T.-Y. (2010). Capsiate inhibits ultraviolet B-induced skin inflammation by inhibiting Src family kinases and epidermal growth factor receptor signaling. *Free Radical Biology and Medicine*, *48*(9), 1133–1143. https://doi.org/10.1016/j.freeradbiomed.2010.01.034

Lee, Y. M., Kim, Y. K., Kim, K. H., Park, S. J., Kim, S. J., & Chung, J. H. (2009). A novel role for the TRPV1 channel in UV-induced matrix metalloproteinase (MMP)-1 expression in HaCaT cells. *Journal of Cellular Physiology*, *219*(3), 766–775. https://doi.org/10.1002/jcp.21729

Li, W. H., Lee, Y. M., Kim, J. Y., Kang, S., Kim, S., Kim, K. H., Park, C.-H., & Chung, J. H. (2007). Transient Receptor Potential Vanilloid-1 Mediates Heat-Shock-Induced Matrix Metalloproteinase-1 Expression in Human Epidermal Keratinocytes. *Journal of Investigative Dermatology*, *127*(10), 2328–2335. https://doi.org/10.1038/sj.jid.5700880

Liao, M., Cao, E., Julius, D., & Cheng, Y. (2013). Structure of the TRPV1 ion channel determined by electron cryo-microscopy. *Nature*, *504*(7478), 107–112. https://doi.org/10.1038/nature12822

Liao, M., Cao, E., Julius, D., & Cheng, Y. (2014). Single particle electron cryo-microscopy of a mammalian ion channel. *Current Opinion in Structural Biology*, *27*, 1–7. https://doi.org/10.1016/j.sbi.2014.02.005

Lieder, B., Hans, J., Hentschel, F., Geissler, K., & Ley, J. (2019). Biological Evaluation of Natural and Synthesized Homovanillic Acid Esters as Inhibitors of Intestinal Fatty Acid Uptake in Differentiated Caco-2 Cells. *Molecules*, *24*(19), 3599. https://doi.org/10.3390/molecules24193599

Liedtke, W. B., & Heller, S. (Eds.). (2007). *TRP ion channel function in sensory transduction and cellular signaling cascades*. CRC/Taylor & Francis.

Liu, T., Zhang, L., Joo, D., & Sun, S.-C. (2017). NF-κB signaling in inflammation. *Signal Transduction and Targeted Therapy*, *2*(1), 17023. https://doi.org/10.1038/sigtrans.2017.23

Mathie, K., Lainer, J., Spreng, S., Dawid, C., Andersson, D. A., Bevan, S., & Hofmann, T. (2017). Structure–Pungency Relationships and TRP Channel Activation of Drimane Sesquiterpenes in Tasmanian Pepper (*Tasmannia lanceolata*). *Journal of Agricultural and Food Chemistry*, *65*(28), 5700–5712. https://doi.org/10.1021/acs.jafc.7b02356

McKnight, G., Shah, J., & Hargest, R. (2022). Physiology of the skin. *Surgery (Oxford)*, *40*(1), 8–12. https://doi.org/10.1016/j.mpsur.2021.11.005

Merck KGaA. (2024). *Keratinocyte Growth Medium 2*. Sigma Aldrich. https://www.sigmaaldrich.com/AT/de/product/sigma/c20111

Murata, S., Kaneko, S., & Morita, E. (2021). Interleukin-8 Levels in the Stratum Corneum as a Biomarker for Monitoring Therapeutic Effect in Atopic Dermatitis Patients. *International Archives of Allergy and Immunology*, *182*(7), 592–606. https://doi.org/10.1159/000512965

Nadezhdin, K. D., Neuberger, A., Nikolaev, Y. A., Murphy, L. A., Gracheva, E. O., Bagriantsev, S. N., & Sobolevsky, A. I. (2021). Extracellular cap domain is an essential component of the TRPV1 gating mechanism. *Nature Communications*, *12*(1), 2154. https://doi.org/10.1038/s41467-021-22507-3

New England Biolabs. (2024). *LunaScript® RT SuperMix Kit*. LunaScript® RT SuperMix Kit. https://www.neb.com/en/products/e3010-luna-script-rt-supermix-kit

Nguyen, A. V., & Soulika, A. M. (2019). The Dynamics of the Skin's Immune System. *International Journal of Molecular Sciences*, *20*(8), 1811. https://doi.org/10.3390/ijms20081811

Nolan, T., Huggett, J., Sanchez, E., Sanders, R., Redshaw, N., & Wilkes, T. (2013). *Good practice guide for the application of quantitative PCR (qPCR)*. https://doi.org/10.13140/RG.2.2.15943.96162

Nygaard, U. H., Niehues, H., Rikken, G., Rodijk-Olthuis, D., Schalkwijk, J., & Van Den Bogaard, E. H. (2015). Antibiotics in cell culture: Friend or foe? Suppression of keratinocyte growth and differentiation in monolayer cultures and 3D skin models. *Experimental Dermatology*, *24*(12), 964–965. https://doi.org/10.1111/exd.12834

Otani, T., & Furuse, M. (2020). Tight Junction Structure and Function Revisited. *Trends in Cell Biology*, *30*(10), 805–817. https://doi.org/10.1016/j.tcb.2020.08.004

Peterson, S. M., & Freeman, J. L. (2009). RNA Isolation from Embryonic Zebrafish and cDNA Synthesis for Gene Expression Analysis. *Journal of Visualized Experiments*, *30*, 1470. https://doi.org/10.3791/1470

Piipponen, M., Li, D., & Landén, N. X. (2020). The Immune Functions of Keratinocytes in Skin Wound Healing. *International Journal of Molecular Sciences*, *21*(22), 8790. https://doi.org/10.3390/ijms21228790

Polishchuk, P. (2017). Interpretation of Quantitative Structure–Activity Relationship Models: Past, Present, and Future. *Journal of Chemical Information and Modeling*, *57*(11), 2618–2639. https://doi.org/10.1021/acs.jcim.7b00274

Qazi, B. S., Tang, K., & Qazi, A. (2011). Recent Advances in Underlying Pathologies Provide Insight into Interleukin-8 Expression-Mediated Inflammation and Angiogenesis. *International Journal of Inflammation*, *2011*, 1–13. https://doi.org/10.4061/2011/908468

Ranzato, E., Patrone, M., Mazzucco, L., & Burlando, B. (2008). Platelet lysate stimulates wound repair of HaCaT keratinocytes. *British Journal of Dermatology*, ???-??? https://doi.org/10.1111/j.1365-2133.2008.08699.x

Rechenberg, W. (1982). Zur Ermittlung von Ausrei ern. *Fresenius' Zeitschrift f r Analytische Chemie*, *311*(6), 590–597. https://doi.org/10.1007/BF00635536

Riss, T. L., Moravec, R. A., Niles, A. L., Duellman, S., Benink, H. A., Worzella, T. J., & Minor, L. (2004). Cell Viability Assays. In S. Markossian, A. Grossman, M. Arkin, D. Auld, C. Austin, J. Baell, K. Brimacombe, T. D. Y. Chung, N. P. Coussens, J. L. Dahlin, V. Devanarayan, T. L. Foley, M. Glicksman, K. Gorshkov, J. V. Haas, M. D. Hall, S. Hoare, J. Inglese, P. W. Iversen, … X. Xu (Eds.), *Assay Guidance Manual*. Eli Lilly & Company and the National Center for Advancing Translational Sciences. http://www.ncbi.nlm.nih.gov/books/NBK144065/

Rosenbaum, T., Gordon-Shaag, A., Munari, M., & Gordon, S. E. (2004). Ca2+/Calmodulin Modulates TRPV1 Activation by Capsaicin. *The Journal of General Physiology*, *123*(1), 53–62. https://doi.org/10.1085/jgp.200308906

Sancho, R., Lucena, C., Macho, A., Calzado, M. A., Blanco-Molina, M., Minassi, A., Appendino, G., & Muñoz, E. (2002). Immunosuppressive activity of capsaicinoids: Capsiate derived from sweet peppers inhibits NF-κB activation and is a potent antiinflammatory compound in vivo. *European Journal of Immunology*, *32*(6), 1753. https://doi.org/10.1002/1521-4141(200206)32:6<1753::AID-IMMU1753>3.0.CO;2-2

Sander, T., Freyss, J., Von Korff, M., & Rufener, C. (2015). DataWarrior: An Open-Source Program For Chemistry Aware Data Visualization And Analysis. *Journal of Chemical Information and Modeling*, *55*(2), 460–473. https://doi.org/10.1021/ci500588j

Silverman, R. B., & Holladay, M. W. (2014). *The organic chemistry of drug design and drug action* (3d edition). Elsevier/AP, Academic Press, is an imprint of Elsevier.

Southall, M. D., Li, T., Gharibova, L. S., Pei, Y., Nicol, G. D., & Travers, J. B. (2003). Activation of Epidermal Vanilloid Receptor-1 Induces Release of Proinflammatory Mediators in Human Keratinocytes. *Journal of Pharmacology and Experimental Therapeutics*, *304*(1), 217–222. https://doi.org/10.1124/jpet.102.040675

Stockert, J. C., Horobin, R. W., Colombo, L. L., & Blázquez-Castro, A. (2018). Tetrazolium salts and formazan products in Cell Biology: Viability assessment, fluorescence imaging, and labeling perspectives. *Acta Histochemica*, *120*(3), 159–167. https://doi.org/10.1016/j.acthis.2018.02.005

Szallasi, A., Cortright, D. N., Blum, C. A., & Eid, S. R. (2007). The vanilloid receptor TRPV1: 10 years from channel cloning to antagonist proof-of-concept. *Nature Reviews Drug Discovery*, *6*(5), 357–372. https://doi.org/10.1038/nrd2280

Szolcsányi, J., & Sándor, Z. (2012). Multisteric TRPV1 nocisensor: A target for analgesics. *Trends in Pharmacological Sciences*, *33*(12), 646–655. https://doi.org/10.1016/j.tips.2012.09.002

Takashima, A., Matsue, H., Bergstresser, P. R., & Ariizumi, K. (1995). Interleukin-7—Dependent Interaction of Dendritic Epidermal T Cells with Keratinocytes. *Journal of Investigative Dermatology*, *105*(1), S50–S53. https://doi.org/10.1038/jid.1995.10

Thermofisher Scientific. (2024). *DMEM, high glucose, GlutaMAX™ Supplement*. Thermofisher. https://www.thermofisher.com/order/catalog/product/10566016?ef_id=CjwKCAjw5ImwBhBtEiwAFHDZx7amhvgBESoejMc1WIlDHSAPW41acHcgNgbORy4yec8zJ5XV0meS1BoC0pIQAvD_BwE:G:s&s_kwcid=AL!3652!3!530347123812!!!g!!!382790548!127140246227&cid=bid_clb_cce_r01_co_cp0000_pjt0000_bid00000_0se_gaw_dy_pur_con&s_kwcid=AL!3652!3!530347123812!!!g!!&gad_so

urce=1&gbraid=0AAAADxi_GSH44YdLfNpND0AfvMSXXwGL&gclid=CjwKCAjw5ImwBhBtEiwAFHDZx7amhvgBESoejMc1WIlDHSAPW41acHcgNgbORy4yec8zJ5XV0meS1BoC0pIQAvD_BwE
Thermofisher Scientific. (2025). *Overview of Cell Lysis and Protein Extraction*. Overview of Cell Lysis and Protein Extraction. https://www.thermofisher.com/at/en/home/life-science/protein-biology/protein-biology-learning-center/protein-biology-resource-library/pierce-protein-methods/traditional-methods-cell-lysis.html

thermoscientific. (2024, April 3). *PierceTM BCA Protein Assay Kit*. https://assets.thermofisher.com/TFS-Assets/LSG/manuals/MAN0011430_Pierce_BCA_Protein_Asy_UG.pdf

Tokumasu, R., Yamaga, K., Yamazaki, Y., Murota, H., Suzuki, K., Tamura, A., Bando, K., Furuta, Y., Katayama, I., & Tsukita, S. (2016). Dose-dependent role of claudin-1 in vivo in orchestrating features of atopic dermatitis. *Proceedings of the National Academy of Sciences*, *113*(28). https://doi.org/10.1073/pnas.1525474113

Tominaga, M. (2005). Molecular Mechanisms of Trigeminal Nociception and Sensation of Pungency. *Chemical Senses*, *30*(Supplement 1), i191–i192. https://doi.org/10.1093/chemse/bjh179

Umumura, S.; Iwata, F.; Ataka, K.; Shiraishi, H. Process for Preparation of 3-Alkoxy-4-hydroxyphenylacetic Acid. U.S. Patent 4,401,830, 30 August 1983.
ISO

Vos, M. H., Neelands, T. R., McDonald, H. A., Choi, W., Kroeger, P. E., Puttfarcken, P. S., Faltynek, C. R., Moreland, R. B., & Han, P. (2006). TRPV1b overexpression negatively regulates TRPV1 responsiveness to capsaicin, heat and low pH in HEK293 cells. *Journal of Neurochemistry*, *99*(4), 1088–1102. https://doi.org/10.1111/j.1471-4159.2006.04145.x

Wiesmann, U. N. (1999). Segregating Cells—Proteases in Tissue Culture. In E. E. Sterchi & W. Stöcker (Eds.), *Proteolytic Enzymes* (pp. 298–311). Springer Berlin Heidelberg. https://doi.org/10.1007/978-3-642-59816-6_17

Xiao, T., Sun, M., Zhao, C., & Kang, J. (2023). TRPV1: A promising therapeutic target for skin aging and inflammatory skin diseases. *Frontiers in Pharmacology*, *14*. https://doi.org/10.3389/fphar.2023.1037925

Xu, X., Yu, C., Xu, L., & Xu, J. (2022). Emerging roles of keratinocytes in nociceptive transduction and regulation. *Frontiers in Molecular Neuroscience*, *15*, 982202. https://doi.org/10.3389/fnmol.2022.982202

Yamanaka, K., Yamamoto, O., & Honda, T. (2021). Pathophysiology of psoriasis: A review. *The Journal of Dermatology*, *48*(6), 722–731. https://doi.org/10.1111/1346-8138.15913

Yang, F., Xiao, X., Cheng, W., Yang, W., Yu, P., Song, Z., Yarov-Yarovoy, V., & Zheng, J. (2015a). Structural mechanism underlying capsaicin binding and activation of the TRPV1 ion channel. *Nature Chemical Biology*, *11*(7), 518–524. https://doi.org/10.1038/nchembio.1835

Yang, F., Xiao, X., Cheng, W., Yang, W., Yu, P., Song, Z., Yarov-Yarovoy, V., & Zheng, J. (2015b). Structural mechanism underlying capsaicin binding and activation of the TRPV1 ion channel. *Nature Chemical Biology*, *11*(7), 518–524. https://doi.org/10.1038/nchembio.1835
Yang, F., & Zheng, J. (2017). Understand spiciness: Mechanism of TRPV1 channel activation by capsaicin. *Protein & Cell*, *8*(3), 169–177. https://doi.org/10.1007/s13238-016-0353-7
Yang, P., Feng, J., Luo, J., Madison, M., & Hu, H. (2017). A Critical Role for TRP Channels in the Skin. In T. L. R. Emir (Ed.), *Neurobiology of TRP Channels* (1st ed., pp. 95–111). CRC Press. https://doi.org/10.4324/9781315152837-6

Yang, R., Xiong, Z., Liu, C., & Liu, L. (2014). Inhibitory effects of capsaicin on voltage-gated potassium channels by TRPV1-independent pathway. *Cellular and Molecular Neurobiology*, *34*(4), 565–576. https://doi.org/10.1007/s10571-014-0041-1

Young, C. N., Koepke, J. I., Terlecky, L. J., Borkin, M. S., Boyd, S. L., & Terlecky, S. R. (2008). Reactive oxygen species in tumor necrosis factor-alpha-activated primary human keratinocytes: Implications for psoriasis and inflammatory skin disease. *The Journal of Investigative Dermatology*, *128*(11), 2606–2614. https://doi.org/10.1038/jid.2008.122

Yousef, H., Alhajj, M., Fakoya, A. O., & Sharma, S. (2025). Anatomy, Skin (Integument), Epidermis. In *StatPearls*. StatPearls Publishing. http://www.ncbi.nlm.nih.gov/books/NBK470464/

Zhang, K., Julius, D., & Cheng, Y. (2021). Structural snapshots of TRPV1 reveal mechanism of polymodal functionality. *Cell*, *184*(20), 5138-5150.e12. https://doi.org/10.1016/j.cell.2021.08.012

8. Aid Directory

AI Tool	Use	Affected Parts of the Work	Remarks
SciSpace	Literature search	Only used for part of the discussion Page 63: (Qazi et al., 2011), (George Qing Wei Ye, 2006), (Murata et al., 2021)Page 65: (Di Meo et al., 2025), (S. Han et al., 2018), (Xu et al., 2022)	—
Zotero	Literature management and citation management	Citations throughout the entire master's thesis	—
OpenAI ChatGPT	Transforming bullet points into fluent text	Method section pages 25–33: • 3.3 Cell Culture, 1st paragraph • 3.3.1 Sub-cultivation • 3.4 MTT Assay Protocol, last paragraph • 3.5 Treatment HaCaT-cell line • 3.6 RNA Isolation and Purification, 2nd paragraph • 3.9 ELISA, last paragraph	Prompt example: “Take the following CONTEXT and revise it, turning bullet points into a fluent text.”Final version was reviewed and edited by the author.
Grammarly	Editing	Spelling, grammar, punctuation, and style (scientific wording, English: USA) throughout the entire master's thesis	Prompt example: “Take the following CONTEXT and revise it. Make it more scientific and objective.”
Microsoft Editor	Editing	Spelling, grammar, punctuation, and style (scientific wording, English: USA) throughout the entire master's thesis	—

9.Appendix

Table 15 Raw data for determining cell viability in HaCaT cells after 24-hour treatment with 10 µM homovanillic acid esters compared to the solvent control ddH_2O (0.1 % ddH_2O)

The data is expressed as a percentage change relative to the ddH_2O control and have been cleaned of outliers using the Nalimov test.

	ddH$_2$O	DMSO	CAP	CTE	1	2	3	4	5	6	7	8	9	10	11	12	13	14	15	16
PLATE 1		66.01	55.56	85.73	87.75	85.56	87.75	54.72	79.49		88.43	70.562	48.15	47.30			56.24			
	121.29	82.36	41.74	70.06	63.15	66.69	68.54	86.74	83.37	180.128	71.40	84.719		44.27	176.502	76.766	58.09	82.660	212.769	77.219
	112.53	117.08	52.02	43.43	66.18	56.24	49.49	69.38	59.94		62.64		47.81	43.93		122.100	73.26	133.887		
	66.18	70.56	67.70		49.66	49.83	50.34	46.12	57.58		53.54		29.44	41.40						
	91.273	195.089																		
	104.873	233.623																		
	109.860	258.557																		
	93.993	242.690																		
PLATE 2	111.31	97.87	144.05	162.93	68.86	57.35	73.70	23.44	98.29	70.07	54.56	87.51	66.86		46.63	99.66	160.54	55.17	67.34	96.84
	101.26	68.25		143.20	68.25	54.99	99.50	22.35	75.52	62.13	51.36	75.52	74.67		56.08	149.66	171.26	59.83	58.56	76.97
	104.35	76.25	143.54	160.20	62.20	45.90	75.34		50.87	55.29	47.66	71.58	69.28	112.76	53.47	158.67			49.66	63.83
PLATE 3	83.09	76.91	143.71	153.57	50.14	44.21	49.66	11.26	58.14	59.11	40.39	65.40	64.44	146.94	58.62	158.84	178.40		57.05	62.98
	120.58	74.66																		
	120.24	74.83																		
	59.18	100.34																		
		51.19																		
PLATE 4		103.64	59.35	72.07	92.85	102.42	101.58	86.59	129.60	108.72	102.88	120.57	90.66	49.82	113.01	74.41	120.96	113.05	131.74	98.47
	89.15	94.23	72.65	84.44	102.97	119.90	109.69	104.14	128.42	108.01	110.24	115.91	87.30	60.24	103.26	56.04	99.71	108.81	137.58	115.65
	97.05	108.30	61.11	126.42	101.08	115.99	97.13	103.30	115.07	96.37	104.06	107.71	92.17	61.61	109.52	46.80	88.68	104.82	123.68	110.24
PLATE 5	113.81	90.37	65.67	135.55	89.48	95.70	91.71	86.33	122.75	79.66	100.78	102.21	79.11	49.93	98.31	47.92	99.42	105.91	106.79	103.81
	32.42	81.20																		
		84.26																		
	141.41	136.30																		
	126.17																			
PLATE 6	98.38	172.32		31.27		135.94		153.80	146.27	138.89	150.18			82.51	151.22	23.87	59.56	164.28	100.07	112.18
	102.95	145.54	39.05	32.55	152.47	141.11	137.93		139.78	151.00	145.31	97.86	129.89	86.31	158.89	27.15	54.41	151.59	144.50	169.15
PLATE 7	99.26	163.17	19.31	36.54	146.57				154.24	142.58	138.01	106.05		60.27	158.23	22.01	69.85	144.21	152.99	134.39
	99.41	154.46	20.15	31.14	149.00	123.54	154.76	127.16	141.40	157.86	151.73	74.39	140.30	64.70	116.31			141.99	138.15	136.53
	81.16	100.64																		
	109.00	96.08																		
	99.23	63.09																		
	110.61																			
PLATE 8	105.79	103.07	103.41	115.92	96.61	100.08	110.28	114.63	114.29	88.72	115.24	100.21	116.33	103.10	85.42	88.20	87.64	82.74	93.63	146.85
	97.43	94.16	105.38	86.48	110.96	106.26	74.58	129.24	142.71	91.69	138.97	116.12	112.25	75.24	52.34	72.18	75.67	86.79	71.61	135.16
PLATE 9	83.49	66.22	108.92	80.91	72.34	63.50	53.85	128.43	106.74	66.48	81.18	107.22	69.01	48.71	35.13		43.90	53.00	48.19	144.75
			80.43		98.45			73.09	119.59	58.46	106.20	66.49				135.57	64.68	57.61		147.13
	111.23	107.01																		
	100.76	104.70																		
		100.41																		
	68.06	114.74																		
	100.00																			

	91.98																			
	94.10																			
	115.64																			
	98.29																			
Mean	**99.15**	**112.71**	**76.87**	**91.80**	**91.00**	**86.96**	**87.40**	**83.57**	**106.20**	**100.89**	**95.74**	**92.36**	**82.35**	**69.36**	**98.31**	**84.99**	**91.90**	**102.90**	**105.89**	**113.66**
Std. dev	19.56	51.11	39.88	46.80	31.56	32.68	30.40	41.74	33.53	39.76	36.87	18.94	30.55	29.06	45.59	47.81	42.20	36.73	46.28	31.66
Std dev [%]	19.73	45.35	51.87	50.98	34.69	37.58	34.78	49.94	31.57	39.41	38.51	20.51	37.09	41.90	46.37	56.25	45.92	35.69	43.70	27.85
Count	28	30	14	15	15	15	14	13	16	13	16	13	13	14	13	13	13	12	13	13

table 16 additional raw data of R16.

Raw data for determining cell viability in HaCaT cells after 24-hour treatment with 10 µM homovanillic acid esters compared to the solvent control ddH_2O (0.1 % ddH_2O) The data are expressed as a percentage change relative to the ddH_2O control.

16	
PLATE 6	79.47
	134.59
	145.25
	129.01
Average	**122.08**
Std. dev	29.20
Std dev [%]	23.91
Count	4
PLATE 7	99.07
	80.99
	88.47
	92.51
Average	**90.26**
Std. dev	7.57
Std dev [%]	8.39
Count	4

Table 17.1 CLDN1 gene expression fold change compared to DMSO control (0.1%)

pretreated HaCaT skin cells (24h homovanillic acid esters 10 µM) and 20 ng/ml TNF-α for 6 h) and the descriptive analysis (mean, SD, SD % and count) Data is cleaned via NALIMOV.

	DMSO+TNFα	ddH20	ddH20+ TNFα	CAP	CTE	1	2	3	4	5
Plate1	1.09	0.52		0.77	1.45	2.24	1.37	3.78	1.5	2.15
	1.01		5.35	0.75	1.36	1.88	1.46	3.84	1.81	2.2
	0.9			0.86	1.46			4.03	1.72	2.17
Plate2	1.04	0.24	0.9	1.1	0.44	1.08	0.21	1.54	0.45	2.23
	1.1	0.26	0.89	0.85	0.6	1.12	0.22	1.57	0.49	2.45
	0.86	0.24	0.81	1.13	0.56	1.27	0.21	1.27	0.5	
Plate3	0.83	0.35	1.17	0.88	0.82	0.27	0.74	1.8	0.8	2.28
	1.14	0.35	1.25	0.88	0.92	0.28	0.72	1.97	0.79	2.29
	1.02	0.36	1.16	0.89	0.93	0.28	0.71	1.86	0.72	2.24
Plate4	0.93	0.28	1.23	1.04	0.83		0.67	1.28	1.27	1.48
	1.04	0.27	1.19		0.88		0.64	1.58	1.42	2.09
	1.03	0.34	1.23	0.83	0.85		0.59	1.87	1.25	2.11
Plate5	1.01	0.28	1.11	1.05	0.81	0.98	0.71	2.57	0.49	1.46
	0.91	0.34	1.19	1.1	0.8	1.23	0.75	4.03	0.5	
	1.08	0.32	1.13	1.11	0.88	1.41	0.79	3.35	0.57	1.63
Mean	1.00	0.32	1.43	0.95	0.906	1.10	0.70	2.42	0.95	2.06
Std. dev	0.09	0.07	1.19	0.14	0.30	0.64	0.37	1.07	0.49	0.32
Std. Dev [%]	9.28	23.29	82.82	14.34	33.36	58.47	52.71	44.08	51.555	15.60
Count	15	13	13	14	15	11	14	15	15	13

Table 17.2 CLDN1 gene expression fold change compared to DMSO control (0.1%)
pretreated HaCaT skin cells (24h homovanillic acid esters 10 µM) and 20 ng/ml TNF-α for 6 h) and the descriptive analysis (mean, SD, SD % and count) Data is cleaned via NALIMOV

	6	7	8	9	10	11	12	13	14	15	16
Plate1	2.58	1.3	1.24	2.72	3.17		3.04	2.83		3.34	2.55
				2.64	3.11		3.06	3.34	1.9	3.7	2.87
			1.31	2.66	3.29	2.03		3.06	1.8		
Plate2	1.09	0.53	0.86	0.36	0.87	0.88	0.9	0.97	0.88	1.56	1.53
	1.06	0.54	0.79	0.37	1.09	0.77	0.94	1.05	0.77	1.6	1.38
	1.1	0.53	0.79	0.45	1.08	0.77	0.93	0.97	0.82	1.2	1.73
Plate3	1.23	0.58	0.93	0.99	1.52	1.18	1.84	2.57	0.58	1.46	1.29
	1.14	0.65	0.89	1.1	1.7	1.19	1.87	2.48	0.63	1.29	1.09
	1.21	0.61	0.83	1.06	1.85	1.15	1.77	2.56	0.52	1.72	1
Plate4	0.95	0.48	0.97	0.6	2.18	0.78	1.53	1.56	1.15	1.98	1.14
	0.68	0.49	1.02	0.82	2.44	0.95	1.72	1.62	1.01	2.13	1.37
	0.92	0.6	0.91	0.84	2.38	0.76	1.29	1.4	1.11	1.94	1.59
Plate5	1.11	0.55	0.74	1.49	2.35	1	1.39	0.06	1.06	3.2	0.58
	1.22	0.65	0.7	1.63	2.32	1.12	1.63	0.07	1.02	3.26	0.92
	0.97	0.55	0.77	1.42	3.05	0.89	1.71	0.09	0.91	3.24	0.77
Mean	1.17	0.62	0.91	1.277	2.16	1.04	1.69	1.64	1.01	2.26	1.42
Std. dev	0.45	0.21	0.18	0.82	0.80	0.34	0.67	1.12	0.40	0.89	0.64
Std. Dev [%]	38.21	34.07	19.63	64.20	36.86	32.86	39.62	67.91	40.12	39.22	45.03
Count	13	13	14	15	15	13	14	15	14	14	14

Table 18.1 IL8 gene expression fold change compared to DMSO control (0.1%)

*pretreated HaCaT skin cells (24h homovanillic acid esters 10 µM) and 20 ng/ml TNF-α for 6 h) and the descriptive analysis (mean, SD, SD % and count) Data is cleaned via NALIMOV. Numbers marked with * were not considered.*

	DMSO+TNFα	ddH20	ddH20+ TNFα	CAP	CTE	1	2	3	4	5
Plate1	1.07	0.04		0.9		*8.74**			1.65	
	1.04	0.04		0.86	2.71	*8.3**		4.9	1.87	
	0.89	0.03		1	2.79	*8.03**	2.26	4.7	1.93	2.03
Plate2	1.02	0.01	1.08	1.4	0.73	1.25	0.5	1.15	1.01	1.83
	0.93	0.01	1.04	1.12	0.72	1.44	0.48	1.47	1.21	1.81
	1.04	0.01	1.04	1.36	0.78	1.57	0.49	1.1	1.17	1.58
Plate3	1.08	0.04	1.19	1.29	1.38	1.92	0.85	1.65	0.63	1.59
	1.08	0.04	1.35	1.25	1.46	2.14	0.93	1.88	0.71	1.94
	0.84	0.04	1.27	1.13	1.32	1.8	0.87	0.95	0.49	1.95
Plate4	1	0.02	1.04	0.95	0.97		0.72	1.29	1.21	1.18
	1.01	0.02	1.07	0.98			0.7	1.39	1.2	1.4
	0.99	0.02	1	0.92	0.91		0.72	1.36	0.88	1.36
Plate5	1.24	0.01	1.04	1.24	0.93	1.63	0.69	2.65	0.63	0.92
	1.21	0.01	0.94	0.87	0.83	1.65	0.69	2.62	0.66	0.66
		0.01	0.85		0.67	1.62	0.68	1.52	0.17	0.71
Mean	1	0.02	1.1	1.1	1.2	1.7	0.81	2	1	1.5
Std. dev	0.11	0.013	0.14	0.19	0.72	0.26	0.46	1.3	0.51	0.47
Std. Dev [%]	11.00	56.52	12.73	17.27	60.00	15.29	56.79	65.00	51.00	31.33
Count	14	15	12	14	13	9	13	14	15	13

Table 18.2 IL8 gene expression fold change compared to DMSO control (0.1%)

*pretreated HaCaT skin cells (24h homovanillic acid esters 10 µM) and 20 ng/ml TNF-α for 6 h) and the descriptive analysis (mean, SD, SD % and count) Data is cleaned via NALIMOV. Numbers marked with * were not considered*

	6	7	8	9	10	11	12	13	14	15	16
Plate1	3.69	1.48	2.06	0.25	5.55	5.24		4.69	4.11	3.84	2.59
			2.11	0.3	5.61		3.93	4.64			3.21
			2.07	0.29	4.6		4.01		4.21		2.23
Plate2	0.86	0.99	1.05	0.85	1.46	0.94	1.05	0.59	1.23	1.44	0.8
	0.89	0.95	1.23		1.6	1.12	1.07	0.97	1.26	1.49	0.82
	0.98	1.06	1.23	1.11	1.34	1.22	1.11	1	1.23	1.44	1.07
Plate3	0.93	0.72	1.34	1.4	2.33	1.55	1.24	2.24	0.37	1.36	
	0.98	0.8	1.35	1.59	2.51	1.55	1.53	2.11	0.39	1.4	
	1.3	0.82	1.27	1.49	2.42	1.54	1.68	2.66	0.42	0.75	
Plate4	0.86	0.98	0.88	0.92	1.65	1.11	1.36	0.85	1.04	1.14	0.32
	0.96	1.04	0.89	1.04	1.64	1.08	1.42	1.08	1.11	1.17	0.36
	0.86	1.27	0.84	1.09	1.48	1.03	1.26	1.09	0.85	1.2	0.33
Plate5	1.1	0.65	0.89	1.4	4.09	1.05	1.51	0.96	1.04	0.93	0.37
	1.04	0.61	0.88	0.38	4	1	1.42	1.01	0.92	1.02	0.72
	1.09	0.64	0.93	0.56	4.62	1.16	1.38	0.94	1.14	0.9	0.69
Mean	1.2	0.92	1.3	0.91	3	1.5	1.7	1.8	1.4	1.4	1.1
Std. dev	0.76	0.26	0.46	0.48	1.6	1.1	0.97	1.4	1.2	0.77	0.99
Std. Dev [%]	63.33	28.26	35.38	52.75	53.33	73.33	57.06	77.78	85.71	55.00	90.00
Count	13	13	15	14	15	13	14	14	14	13	12

Table 19.1 raw data of IL-8 release shown as fold change compared DMSO control (0.1%)

pretreated HaCaT skin cells (24h homovanillic acid esters 10 µM) and 20 ng/ml TNF-α for 6 h) and the descriptive analysis (mean, SD, SD % and count) Data is cleaned via NALIMOV. R11 was tested 11th times with the 11th value being 0.81 which was taken into account for the descriptive analysis and the statistical analysis.

	DMSO+TNFα	ddH_2O	ddH_2O +TNFα	CAP	CTE	1	2	3	4	5
Plate1	0.99		1.44	1	1.45	0.64	1.06	0.87	1.11	0.94
	1.01	0.24	1	0.93	1.48	0.73	1.07		1.11	0.87
Plate2	0.99	-0.01	1.32	1.22	1.42	1.17	1.32	1.05	1.15	0.88
	1.01	-0.05	1.38	1.24	1.45	1.14	1.29	1.19	1.23	0.91
Plate3	0.99	0.01	1.05	1.33	1.17	1.15	0.63	0.71	0.4	0.63
	1.01	0.02	1.83	1.31	1.13	1.17	0.71	0.75	0.41	0.72
Plate4	0.99		1.55	0.92	1.08	0.84	0.96	0.66	0.66	0.64
	1.01	-0.07		1	1.14	0.91	1	0.79	0.73	0.66
Plate5		-0.36	0.71	0.78		1.35	1.29	1.09	0.99	0.42
		-0.29	0.76	0.99	1.34	1.31	1.14	1.14	0.96	0.44
Mean	1	-0.064	1.2	1.1	1.3	1	1	0.92	0.88	0.71
Std. dev	0.011	0.19	0.37	0.19	0.16	0.24	0.24	0.2	0.31	0.19
Std. Dev [%]	1.10	- 296.88	30.83	17.27	12.31	24.00	24.00	21.74	35.23	26.76
Count	8	8	9	10	9	10	10	9	10	10

table 19.2 raw data of IL-8 release shown as fold change compared DMSO control (0.1%)

pretreated HaCaT skin cells (24h homovanillic acid esters 10 µM) and 20 ng/ml TNF-α for 6 h) and the descriptive analysis (mean, SD, SD % and count) Data is cleaned via NALIMOV. R11 was tested 11th times with the 11th value being 0.81 which was taken into account for the descriptive analysis and the statistical analysis.

	6	7	8	9	10	11	12	13	14	15	16
Plate1	1.26	1.12	1.47	1.04	1.15	0.96	0.97	1.05	1	1.28	0.9
	1.16	1.74	1.44	1.1	1.1	1.11	1	1.17	1.07		0.87
Plate2	0.95	1.4	1.13		1.02	0.92	0.93	1.09	1.29	0.77	0.69
	1.07	1.5	1.07	1.68	1.03	1.01	0.93	1.18	1.17	0.84	0.72
Plate3	0.83	0.62	1.08	0.96	0.93	0.8	0.78	0.93	0.72	0.73	0.53
	0.93	0.64	1.23	1.12	0.8	0.73	0.71	1.07	0.72	0.7	0.53
Plate4	1	0.69	1	0.91	0.12	0.83	0.65	0.69	0.94	0.74	0.33
	0.98	0.66	1.02	0.93	0.12	0.89	1.04	0.74	0.83	0.71	0.33
Plate 5	0.84	1.02	0.98	1.09	0.45	0.57	0.93	0.56	0.79	0.54	0.52
		0.97	1.19	1.12	0.25		0.8	0.49	0.48	0.61	0.43
Mean	1	1	1.2	1.1	0.71	0.87	0.87	0.9	0.9	0.77	0.59
Std. dev	0.14	0.4	0.17	0.23	0.4	0.16	0.13	0.26	0.24	0.21	0.2
Std. Dev [%]	14.00	40.00	14.17	20.91	56.34	18.39	14.94	28.89	26.67	27.27	33.90
Count	9	10	10	9	11	9	10	10	10	9	10

table 20 CLDN1 gene expression expressed as fold change compared to the untreated sample (without capsazepine (CAPSZ))

pretreated HaCaT skin cells (24h homovanillic acid esters 10 µM as well as 1 µM CAPZ and 20 ng/ml TNF-α for 6 h) and the descriptive analysis (mean, SD, SD % and count) Data is cleaned via NALIMOV.

	CTE +	CTE	15+	15	16+	16	5+	5
PLATE1	0.99	1		1.14	1.74	1.14	1.02	1.07
	1	1.03	1.15	0.87	1.76	1.06	0.6	1.01
	1.11	0.97	1.12	0.99			1.05	0.93
PLATE2	1.2	0.73	1.47	1.05	1.12	1.02	1.94	1.06
	1.07	1.11	1.09	0.93	1.07	0.97	2.08	0.99
	0.96	1.16	1.52	1.02	1.07	1.01	1.77	0.94
PLATE3	0.81	1.04	1.43	1.13	1.2	0.95	0.97	1.02
	0.76	0.96	1.33	0.94	1.08	1	0.71	0.97
	0.76	1	1.3	0.92	1.07	1.05	0.89	1.01
PLATE4	0.98	0.93	1.15	1	0.98	1.08	1.01	0.92
	0.96	1.07	1.1	0.98	0.98	0.95	1.02	1.03
	0.98	1	1.16	1.02	0.96	0.97	1.02	1.05
PLATE5	*3.9**	1.16			1.09	1.05	1.75	
	*3.77**	0.91	1.49	1.21	1.21	0.9	2.07	1.14
		0.93	1.58	1.06	1.11	1.05	2.06	1.08

Mean	0.97	1.00	1.30	1.02	1.17	1.01	1.33	1.02
Std. dev	0.13	0.11	0.18	0.09	0.25	0.06	0.54	0.06
Std. Dev [%]	13.90	10.82	13.89	9.23	21.68	6.21	40.63	6.16
Count	12	15	13	14	14	14	15	14

table 21 IL8 gene expression expressed as fold change compared to the untreated sample (without capsazepine (CAPSZ))

*pretreated HaCaT skin cells (24h homovanillic acid esters 10 µM as well as 1 µM CAPZ and 20 ng/ml TNF-α for 6 h) and the descriptive analysis (mean, SD, SD % and count) Data is cleaned via NALIMOV. Numbers marked with * were not considered.*

	CTE +	CTE	15+	15	16+	16	5+	5
PLATE1	1.16	1.03	1.14	1.12	1.03	1.05	1.01	1.05
	1.37	1.03	0.93	0.87	0.91	0.95	0.9	0.95
	1.21	0.95	1.22	1.01	0.96	1	1	1
PLATE2	1.08	0.96	1.21	1.05	0.9	1.04	0.72	1
	1.08	1.01	1.24	1	0.92	0.98	0.71	0.99
	0.9	1.03	1.21	0.94	0.9	0.98	0.66	1.01
PLATE3	1.16	0.97		1.1	0.72	1.04	0.81	1
	1.02	1.04		1.02	0.82	1	0.78	1.07
	0.81	0.99	*3.69**	0.88	0.8	0.96	0.67	0.93
PLATE4	0.4	0.92	0.76	1.02	1.02	0.82	0.9	0.99
	0.83		0.67	1.03	0.96	1.09	0.87	0.98
	0.75	0.97	0.5	0.95	1.04	1.09	0.87	1.03
PLATE5	1.36	0.93	0.77	0.99	0.79			1.08
	1.46	1.03	1.02	0.89	0.87	1.09		
	1.43	1.04	1.08	1.13		1.15	1	1.03

Mean	1.07	0.99	0.98	1.00	0.90	1.02	0.84	1.01
Std. dev	0.29	0.04	0.25	0.08	0.10	0.08	0.12	0.04
Std. Dev [%]	27.41	4.28	25.57	8.25	10.65	7.98	14.86	4.16
Count	15	14	12	15	14	14	13	14

table 22 IL-8 release expressed as fold change compared to the untreated sample (without capsazepine (CAPSZ))

pretreated HaCaT skin cells (24h homovanillic acid esters 10 µM as well as 1 µM CAPZ and 20 ng/ml TNF-α for 6 h) and the descriptive analysis (mean, SD, SD % and count) Data is cleaned via NALIMOV.

	CTE	CTE +	16	16+	15	15+	5	5+
Plate1	1.09	1.07	0.87	0.83	0.93	0.96	0.97	1.09
	0.91	0.89	1.13	1.17	1.07	0.91	1.03	1.15
Plate2	0.95	1.24	0.98	0.99	1	1.26	0.98	0.98
	1.05	1.26	1.02	1.05	1	1.33	1.02	1.09
Plate3	0.9	1.13	0.8	0.68	0.96	1.22	0.97	0.91
	1.1	1.16	1.2	0.65	1.04	1.25	1.03	0.97
Plate4	1.03	0.99		0.94		0.64		0.91
	0.87	0.98		0.93		0.7		0.83
Plate 5	0.42	1.16	0.91	0.94	1	1.54	1.01	0.9
			1.09	1	1	1.64	0.99	0.8
Mean	0.92	1.1	1	0.92	1	1.1	1	0.96
Std. dev	0.21	0.12	0.14	0.16	0.04	0.33	0.026	0.12
Std. Dev [%]	22.83	10.91	14.00	17.39	4.30	30.00	2.60	12.50
Count	9	9	8	10	8	10	8	10

table 23 raw SAR Data (part 1: length group)

fold changes (IL-8 and CLDN1 gene expression IL-8 release) used to make assumptions about the effect of different structural modifications (showing only the lenght group)

	IL-8 Gene Expr. Fold change_1	IL-8 release_1	CLDN1 Expression Fold change_1	IL-8 Gene Expr. Fold change_2	IL-8 release_2	CLDN1 Expression Fold change_2	DELTA_IL-8 Gene Expr.	DELTA_IL-8 release	DELTA_CLDN1 Expression	Il 8 gene exp fold change	Il 8 release fold change	CLDN1 gene expression fold change
R1	1.53	0.92	0.89	0.52	0.99	0.69	-1.01	0.07	-0.20	0.34	1.07	0.78
R1	1.53	0.92	0.89	0.99	1.06	0.84	-0.54	0.14	-0.04	0.65	1.15	0.95
R2	0.99	0.95	0.72	0.52	0.99	0.69	-0.48	0.04	-0.04	0.52	1.04	0.95
R2	0.99	0.95	0.72	0.89	0.96	0.96	-0.11	0.01	0.23	0.89	1.01	1.32
R2	0.99	0.95	0.72	0.99	1.06	0.84	-0.01	0.11	0.12	0.99	1.12	1.16
R2	0.99	0.95	0.72	1.18	0.82	1.31	0.18	-0.13	0.59	1.18	0.86	1.81
R2	0.99	0.95	0.72	1.53	0.92	0.89	0.53	-0.03	0.16	1.53	0.97	1.22
R4	1.83	0.72	2.32	0.52	0.99	0.69	-1.31	0.27	-1.63	0.28	1.37	0.30
R4	1.83	0.72	2.32	0.89	0.96	0.96	-0.94	0.24	-1.36	0.49	1.33	0.41
R4	1.83	0.72	2.32	0.94	0.88	0.84	-0.88	0.16	-1.48	0.52	1.21	0.36
R4	1.83	0.72	2.32	0.99	1.06	0.84	-0.84	0.34	-1.48	0.54	1.47	0.36
R4	1.83	0.72	2.32	0.99	0.95	0.72	-0.83	0.23	-1.60	0.54	1.32	0.31
R4	1.83	0.72	2.32	1.18	0.82	1.31	-0.65	0.10	-1.01	0.65	1.13	0.56
R4	1.83	0.72	2.32	1.53	0.92	0.89	-0.30	0.20	-1.43	0.84	1.28	0.38
R5	0.94	0.88	0.84	0.52	0.99	0.69	-0.43	0.11	-0.15	0.55	1.13	0.82
R5	0.94	0.88	0.84	0.89	0.96	0.96	-0.05	0.09	0.12	0.94	1.10	1.14
R5	0.94	0.88	0.84	0.99	1.06	0.84	0.04	0.18	0.04	1.05	1.21	1.01
R5	0.94	0.88	0.84	0.99	0.95	0.72	0.05	0.07	-0.11	1.06	1.08	0.86
R5	0.94	0.88	0.84	1.18	0.82	1.31	0.24	-0.06	0.47	1.25	0.93	1.56
R5	0.94	0.88	0.84	1.53	0.92	0.89	0.58	0.05	0.05	1.62	1.05	1.06
R6	1.05	1.02	0.93	0.52	0.99	0.69	-0.54	-0.03	-0.25	0.49	0.97	0.74
R6	1.05	1.02	0.93	0.89	0.96	0.96	-0.16	-0.06	0.02	0.84	0.94	1.03
R6	1.05	1.02	0.93	0.94	0.88	0.84	-0.11	-0.14	-0.10	0.89	0.86	0.90
R6	1.05	1.02	0.93	0.99	1.06	0.84	-0.07	0.04	-0.09	0.94	1.04	0.90
R6	1.05	1.02	0.93	0.99	0.95	0.72	-0.06	-0.07	-0.21	0.94	0.93	0.78
R6	1.05	1.02	0.93	1.18	0.82	1.31	0.13	-0.20	0.38	1.12	0.80	1.40
R6	1.05	1.02	0.93	1.53	0.92	0.89	0.47	-0.10	-0.05	1.45	0.91	0.95
R6	1.05	1.02	0.93	1.61	0.79	2.55	0.56	-0.24	1.62	1.53	0.77	2.74
R6	1.05	1.02	0.93	1.83	0.72	2.32	0.77	-0.30	1.39	1.73	0.71	2.49

table 24 raw SAR Data (part 2: ramification group)

fold changes (IL-8 and CLDN1 gene expression IL-8 release) used to make assumptions about the effect of different structural modifications (showing only the ramification group)

	IL-8 Gene Expr. Fold change_1	IL-8 release_1	CLDN1 Expression Fold change_1	IL-8 Gene Expr. Fold change_2	IL-8 release_2	CLDN1 Expression Fold change_2	DELTA_IL-8 Gene Expr.	DELTA_IL-8 release	DELTA_CLDN1 Expression	IL-8 Gene Expr. Fold change	IL-8 release fold change	CLDN1 Expression fold change
R7	0.89	0.96	0.96	0.52	0.99	0.69	-0.37	0.03	-0.27	0.58	1.03	0.72
R7	0.89	0.96	0.96	0.99	1.06	0.84	0.10	0.10	-0.12	1.11	1.10	0.88
R7	0.89	0.96	0.96	1.18	0.82	1.31	0.29	-0.15	0.35	1.33	0.85	1.37
R7	0.89	0.96	0.96	1.53	0.92	0.89	0.64	-0.04	-0.07	1.72	0.96	0.93
R9	0.52	0.99	0.69	0.99	1.06	0.84	0.47	0.07	0.15	1.91	1.07	1.23
R10	1.83	0.96	1.67	0.52	0.99	0.69	-1.31	0.03	-0.98	0.28	1.03	0.41
R10	1.83	0.96	1.67	0.89	0.96	0.96	-0.94	0.00	-0.71	0.49	1.00	0.57
R10	1.83	0.96	1.67	0.94	0.88	0.84	-0.89	-0.08	-0.83	0.51	0.91	0.50
R10	1.83	0.96	1.67	0.99	1.06	0.84	-0.84	0.10	-0.83	0.54	1.10	0.50
R10	1.83	0.96	1.67	0.99	0.95	0.72	-0.84	-0.01	-0.94	0.54	0.99	0.43
R10	1.83	0.96	1.67	1.05	1.02	0.93	-0.78	0.06	-0.74	0.58	1.06	0.56
R10	1.83	0.96	1.67	1.18	0.82	1.31	-0.65	-0.14	-0.36	0.64	0.85	0.79
R10	1.83	0.96	1.67	1.27	0.96	0.94	-0.56	0.00	-0.73	0.69	1.00	0.56
R10	1.83	0.96	1.67	1.30	0.89	0.92	-0.53	-0.08	-0.75	0.71	0.92	0.55
R10	1.83	0.96	1.67	1.42	0.86	1.56	-0.41	-0.10	-0.11	0.77	0.90	0.94
R10	1.83	0.96	1.67	1.53	0.92	0.89	-0.31	-0.04	-0.78	0.83	0.96	0.53
R10	1.83	0.96	1.67	1.53	0.91	1.63	-0.30	-0.05	-0.04	0.83	0.95	0.98
R10	1.83	0.96	1.67	1.61	0.79	2.55	-0.22	-0.18	0.88	0.88	0.82	1.53
R10	1.83	0.96	1.67	1.83	0.72	2.32	0.00	-0.24	0.65	1.00	0.75	1.39
R11	1.30	0.89	0.92	0.52	0.99	0.69	-0.78	0.11	-0.24	0.40	1.12	0.75
R11	1.30	0.89	0.92	0.89	0.96	0.96	-0.41	0.08	0.03	0.68	1.09	1.04
R11	1.30	0.89	0.92	0.94	0.88	0.84	-0.36	-0.01	-0.08	0.72	0.99	0.91
R11	1.30	0.89	0.92	0.99	1.06	0.84	-0.32	0.18	-0.08	0.76	1.20	0.91
R11	1.30	0.89	0.92	0.99	0.95	0.72	-0.31	0.06	-0.20	0.76	1.07	0.78
R11	1.30	0.89	0.92	1.05	1.02	0.93	-0.25	0.14	0.01	0.81	1.15	1.01
R11	1.30	0.89	0.92	1.18	0.82	1.31	-0.12	-0.07	0.39	0.91	0.92	1.42
R11	1.30	0.89	0.92	1.53	0.92	0.89	0.22	0.04	-0.04	1.17	1.04	0.96
R11	1.30	0.89	0.92	1.61	0.79	2.55	0.31	-0.10	1.63	1.24	0.89	2.77
R11	1.30	0.89	0.92	1.83	0.72	2.32	0.53	-0.16	1.40	1.40	0.81	2.52
R12	1.42	0.86	1.56	0.52	0.99	0.69	-0.90	0.13	-0.87	0.36	1.15	0.44
R12	1.42	0.86	1.56	0.89	0.96	0.96	-0.53	0.10	-0.60	0.63	1.11	0.61
R12	1.42	0.86	1.56	0.94	0.88	0.84	-0.48	0.01	-0.72	0.66	1.02	0.54
R12	1.42	0.86	1.56	0.99	1.06	0.84	-0.43	0.20	-0.72	0.70	1.23	0.54
R12	1.42	0.86	1.56	0.99	0.95	0.72	-0.42	0.09	-0.84	0.70	1.10	0.46
R12	1.42	0.86	1.56	1.05	1.02	0.93	-0.36	0.16	-0.63	0.74	1.18	0.60
R12	1.42	0.86	1.56	1.18	0.82	1.31	-0.24	-0.05	-0.25	0.83	0.95	0.84
R12	1.42	0.86	1.56	1.27	0.96	0.94	-0.15	0.10	-0.62	0.90	1.11	0.60
R12	1.42	0.86	1.56	1.30	0.89	0.92	-0.12	0.02	-0.64	0.92	1.03	0.59
R12	1.42	0.86	1.56	1.53	0.92	0.89	0.11	0.06	-0.68	1.08	1.07	0.57

R12	1.42	0.86	1.56	1.61	0.79	2.55	0.19	-0.08	0.99	1.14	0.91	1.63
R12	1.42	0.86	1.56	1.83	0.72	2.32	0.41	-0.14	0.76	1.29	0.84	1.49
R13	1.53	0.91	1.56	0.52	0.99	0.69	-1.01	0.08	-0.94	0.34	1.09	0.42
R13	1.53	0.91	1.56	0.89	0.96	0.96	-0.64	0.05	-0.67	0.58	1.06	0.59
R13	1.53	0.91	1.56	0.94	0.88	0.84	-0.59	-0.04	-0.79	0.62	0.96	0.51
R13	1.53	0.91	1.56	0.99	1.06	0.84	-0.54	0.15	-0.79	0.65	1.16	0.52
R13	1.53	0.91	1.56	0.99	0.95	0.72	-0.53	0.04	-0.91	0.65	1.04	0.44
R13	1.53	0.91	1.56	1.05	1.02	0.93	-0.47	0.11	-0.70	0.69	1.12	0.57
R13	1.53	0.91	1.56	1.18	0.82	1.31	-0.35	-0.09	-0.32	0.77	0.90	0.80
R13	1.53	0.91	1.56	1.27	0.96	0.94	-0.26	0.05	-0.69	0.83	1.05	0.58
R13	1.53	0.91	1.56	1.30	0.89	0.92	-0.23	-0.03	-0.71	0.85	0.97	0.57
R13	1.53	0.91	1.56	1.42	0.86	1.56	-0.11	-0.05	-0.07	0.93	0.95	0.96
R13	1.53	0.91	1.56	1.53	0.92	0.89	0.00	0.01	-0.74	1.00	1.01	0.54
R13	1.53	0.91	1.56	1.61	0.79	2.55	0.09	-0.13	0.92	1.06	0.86	1.57
R13	1.53	0.91	1.56	1.83	0.72	2.32	0.30	-0.19	0.69	1.20	0.79	1.42

table 25 raw SAR Data (part 3: double bond group)

fold changes (IL-8 and CLDN1 gene expression IL-8 release) used to make assumptions about the effect of different structural modifications (showing only the double bond group)

	IL-8 Gene Expr. Fold change_1	IL-8 release_1	CLDN1 Expression Fold change_1	IL-8 Gene Expr. Fold change_2	IL-8 release_2	CLDN1 Expression Fold change_2	DELTA_IL-8 Gene Expr.	DELTA_IL-8 release	DELTA_CLDN1 Expression	CXCL8 gene expression fold chang
R14	1.27	0.96	0.94	0.52	0.99	0.69	-0.75	0.03	-0.25	0.41
R14	1.27	0.96	0.94	0.89	0.96	0.96	-0.38	0.00	0.02	0.70
R14	1.27	0.96	0.94	0.94	0.88	0.84	-0.33	-0.08	-0.10	0.74
R14	1.27	0.96	0.94	0.99	1.06	0.84	-0.28	0.10	-0.10	0.78
R14	1.27	0.96	0.94	0.99	0.95	0.72	-0.27	-0.01	-0.21	0.78
R14	1.27	0.96	0.94	1.05	1.02	0.93	-0.22	0.06	-0.01	0.83
R14	1.27	0.96	0.94	1.18	0.82	1.31	-0.09	-0.14	0.37	0.93
R14	1.27	0.96	0.94	1.30	0.89	0.92	0.03	-0.07	-0.02	1.03
R14	1.27	0.96	0.94	1.53	0.92	0.89	0.26	-0.03	-0.05	1.20
R14	1.27	0.96	0.94	1.61	0.79	2.55	0.34	-0.17	1.61	1.27
R14	1.27	0.96	0.94	1.83	0.72	2.32	0.56	-0.24	1.38	1.44
R15	1.61	0.79	2.55	0.52	0.99	0.69	-1.10	0.21	-1.86	0.32
R15	1.61	0.79	2.55	0.89	0.96	0.96	-0.72	0.18	-1.59	0.55
R15	1.61	0.79	2.55	0.94	0.88	0.84	-0.67	0.09	-1.71	0.58
R15	1.61	0.79	2.55	0.99	1.06	0.84	-0.63	0.28	-1.71	0.61
R15	1.61	0.79	2.55	0.99	0.95	0.72	-0.62	0.17	-1.83	0.62
R15	1.61	0.79	2.55	1.18	0.82	1.31	-0.43	0.03	-1.24	0.73
R15	1.61	0.79	2.55	1.53	0.92	0.89	-0.09	0.14	-1.67	0.95
R15	1.61	0.79	2.55	1.83	0.72	2.32	0.21	-0.06	-0.23	1.13
R16	1.13	0.59	1.42	0.52	0.99	0.69	-0.61	0.41	-0.73	0.46
R16	1.13	0.59	1.42	0.89	0.96	0.96	-0.24	0.38	-0.46	0.79
R16	1.13	0.59	1.42	0.94	0.88	0.84	-0.18	0.29	-0.58	0.84
R16	1.13	0.59	1.42	0.99	1.06	0.84	-0.14	0.48	-0.57	0.88
R16	1.13	0.59	1.42	0.99	0.95	0.72	-0.13	0.37	-0.69	0.88

R16	1.13	0.59	1.42	1.05	1.02	0.93	-0.07	0.44	-0.48	0.94
R16	1.13	0.59	1.42	1.18	0.82	1.31	0.05	0.23	-0.11	1.05
R16	1.13	0.59	1.42	1.27	0.96	0.94	0.14	0.37	-0.48	1.13
R16	1.13	0.59	1.42	1.30	0.89	0.92	0.18	0.30	-0.49	1.16
R16	1.13	0.59	1.42	1.42	0.86	1.56	0.29	0.28	0.15	1.26
R16	1.13	0.59	1.42	1.53	0.92	0.89	0.40	0.34	-0.53	1.36
R16	1.13	0.59	1.42	1527.00	0.91	1.63	0.40	0.33	0.21	1.36
R16	1.13	0.59	1.42	1.61	0.79	2.55	0.49	0.20	1.14	1.43
R16	1.13	0.59	1.42	1.83	0.72	2.32	0.70	0.14	0.91	1.62
R16	1.13	0.59	1.42	1.83	0.96	1.67	0.70	0.38	0.25	1.63

Abstract

This master's thesis investigates the anti-inflammatory and barrier-enhancing effects of homovanillic acid esters on human epidermal keratinocytes, with a particular focus on the aliphatic side chain of these structures. Homovanillic acid esters are structurally related to capsaicin (the active component in chili peppers) and its non-pungent analogue capsiate, but differ in chain length, branching, and the presence of double bonds in the aliphatic side chain. To evaluate their ability to modulate *CLDN1* and *CXCL8* gene expression, as well as the release of IL-8 a total of sixteen analogs were tested.

The HaCaT cell line was used as a model for non-neuronal skin cells due to its capacity to transition between proliferative and differentiated states depending on calcium concentration (Colombo et al., 2017). Cells were treated with selected TRPV1 agonists and antagonists, including capsaicin (Chen et al., 2019), capsiate (Ilie et al., 2019), and capsazepine (Gonzalez-Reyes et al., 2013), followed by inflammatory stimulation using TNF-α. Gene expression of key markers such as *CLDN1* (Deng et al., 2019) and *CXCL8* (Reinke & Sorg, 2012; Gendrisch et al., 2021) was assessed via RT-qPCR, while IL-8 secretion was quantified using ELISA. These results were further explored through a structure–activity relationship (SAR) analysis to identify structural features associated with biological activity.

Initial findings indicated that several homovanillic acid esters reduced IL-8 release and enhanced *CLDN1* gene expression. In particular, one compound, characterized by a six-carbon side chain and a double bond at the gamma-position, stood out by significantly increasing *CLDN1* expression and decreasing IL-8 release.

This research underscores the therapeutic potential of different non-pungent capsaicin analogs in keratinocytes for conditions characterized by inflammation and impaired barrier function, such as psoriasis and atopic dermatitis (C. Cao et al., 2020). Identifying the structural modifications necessary leading to anti-inflammatory properties and enhanced barrier function with minimal side effects could pave the way for innovative treatments for skin-related inflammatory disorders.

Zusammenfassung

Diese Masterarbeit untersucht Homovanillinsäureester, strukturelle Analoga von Capsaicin, im Hinblick auf ihre entzündungshemmenden und barrierefördernden Effekte in humanen epidermalen Keratinozyten. Der Fokus liegt auf den strukturellen Unterschieden innerhalb der aliphatischen Seitenkette dieser Verbindungen, die *CLDN1*- und *CXCL8*-Genexpression sowie die Sekretion von IL-8 beeinflussen. Eine zentrale Hypothese der Arbeit ist, dass bestimmte strukturelle Merkmale die biologische Aktivität der Verbindungen maßgeblich bestimmen.

Die Untersuchungen wurden an der HaCaT-Zelllinie durchgeführt, einem *in-vitro*-Modell für humane Keratinozyten, das zwischen proliferativen und differenzierten Zuständen wechseln kann (Colombo et al., 2017). Dabei wurden insgesamt 16 Analoga getestet. Zur funktionellen Charakterisierung wurden zusätzlich bekannte TRPV1-Modulatoren (Capsaicin, Capsiat (Ilie et al., 2019) und Capsazepin (Gonzalez-Reyes et al., 2013)) eingesetzt. Nach Behandlung der Zellen mit den Verbindungen wurde eine Entzündungsreaktion durch TNF-α induziert. Anschließend erfolgte die Quantifizierung der Genexpression von *CLDN1* (Tight-Junction-Protein) (Deng et al., 2019) und *CXCL8* (Gen des proinflammatorischen Zytokins IL-8) (Reinke & Sorg, 2012; Gendrisch et al., 2021) mittels RT-qPCR sowie die Messung der IL-8-Sekretion mittels ELISA. Eine begleitende Struktur-Wirkungs-Beziehungsanalyse (SAR) diente der Identifikation von Merkmalen, die mit der biologischen Aktivität zusammenhängen.

Einige der getesteten Homovanillinsäureester führten zu einer erhöhten *CLDN1*-Expression und reduzierten IL-8-Werten. Besonders auffällig war eine Verbindung mit einer sechs Kohlenstoffatome langen aliphatischen Seitenkette und einer Doppelbindung am gamma Kohlenstoffatom, die eine klare Wirkung auf Barrierefunktion und Entzündungsmarker in humanen Keratinozyten zeigte.

Diese Ergebnisse unterstreichen das Potenzial strukturell optimierter Homovanillinsäureester als Ausgangspunkt für neue dermatologische Therapien bei entzündlichen Hauterkrankungen wie Psoriasis oder atopischer Dermatitis (Cao et al., 2020). Die gezielte Analyse struktureller Einflüsse könnte zu neuen Behandlungsstrategien führen, die Entzündung reduzieren und gleichzeitig die Hautbarriere stärken, bei gleichzeitig geringeren Nebenwirkungen als herkömmliche Wirkstoffe.